A FINITE ELEMENT SOLUTION OF THE LAMINAR FLAME EQUATIONS AT THE LOWER FLAMMABILITY LIMIT

L.A. McLean

ABSTRACT

In this work a general numerical finite element solution of the laminar flame equations is formulated using Galerkin's concept of error minimization. A computer program developed from the resulting discrete equations is then tested using simple models for which exact solutions are available. At the same time, using these simple models, the code is evaluated. It is found to be generally satisfactorily and to be particularly well suited to solving global aspects of reacting flow problems such as the flame speed. Since element weighting (upwinding) is included in the numerical model, its effect on the solution accuracy is examined and is found to greatly improve the species profile accuracy with a small sacrifice in the accuracy of the reaction front progression rate.

So that the code may be generally useful for solving flame problems where little information of the species transport properties is available, the corresponding flame parameters are calculated in the code using a modified Chapman-Enskog model with Lennard-Jones correction factors. The reliability of this method is examined in detail. It is concluded that the error level is acceptable in pertinent temperature ranges.

Finally, the general program is applied to particular hydrocarbon flames, modelled as simplex global one-dimensional laminar reaction fronts. The code yields profile results, flame speeds and flame thickness. The flammability limit of a methane flame is estimated using a unique flame speed profile trajectory method developed and the predicted results compare to conventional flammability limit measurements to within 13%.

Extension and refinement of the procedure is discussed.

ACKNOWLEDGEMENTS

The author is grateful to all the members of the combustion research group at Concordia University: They have contributed immeasurably to the research involved and to the production of this thesis. In particular, the author thanks Dr. A.J. Saber, his research advisor and the leader of the group. Dr. Saber gave freely of his time and shared his insight at times when problems seemed insurmountable and understanding seemed elusive.

He would also like to acknowledge the personal support of his parents, family, Morg and M.J.P.. In particular, however, the author is indebted to the NATURAL SCIENCES and ENGINEERING COUNCIL of CANADA (NSERC) for financially supporting this research investigation.

This work has been carried out under NSERC Operating Grant Number A4208,
"Coal Producer Gas Flammability Limits."

TABLE OF CONTENTS

Table of Contents (cont'd.)

Table of Contents (cont'd.)

LIST OF TABLES

LIST OF FIGURES

LIST OF FIGURES (cont'd)

LIST OF FIGURES (cont'd)

LIST OF SYMBOLS

AFT	adiabatic flame temperature [K]
A_r	heat loss area [cm^2]
c_p	specific heat at constant pressure [$\frac{cal}{g-K}$]
c_v	specific heat at constant volume [$\frac{cal}{g-K}$]
D	diffusion coefficient for the fuel species in air. [$\frac{cal}{g-K}$]
D_{AM}	diffusion coefficient between species A and the mixture [cm^2/s]
D_s	self-diffusion coefficient [cm^2/s] for fuel species
E	activation energy [cal/mole]
f	upwinding factor
G	convection rate [g/cm^2-s]
h	element size [cm]
H	convection heat transfer coefficient [$\frac{cal}{cm^2-s-K}$]
H_c	heat of combustion [$\frac{cal}{g-s-cm^2}$]
k	thermal conductivity [$\frac{cal}{cm-s-K}$]
$k_1;k_2$	reaction rate correction factors
L	lewis number = $\frac{\rho DCp}{k}$
m	reaction order
M	molecular weight
N	number of elements
p	pressure [atm]

P	Peclet number = $\frac{c_p G}{k}$
$\tilde{P}$	Ph
q_c	heat loss across a convection sheet $[\frac{cal}{s\text{-}cm^2}]$
q_L	heat loss rate to surroundings $[\frac{cal}{s\text{-}cm^2}]$
q_r	heat loss due to radiation $[\frac{cal}{s\text{-}cm^2}]$
R	universal gas constant
R_F	rate of fuel consumption per unit vol. $[\frac{g}{cm^3\text{-}s}]$
T	temperature [K]
T_c	cutoff temperature [K]
T_i	ignition temperature [K]
T_o	unburnt gas temperature [K]
T_w	wall temperature [K]
T_∞	ambient temperature [K]
u	gas velocity [cm/s]
V_o	stoichiometric flame velocity [cm/s]
$W_1;W_2$	elemental weighting functions (mathematical)
x	displacement through the flame [cm]
$X_i;X_j$	mole fractions of ith and jth species
Y	fuel mass fraction
Y_o	fuel mass fraction in unburnt mixture
$\alpha = Y/Y_o$	normalized fuel fraction

Γ	boundary surface between the solution regime and the surroundings (mathematical)
δ	flame thickness [cm]
ε	molecular energy $[\frac{cal}{cm-s}]$
ε_r	surface emissivity
ε/k	molecular energy parameters [K]
μ	viscosity $[\frac{g}{cm-s}]$
ρ	mass density $[g/cm^3]$
ρ_0	mass density of unburnt mixture $[g/cm^3]$
σ_r	Stefan-Boltzmann constant
σ	molecular collision diameter [angstroms]
$\phi_1; \phi_2$	elemental functions (mathematical)
Ω_D	Lennard-Jones diffusivity correction factor
$\Omega_\mu = \Omega_k$	Lennard-Jones viscosity correction factor

CHAPTER 1

PERSPECTIVE

1.1 The General Framework

Combustion of fuels, either solid, liquid or gaseous is the dominant means by which man produces the energy used in everyday activities (1,2,3). This combustion-derived energy is converted to several forms. A form of this energy, electricity, convenient for distribution from a central location to light and heat buildings, is often produced in "central power stations" by burning natural fuels such as coal, natural gas and oil (3). Also, another form, mechanical energy, needed to drive vehicles of all sorts (automobiles, trains, aircraft and ships) is conveniently derived from the combustion of these fuels in heat engines (3,4).

There are alternate processes to supply energy needs which have long been available and new processes are quickly being researched and developed (5). These alternatives include hydropower, presently an important source of centralized power; nuclear power, becoming increasingly important; and solar power, wind power and wave power all of which will be actively developed in the future (6). These processes are replacing combustion in technologically accessible uses.

With few exceptions, however, these alternative

processed are inappropriate in mobile applications where the energy source must be compact and portalbe and conversion rates high (3). The combustion of fuels to release stored chemical energy is a common process used in such applications.

Hydrocarbon fuels, composed of chemically-linked carbon and hydrogen, have a high heating value and have been abundant and cheap (5). Hence, most common fuels are hydrocarbons, and a vast capital investment in machinery fueled by these fuels, has resulted (3,7). However, hydrocarbon fuels are an exhaustible resource, and so, much effort is being expended to ensure that they are used efficiently (8,9,10,11). Some of this effort involves increasing the knowledge of the fundamental burning processes in combustion studies.

The science of combustion combines many other traditional disciplines encountered in the study of chemistry and physics (Fig. 1.1). Most combustion processes take place in hot flowing multicomponent fluids undergoing exothermic reactions. Therefore, the physics of fluids, including diffusion, heat transfer, thermodynamics and fluid mechanics play an important role. Also, because of the relationship between molecular structure and fluid parameters such as thermal conductivity, specific heat, viscosity and diffusivity, physical chemistry and quantum mechanics are important. Furthermore, the laws governing chemical transformations, including

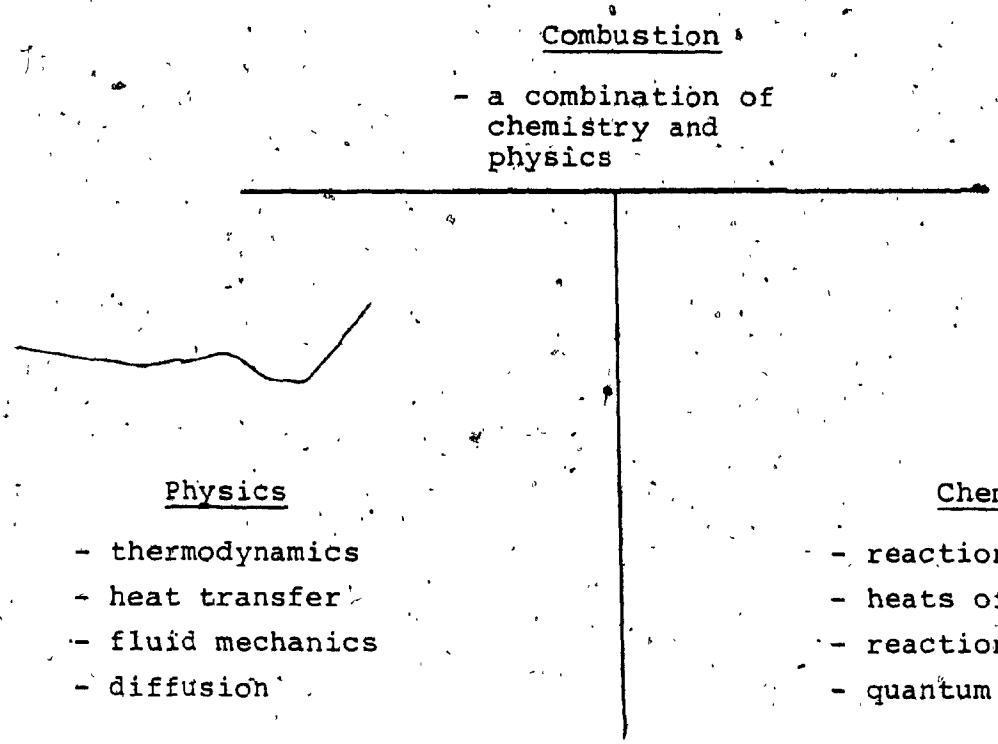

Fig. 1.1: A breakdown of the science of combustion

chemical kinetics, chemical thermodynamics and reaction mechanisms are important (12,13,15). If, in the analysis of a particular problem, all the phenomena happen simultaneously, the task of solving it is formidable indeed. Fortunately, however, many phenomena do not play dominant roles and models of many combustion engineering systems can be simplified (12).

1.2 The Premixed Laminar Flame

Two general classes of flames are observed in engineering systems, diffusion flames where the reactant mixing process is part of the combustion process and premixed flames where the mixing process is independent of the combustion process. A premixed flame which propagates so that the fluid mechanics of the flame involves little or no turbulence, is called a premixed laminar flame.

The premixed laminar flame occurs in Bunsen burners commonly found in science laboratories, flat flame burners a modern device for studying flames and flame tubes like those used in flammability limit testing (13). This flame phenomenon has been attributed particular theoretical importance because it can exist as a steady self-sustaining exothermic reaction propagating axially if surface curvature and aerodynamic effects can be eliminated (14). Some salient

features of such a flame are illustrated in Fig. 1.2.

In this figure the flame is broken down into four regions, an induction region composed of an uneffected fuel/oxidizer mixture, a preheat region where the reactants are thermally elevated to the combustion temperature, a reaction region where the gases react and a post flame region comprised of hot gas products.

The phenomena associated with laminar flame propagation have been known for many years (16) and computer packages designed to solve particular problems do exist (17,18,19,20). There are, however, several specific areas where lack of knowledge has delayed a complete and reliable solution to laminar flame problems. What follows is a partial list:

1) Transport information for complicated gas mixtures encountered in flames, particularly at elevated temperatures, is incomplete.
2) Information regarding mechanisms of extinction is lacking.

Codes which presently exist usually simplify or neglect transport properties and almost always ignore the extinction problem.

1.3 Flame Extinction

Extinction of flames is a widely observed phenomenon

INDUCTION REGION	PREHEAT REGION	REACTION REGION	POST FLAME REGION
- room temperature - fuel/oxidant unreacted	- rising temperature - diffusion of species	- high reaction rate	- hot products

Fig. 1.2: Schematic of a Flame

in combustion systems, and as such a general flame propagation model is incomplete without acknowledging it. Nevertheless, no adequate general theory exists to explain this phenomenon and very little is known concerning the mechanisms of extinction. As such, modelling is difficult.

One class of extinction of particular interest in propagating laminar flames is the self-extinction of flames propagating in mixtures of flammable gases. This takes place when the mixture is overladen with either of the two major components, fuel or oxidant. Such a mixture is said to be outside the flammability limits.

The measured values of flammability limits for gas mixtures is dependent on the procedure used (21,22,23). Noteable, however, is that the flammability limits broaden as aerodynamic buoyancy and multidimensional effects are reduced (22).

1.4 This Work

The present work addresses aspects of hydrocarbon combustion processes. It begins with a description of the physical and chemical processes involved in general premixed laminar flame propagation, hence the general governing differential equations are formulated. Next, a computational code to solve the equations is developed, using a finite

element formulation. The code is tested and applied to the specific case of hydrocarbon combustion.

The computational solution includes an allowance for heat loss from the flame zone in the form of heat flow across a convection boundary layer and in the form of radiation heat transfer to the surroundings.

Transport properties in the flame are calculated using a modified Chapman-Enskog theory with a correction factor calculated using Lennard-Jones potential theory. The flammability limits are estimated using a unique velocity profile trajectory approach.

The present work addresses aspects of combustion as they specifically relate to hydrocarbon combustion processes. The treatment, however, is general, recognizing that other important fuels exist, including methanol and hydrogen, both of which are being studied with interest (24).

CHAPTER 2

THE PHYSICAL AND MATHEMATICAL MODEL

A flame which has been established in a laminar premixed gas flow and continues to exist after all fluid dynamic, chemical and heat flow transients become negligible is called a steady-state premixed laminar flame. A gas mixture which will self-propagate an established flame in this manner until the mixture is exhausted is said to be a flammable mixture.

Such a flame is often modelled as one-dimensional and the equations describing a one-dimensional premixed laminar flame have been established for many years (1). In this work these equations are modified to account for heat loss in the form of radiation to the surroundings and heat flow across a convection boundary layer. They are derived in detail in Appendix A.

2.1 The Governing Equations

Several simplifying assumptions are made:

1). Viscosity, turbulence, ordered kinetic energy and all other effects of velocity are neglected. This is the case when the velocity is small.

2) Body forces are neglected. This is a common

assumption in dealing with gas flows where buoyant forces do not play a major role.

3) Soret and Dufour effects are neglected. These second order effects are often found to be much smaller than other diffusion and heat transfer mechanisms (2).

The overall continuity equation is:

$$G = \rho u = \text{constant} \qquad (2.1)$$

where, ρ = mass density $[g/cm^3]$

u = gas velocity $[cm/s]$

G = convection rate $\left[\frac{g}{cm^2\text{-}s}\right]$

The momentum equation is:

$$p = \text{constant} \qquad (2.2)$$

where, p = pressure [atm]

This form is extremely simple because of assumptions one and two. In support of equation 2.2, Strehlow shows the total pressure drop across a flame to be around one percent (3).

The species and the energy equations are derived with some additional assumptions:

4) Specific heats are constant and uniform. This is a common assumption (6).

5) Thermal conductivity divided by specific heat is proportional to thermal diffusivity times the overall density. These are both constant and uniform through the flame. That is,

the Lewis number is constant. These assumptions are reasonable for a perfect gas. (9)

6) The chemistry is governed by a simplex global reaction. The form of the reaction is:

fuel + oxidant → products

In reality, in most combustion systems many reactions take place simultaneously to produce the global chemistry (4).

Applying these assumptions, the species equation is:

$$LY_o \frac{d^2\alpha}{dx^2} - GY_o \frac{c_p}{k} \frac{d\alpha}{dx} = -\frac{R_F C_p}{k} \qquad (2.3)$$

where

k = thermal conductivity $[\frac{cal}{C\text{-}S\text{-}o_K}]$

c_p = specific heat at constant pressure $[\frac{cal}{g\text{-}o_K}]$

D = diffusion coefficient for the fuel species $[cm^2/s]$

L = Lewis number

Y_o = fuel fraction in unburnt mixture

$\alpha = Y/Y_o$ = normalized fuel fraction

x = displacement through the flame [cm]

R_F = rate of reduction of fuel per unit volume, $[g/cm^3\text{-}s]$

and the energy equation is:

$$\frac{d^2T}{dx^2} - \frac{Gc_p}{k} = \frac{HR_F}{k} + \frac{q_L}{k} \qquad (2.4)$$

where T = temperature (°K)

H = heat of combustion $(\frac{cal}{g\text{-}s\text{-}m^2})$

q_L = heat flow rate to surroundings $(\frac{cal}{s\text{-}cm^2})$

The governing equations must be solved in the context of the appropriate boundary conditions.

2.2 Boundary Conditions

The completely defined problem must make reference to the environment surrounding the solution regime. This is done by requiring certain conditions at the boundary of the solution regime. For the laminar flame problem, when heat loss is neglected the following "boundary conditions" are usual:

COLD BOUNDARY: $X=0$, $T=To$; $\alpha=1$

HOT BOUNDARY: $X=\infty$, $\frac{dT}{dX}=0$, $\frac{d\alpha}{dX}=0$

where To = initial gas temperature

If the hot boundary is fixed at a finite distance from the cold boundary and heat loss is not neglected, the temperature gradient at the hot boundary is not zero unless the temperature of the gas flow has equilibrated with the surroundings. The Cauchy boundary condition is more correct:

$$\left.\frac{dT}{dX}\right|_{\Gamma_{HOT}} = -\left.\frac{q}{k}\right|_{\Gamma_{HOT}}$$

where Γ_{HOT} = the boundary surface between the hot gases and the surroundings

q = heat flow rate $[\frac{cal}{s\text{-}cm^2}]$

The Cauchy condition at a boundary implies that heat flow (q) exists at the boundary.

2.3 Reaction Kinetics

The simplex global reaction rate of the Arrhenius type is used:

$$R_F = (F(\alpha,T))\exp(-E/RT)$$

where

E = activation energy

R = universal gas constant

$F(\alpha,T)$ = a function of "α" and "T" derived from chemistry considerations

Classically, "F" is of the form $(f)^m$ where m is the order of the reaction (5,6). Since, the order of the reaction represents the number of particles which must collide for the reaction to proceed, it is normally a natural number (7). However, because many reactions take place simultaneously in a simplex global reaction, "m" is often allowed to take on a decimal value, usually between one and two (8). To account

for the possiblity that a reaction order can lie between one and two it is postulated, in this work, that the simplex reaction is comprised of two reaction rate components each having the same activation energy. These components have first and second order reactions respectively, and the overall reaction rate is represented as:

$$R_F = \left[\frac{-k_1 \alpha Y_o \rho_o T_o}{T} - k_2\left(\frac{\alpha Y_o \rho_o T_o}{T}\right)^2\right] \exp -\frac{E}{RT} \qquad (2.5)$$

where k_1 and k_2 are factors used to correct the overall reaction rate to experimental values and to account for the proportions of first and second order reactions involved.

2.4 The Steady-State Convection Rate

Using a control volume analysis of the flame, the following relationship is found (see Appendix C):

$$G = \frac{\int_{-\infty}^{\infty}\left[\frac{R_F c_p}{k}\right] dx}{\int_1^0 Y_o\left[\frac{c_p}{k}\right] d\alpha} \qquad (2.6)$$

where, G = convection rate [g/cm^2-s]

This value, G, the "convection rate", is an invariant in the flame for the steady-state. This convection rate formulation also applies in the general case, where "α" is a

single species vector chosen arbitrarily from a multi-species flame where many species vectors are needed to describe the flame (9).

2.5 Cold Boundary Difficulty

The kinetic statement described above demands that reactions in a premixed gas begin immediately upon mixing of the reactants. Hence, a steady-state situation can only exist when the reactants are completely consumed. However, steady-state flames are observed (10). The difficulty in producing a steady-state flame model incorporating a continous kinetic statement is called the cold boundary difficulty. The model described above, therefore, demands modification to allow for steady-state flame situations.

The cold boundary difficulty is usually handled by demanding that the reaction rate function vanish for temperatures less than a certain "cut-off temperature". A cut-off temperature must therefore be selected (11). Here it is presumed that the selection of cut-off temperature is not critical if that temperature falls in a range where the reaction rates are small (12). It is on this basis that the solutions to the differential equations are found. The details of the procedure used here to select an appropriate cut-off temperature are detailed below.

2.6 Flame Extinction and Flammability Limits

The equations described above have been applied successfully in many flame propagation problems. However, they do not account for the phenomena of flame extinction and the related problem of flammability limits.

When a flammable gas mixture is diluted progressively with any miscible ingredient (active or passive) a point, called the flammability limit, can be determined experimentally beyond which the mixture is non-flammable. This experimentally-observed phenomenon lacks an adequate general theory (13).

Standard tests have been applied to premixed gases for many years to determine flammability limits (14). These standard tests are done in specially designed flame tubes in which a flame is started with a spark igniter. The flame which forms propagates in an environment where multidimensional phenomena are involved, including buoyancy, thrust and uneven heat loss from the flame zone (15). These phenomena probably influence the flammability limits (14). This attitude is supported by the virtual elimination of all one-dimensional theories in explaining these limits (15). For instance chemical kinetic instability is described as an unlikely phenomenon (16). Also, based on experimental evidence, radiation heat loss to the surroundings is generally discredited as a likely mechanism (17,18,19). One postulate poses the existence of a true ignition or cut-off temperature (similar to the one

already proposed to deal with the cold boundary difficulty) (20,21). For a flame temperature below such a cut-off temperature, steady-state flame propagation cannot exist. This concept has no apparent experimental or theoretical basis.

Nevertheless, some investigators have postulated that the conventional flammability limits derived from these standard tests are physico-chemical constants (22,23). More recent evidence does not support this view. For example, flames of hydrocarbon and air and of ethylene and air have been stabilized on flat flame burners in mixtures leaner than the conventional lean flammability limit (24,25,26,27). Apparently, if a fundamental flammability limit exists, it is not the traditional limit.

Sorenson et al, by eliminating aerodynamic and multi-dimensional phenomena from a Bunsen burner flame, find the lower flammability limit of a propane-air flame by studying the flame speed for different mixture ratios. Their work, in agreement with earlier study, shows that flame speed plunges as the mixture is weakened near the flammability limit (28) and they find the flame speed approaches zero when the fuel present in the mixture is still substantial (29). As the flame speed approaches zero, so does the reaction rate of the fuel (30), hence this point is the flammability limit and may be of considerable theoretical importance. Here it is called the natural flammability limit.

Since the flame speed drops rapidly as mixture weakens

near the flammability limit and because Sorenson et al shows that the drop continues until the flame speed approaches zero at the natural flammability limit, therefore it is asserted here that a target line tangent at the point of inflection of the flame speed-equivalence ratio curve will intersect the equivalence ratio axis at a point near the flammability limit of the gas mixtures. This working hypothesis is tested below using a methane-air model.

CHAPTER 3

SOLUTION METHOD

The solution of the equations presented in Chapter 2 describing laminar reactive flow are presented here. Although these equations have non-linear coefficients, the nonlinearities are weak, and under the assumptions made in Chapter 2, the coefficients may be considered linear. Nevertheless analytical solutions for these equations are difficult because of the nonlinear source terms which characterize them.

As a consequence of this difficulty and before the development of high speed computers, combustion problems of this sort could be solved only after applying simplifications which made the solutions unrealistic (1). These simplifications are now often unwarranted because the computer makes more comprehensive numerical approaches feasible and ultimately the results obtainable in this way promise to be realiable and available. However, the time and data storage requirements to solve the complex flow field problems tax the capabilities of even the most sophisticated contemporary computers (2). Further, there is presently a trend toward smaller computing units in which memory and storage is even more restrictive. Hence, there is a demand for efficient computing schemes with low storage requirements.

Solving computationally a set of differential equations involves the formulation of a corresponding set of approximate

algebraic equations which can be manipulated numerically. There are at least two methods to formulate such algebraic equations; the finite difference method and the finite element method. Apparently finite difference approximation has been used exclusively to solve the laminar flame equations. However, the alternative procedure, the finite element method, is powerful in some situations. This method is considered here.

The finite element method, like the finite difference method, is applied to continuum flow problems by dividing the solution regime into many small regions called elements (3,4). The numerical approximation is improved as the elements become smaller (5,6).

Consider flame properties, which change quickly within a large flow regime. In this case, a fine mesh is required to obtain acceptable resolution. Thus, problems arise when computer storage availability limits mesh refinement, restricting solution accuracy.

An approach to lowering computational demands involves varying the mesh size through the flowfield. In this way accuracy is increased by using a coarse mesh in non-critical zones where the reaction rate is small and a fine mesh in the critical zone where the reaction rate is large. In contrast to the finite element method, the order of accuracy achieved using the finite difference method is lower when mesh size is variable than when mesh size is constant throughout

the continuum (6,7). In the finite element formulation, however, lattice variations may be applied without any special considerations: the order of the accuracy is unaffected. Some work has been done towards optimizing element size variations and the results are promising (2,8,9).

Another computational advantage of the finite element approach is that the variations within an element is approximated by a simple analytic function called an elemental function or interpolation function. Finite difference formulations, in contrast, do not consider explicitly the functional variation between the nodes. It can be appreciated that when this elemental function accurately represents the true function, node spacing can be increased with a potential economy of computer storage space and computational time.*

Other advantages of the finite element method, of particular importance in flame calculations can be appreciated when the formulation procedure is understood. To formulate the finite element equations, a global approximating function composed of the elemental functions is formed. The specific global approximating function is sought to minimize the error,

* Another important advantage accrues from this feature of the finite element method because these elemental functions can be chosen independently in the interior of a solution regime and at the geometric boundaries (10). Hence, for complicated geometrics (such as might exist in the combustion chamber of a gas turbine engine for instance), boundary hugging curves may be formed without upsetting the simplicity of the interior lattice.

or residual that is produced by substituting this function into the governing differential equation. To do this, the "inner product" of the residual and a preselected weighting function is equated to zero. This procedure, called Galerkin's method (11,12) is applied in this work. The discrete equations derived in this manner in Appendix B are summarized in Table 3-1.

The global approximating function so formed assures conservation of energy and mass across the solution regime as a consequence of the integral nature of the procedure. This is not true for many finite difference procedures (13,14).

Considering the natural flammability limit problem dealt with here will illustrate an important aspect of this conservation feature. In studying the problem, the flame speed, which is dependent on the integral of the reaction rate across the flame is important (17). If the species and energy are not conserved in the solution regime, this integration is inaccurate and both flame speed and flammability limits are poorly predicted.

3.1 The Formulation of the Finite Element Solution

3.1.1 Discretizing the Solution Regime and Choosing the Elemental Functions

Discretizing the solution regime is facilitated by knowledge of the form of the solution profiles. To discuss

Table 3.1 DISCRETE EQUATIONS

SPECIES EQUATIONS

$$L_e Y_o \int_D \frac{\partial \tilde{\alpha}}{\partial x} \frac{\partial W_i}{\partial x} \, dD + \frac{GY_o}{k} C \int_D \frac{\partial \tilde{\alpha}}{\partial x} W_i \, dD + \text{const} \int_D (\tilde{\alpha} W_i) dD - \int_\Gamma L_e Y_o W_i \frac{\partial \alpha}{\partial x}\Big|_{d\Gamma} = 0 \qquad (3.1)$$

ENERGY EQUATION

$$\int_D \frac{\partial \tilde{T}}{\partial x} \frac{\partial W_i}{\partial x} + \frac{cG}{k} \frac{\partial \tilde{T}}{\partial x} W_i + \frac{H_c R_F}{k} W_i \, dD - \int_\Gamma W_i \frac{d\tilde{T}}{dx}\Big|_\Gamma d\Gamma = 0 \qquad (3.2)$$

ELEMENTAL FUNCTIONS

$$\phi_1 = 1 - \frac{x}{h} \; ; \; \frac{\partial \phi_1}{\partial x} = -\frac{1}{h} \qquad (3.3)$$

$$\phi_2 = \frac{x}{h} \; ; \; \frac{\partial \phi_2}{\partial x} = \frac{1}{h} \qquad (3.4)$$

WEIGHTING FUNCTIONS

$$W_1 = \phi_1 + \psi_1 \; ; \; \psi_1 = \frac{3f}{h^2}(x^2 - hx) \qquad (3.5)$$

$$W_2 = \phi_2 + \psi_2 \; ; \; \psi_2 = -\frac{3f}{h^2}(x^2 - hx) \qquad (3.6)$$

the solution profiles of the laminar flame equations, the solution regime is separated into five regions which are illustrated in Fig. 3.1. The profiles in the induction region and the post flame region, shown in the figure, are characterized by moderate changes in associated flame variables, compared to the regions of the narrow band between these, where the profiles change very rapidly. The rapid change in this band is due to the large reaction rate associated with the flame, coupled with large transport of heat and species in this region. This middle region called the flame region is further subdivided into a preheat zone, where transport phenomena dominate the profile shapes and a reaction zone where the reaction rate eclipses the effects of transport phenomena on the profile shapes.

To accomodate these profile variations, the element sizes across the solution regime are varied relative to one another as indicated in Fig. 3.1. The exact sizes of the elements, depend on particular flame constants and the elemental functions used. Linear elemental functions are used here for simplicity (See Table 3.1).

3.1.2. Choosing the Weighting Functions - the Convection-Diffusion Problem

Heinrich, Huyakom, Zienkiewicz and Mitchell study the simple convection-diffusion flow situation and find that

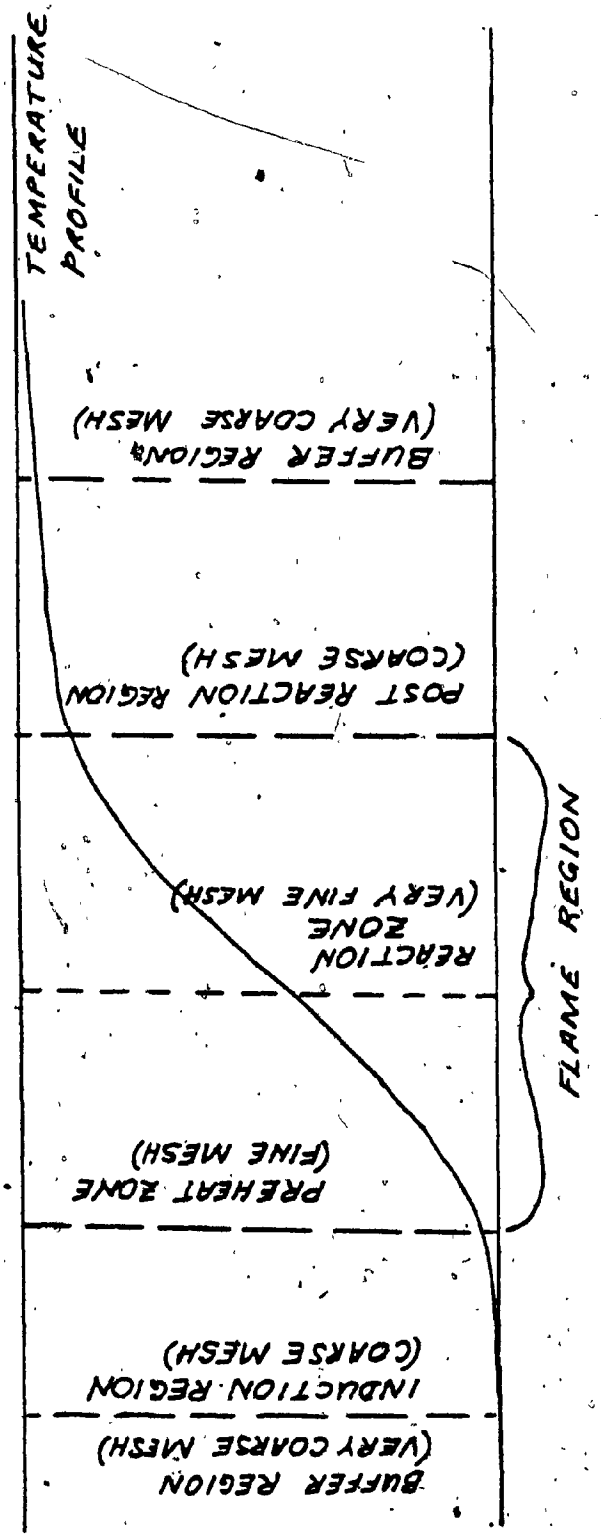

Fig. 3.1 - Regions of a Laminar Flame

the results produced are good when the following weighting functions are used: (15)

$$W_N = \phi_N + \psi_N$$

where $\phi_N = [1 - \frac{x}{h}, \frac{x}{h}]$

$$\psi_N = [\frac{3f}{h^2}(x^2-hx), -\frac{3f}{h^2}(x^2-hx)]$$

W_N = weighting function

f = a constant or function which is preselected

The value of "f" is given a positive sign when the convection rate "G" is positive.

The reaction flow problem studied here has an extra term in the equations, however, it is found that the same weighting function yields good results if the function "f" is made one everywhere in the solution regime.

3.2 Linearization

The non-linear source term which makes analytical solutions of the equations difficult is also responsible for much of the difficulty encountered in solving them numerically.

In fact, the stability considerations of this term, which makes the equations "stiff" can overshadow all others (16). Not surprisingly, early numerical solutions concentrate on simplified equations, stripped of heat conduction and

diffusion terms. The codes developed to solve these equations are now simple and efficient.

3.2.1 Early Solutions

By linearizing the equations locally, Moretti develops a simple algorithm (17,18). The Moretti procedure, however, is less efficient than others where the non-linearity of the reaction rate is acknowledged locally as well as globally.

In another case, Treanor uses a modified Runge-Kutta method in which the rate of change of the reaction expression for the ith specie is dominated by its rate of change with respect to the ith specie alone (19). This partial acknowledgement of the local non-linearity results in a convenient and conceptually simple numerical approach.

Tyson's technique is shown to be more efficient than the method used by Treanor (20,21,22). In the Tyson approach the rate of change of each reaction rate expression is computed with full regard for its rate of change with respect to each specie present. This coupled with the stable nature of the implicit algorithm used, make this the most efficient approach presently available for solving these equations (20). Using Tyson's method, Bittker et al. develop a general computer code often used today (23).

3.2.2 Modern Solutions

To apply the methods of earlier work directly to the laminar steady flow flame problem, it is necessary to postulate that convection is the only important transport mechanism. This denies the dependance of the movement of species and transfer of heat in the flame on the large temperature and concentration gradients that exist.

More complete laminar flame equations accept the importance of heat conduction and concentration driven species diffusion and include these mechanisms of transport in the models. Some of these models are discussed below. This work is summarized in Table 3.2.

In an early attempt, Hirschfelder et al use a "shooting" technique to solve the equations (24). Unfortunately, although this method is simple, it is inappropriate when the analysis includes many species and many simultaneous reactions.

In another approach, Dixon-Lewis uses an explicit finite difference algorithm to solve the time dependent equations (25). He claims that explicit algorithms are more appropriate than implicit algorithms for handling many reaction species.

Spalding et al, using an adaptation of an approach to solve boundary layer problems, eliminates the troublesome convection terms from the transient Eulerian equations and

TABLE 3.2

AUTHOR	SYSTEM	CPU TIME	COMPUTER	NO. OF GRID PTS.	NOTES
DIXON -LEWIS (1967) (25)	HYDROGEN -OXYGEN	-	ENLISH ELECTRIC KDF9	-	EXPLICIT 1-D
WILDE (1971) (34)	O_3-O_2 H_2-Br_2 MULTI	20 MIN to 8 HRS	EMR/ASI 6020	-	-
SPALDING ET AL. (1971) (27)	HYDRAZINE - AIR	.5 - 1 MIN	IBM7094	33-43	NO CONVECTION TERM EXPLICIT 1-D
BLEDJIAN (1973) (35)	O_3-O_2	-	-	-	METHODS OF LINES - RUNGE KUTTA TIME DEPENDENT
BUTLERS ET AL (1976) (33)	-	9 MIN	CDC7600	-	IMPLICIT 2-D TURBULENCE MOMENTUM
TSATSARONIS (1973) (31)	METHANE -AIR 13 SPECIES	60-80 MIN	RX-SIGMA9	33-43	500-600 ITERATIONS SPALDING METHOD LENNARD-JONES TRANSPORT
ALY ET AL (1979) (32)	PROPANE -AIR	30-50S	IBM360/75	100X10	IMPLICIT 2-D PICARD LINEARIZATION

solves the resulting set of equations using an explicit finite difference approach (26,27,28,29,30).

Later, Tsatsaronis uses Spalding's algorithm to write a code which solves a one-dimensional methane/air system in detail (31). He predicts unknown transport properties using a modified Chapman-Enskog model.

Aly solves the steady-state two-dimensional equations using Picard linearization on his finite difference model. He predicts extinction due to quenching by postulating an ignition temperature below which reactions cannot take place (32).

Butler et al, solve the fully time-dependent two dimensional flame equations implicitly allowing multicomponent reactions and non-laminar flows. The equations are fully coupled with the momentum equations in this procedure (33).

Other workers include Wilde (34) who uses Newton-Raphson-Kantorovich linearization and Bledjian (35) who uses the method of lines to produce time-dependent equations which are solved using a Runge-Kutta method.

The most recent work solves the equations implicitly, in contrast to earlier explicit solutions. Based on examination of the above past work an implicit approach is adopted in this work. The linearization procedure used is called Picard linearization and has been used successfully to solve similar equations (32).

3.3 Matrix Formulation

The discrete global equation which is given in Table 3.1 in tensor form may be transformed to equations for individual elements. These transformed equations are represented as 2×2 elemental matrices in Table 3.3 as they are derived in Appendix B. By piecing the elemental matrix equations together and invoking boundary conditions, the resulting matrix, a global equation, is constructed. When solved, this numerical matrix equation yields the solution profiles.

3.3.1 Boundary Conditions

The heat transfer at the hot (Cauchy) boundary of the energy profile is small. Therefore it is approximated as a natural (Neumann) boundary condition, where:

$$\frac{dT}{dx} = 0$$

This is the conventional assumption.

In the elemental matrices already discussed the boundary terms are not considered since only the interior elements are considered. Therefore, when the global equations are constructed it is necessary to impose them by special considerations.

$$\left[\begin{array}{c|c} \frac{1}{h}+\frac{GC_p}{k}\left[-\frac{1}{2}+\frac{f}{2}\right]+ & -\frac{1}{h}+\frac{GC_p}{k}\left[\frac{1}{2}+\frac{f}{2}\right]+ \\ \left[\frac{\sigma_r \epsilon_r A_r}{k} T_e^3+\frac{A_r H}{k}\right]\left(\frac{h}{3}-\frac{fh}{4}\right) & \left[\frac{\sigma_r \epsilon_r A_r}{k} T_e^3+\frac{A_r H}{k}\right]\left(\frac{h}{6}-\frac{fh}{4}\right) \\ \hline -\frac{1}{h}+\frac{GC_p}{k}\left[\frac{1}{2}-\frac{f}{2}\right]+ & \frac{1}{h}+\frac{GC_p}{k}\left[\frac{1}{2}+\frac{f}{2}\right]+ \\ \left[\frac{\sigma_r \epsilon_r A_r}{k} T_e^3+\frac{AH}{k}\right]\left(\frac{h}{6}+\frac{fh}{4}\right) & \left[\frac{\sigma_r \epsilon_r A_r}{k} T_e^3+\frac{A_r H}{k}\right]\left(\frac{h}{3}+\frac{fh}{4}\right) \end{array}\right] \left\{\begin{array}{c} T_1 \\ T_2 \end{array}\right\} = \left[\begin{array}{c} \left[\frac{\sigma_r A_r \epsilon_r}{k} T_\infty^4+\frac{A_r H}{k} T_\infty+\frac{H_c R_f}{k}\right]\left(\frac{h}{2}-\frac{fh}{2}\right) \\ \hline \left[\frac{\sigma_r A_r \epsilon_r}{k} T_\infty^4+\frac{A_r H}{k} T_\infty+\frac{H_c R_f}{k}\right]\left(\frac{h}{2}-\frac{fh}{2}\right) \end{array}\right]$$

Table 3.3a - Evaluated Energy Matrix (Elemental)

$$\begin{bmatrix} \frac{LY_0}{h} + \frac{GC_p}{k} Y_0\left[-\frac{1}{2}+\frac{f}{2}\right]+ & -\frac{LY_0}{h} + \frac{GC_p}{k} Y_0\left[\frac{1}{2}-\frac{f}{2}\right]+ \\ CONST\cdot\left(\frac{h}{3}+\frac{fh}{4}\right) & CONST\cdot\left(\frac{h}{6}-\frac{fh}{4}\right) \\ \hline -\frac{LY_0}{h} + \frac{GC_p}{k} Y_0\left[-\frac{1}{2}-\frac{f}{2}\right]+ & \frac{LY_0}{h} + \frac{GC_p}{k} Y_0\left[\frac{1}{2}+\frac{f}{2}\right]+ \\ CONST\cdot\left(\frac{h}{6}+\frac{fh}{4}\right) & CONST\cdot\left(\frac{h}{3}+\frac{fh}{4}\right) \end{bmatrix} \begin{Bmatrix} \alpha_1 \\ \alpha_2 \end{Bmatrix} = \begin{bmatrix} 0 \\ 0 \end{bmatrix}$$

Table 3.3b - Evaluated Species Matrix (Elemental)

It can be seen that the discrete global equations in Table 3.1 contain an explicit gradient term effective only at the boundaries. Then, for the natural condition, this boundary integral disappears. This applies at the hot boundary for the energy and the species matrices. For the cold boundary the situation is different.

The cold boundary is an essential (Dirichlet) boundary and is dealt with by forcing it on the global matrix using the Payne-Irons method (36). Details of the Payne-Irons method are discussed in the reference.

3.4 Flame Parameters

To solve the governing equations, estimates of the transport properties of the flame and the gas mixtures are necessary. The structure of the calculation procedure used here is adapted from modifications of the Chapman-Enskog kinetic theory of gases. These formulations are drawn from the literature. However, adaptations have been made to produce a computationally convenient procedure and modifications of the traditional formulations are made to improve correspondence with experimental results.

3.4.1 Specific Heats

Theoretical calculation of the heat capacities of

component species is possible (37). However such calculations are generally complex. Therefore curvefitted polynomials, which are accurate in the appropriate temperature ranges are chosen here to replace such calculations. The approximate formulas used in this work for methane and air are summarized in Table 3.4.

3.4.2 Thermal Conductivity

The Chapman-Enskog kinetic theory, modified to account for a particle velocity distribution of a Maxwellian nature is usual in combustion applications (31). The theory modified to include non-rigid molecules with energy interactions of a non-discrete nature and relaxation times for energy exchange between internal and translational storage modes yields a formula for thermal conductivity which is: (38)

$$k = \left[\frac{\rho D_s}{\mu} + \frac{3}{2}\frac{R}{C_v}\left(\frac{5}{2}-\frac{\rho D_s}{\mu}\right) - \frac{2}{3}\frac{R}{C_v}\left(\frac{5}{2}-\frac{\rho D_s}{\mu}\right)\left(1-\frac{3}{2}\frac{R}{C_v}\right)\right.$$

$$\left. x\left(1 - \exp\left(-\frac{2}{3}\frac{C_v}{RZ}\right)\right)\right]\mu C_v \qquad (3.7)$$

where D_s = self-diffusion coefficients

μ = viscosity

C_v = specific heat at const. volume

Viscosity is calculated here using the same theory by:

$$\mu = 2.6693E\text{-}5\ \frac{\sqrt{TM}}{\sigma^2 \Omega_\mu}\ \frac{gm}{cm\text{-}s} \qquad (3.8)$$

TABLE 3.4 SPECIFIC HEAT FORMULAS

TEMPERATURE RANGE	GAS	FORMULA	SOURCE	ERROR
260< T<610°K	AIR	C_p=.249679-7.55179E-5T +1.69194E-7T^2-6.46128E-11T^3	(41) TPRC DATA SERIES,	±2%
600< T<1500°K	AIR	C_p=.208831+7.71027E-5T -8.56726E-9T^2-4.75772E-12T^3	" (41)	"
1500<T<2300°K	AIR	C_p=.4278118-1.9218E-4T +6.92316E-8T^2	CURVEFITTED DATA: (42) U.S. NAT.B.S.	±2%
270<T<790°K	METHANE	C_p=.458066-2.61341E-4T +2.07904E-6T^2-1.25017E-9T^3	TPRC DATA SERIES (41)	±2%
790<T<1500°K	METHANE	C_p=.0258866+1.60802E-3T -6.67069E-7T^2+1.06432E-10T^3	" (43)	"
1400<T<2500°K	METHANE	C_p=.588868+6.44119E-4T -1.174567E-7T^2	CURVEFITTED DATA (44)	±2.5%

where;

Ω_μ = Lennard-Jones correction factor

σ = molecular collision diameter [angstroms]

M = molecular weight

and the specific heat at constant volume is calculated from thermodynamics as:

$$C_v = C_p - R$$

where C_p = specifc heat at constant pressure [cal/g-0_k]

Here the coefficient $\frac{\rho D_s}{\mu}$ is calculated using the formula developed in appendix D.

$$\frac{\rho D_s}{\mu} = 1.20085 \frac{\Omega_\mu}{\Omega_D} \qquad (3.9)$$

where Ω_D = Lennard-Jones Correction Factor.

The Lennard-Jones correction factors are widely available in tabular form (39). They are found to be dependent on temperature and the molecular energy parameter "ε/k" (39). Here, for computation convenience, this dependence is functionalized using curvefitting techniques. The functions are displayed in Table 3.5.

3.4.3 Gas Mixtures

The flame of interest occurs in a gas mixture, and in general the mixture properties are different from the properties of the individual components. The mixture properties must be

TABLE 3.5: LENNARD-JONES POTENTIAL CORRECTION FACTORS

RANGE	FORMULA	ERROR
$.85 \leq \frac{kT}{\epsilon} \leq 5.2$ $.75 \leq \frac{kT}{\epsilon} \leq 5.45$	$\Omega_\mu = .8567 + .08654\frac{kT}{\epsilon} - .014957\left(\frac{kT}{\epsilon}\right)^2 + \frac{2.1916}{e^{1.2\left(\frac{kT}{\epsilon}\right)}}$	$\pm 1.2\%$ $\pm 2.0\%$
$3.8 \leq \frac{kT}{\epsilon} \leq 33.2$ $3.4 \leq \frac{kT}{\epsilon} \leq 38$	$\Omega_\mu = .813 - .004\frac{kT}{\epsilon} + 1.325e^{-\sqrt{\frac{kT}{\epsilon}}}$	$\pm 1\%$ $\pm 2\%$
$2.1 \leq \frac{kT}{\epsilon} \leq 5.4$ $.8 \leq \frac{kT}{\epsilon} \leq 6.1$	$\Omega_D = .92553 - .025427\frac{kT}{\epsilon} + .0014162\left(\frac{kT}{\epsilon}\right)^2 + \frac{1.3875}{e^{.95(kT/\epsilon)}}$	$\pm 1\%$ $\pm 2.2\%$
$5.4 \leq \frac{kT}{\epsilon} \leq 36$ $2.4 \leq \frac{kT}{\epsilon} \leq 42$	$\Omega_D = .7184 - .00338\frac{kT}{\epsilon} + 1.3296e^{-\sqrt{\frac{kT}{\epsilon}}}$	$\pm 1\%$ $\pm 2\%$

evaluated. For determination of the thermal conductivity of the gas mixture using the individual species values, the approximation of C.R. Wilke is used (40).

$$k_{mix} = \sum_{i=1}^{n} \left[\frac{x_i k_i}{\sum_{j=1}^{n} x_j \Phi_{ij}} \right] \tag{3.10}$$

where

$$\Phi_{ij} = \frac{\left(1+\left[\frac{u_i}{u_j}\right]^{1/2}\left[\frac{M_j}{M_i}\right]^{1/4}\right)^2}{\sqrt{8}\left(1+\frac{M_i}{M_j}\right)^{1/2}} \tag{3.11}$$

The specific heat of the mixture is found from thermodynamics to be:

$$C_p(mix) = \sum_{i=1}^{n} C_{pi} X_i \tag{3.12}$$

Next, the binary diffusion coefficient is calculated using the Chapman-Enskog theory

$$D = 1.85834E\text{-}3 \frac{\sqrt{T^3 \left(\frac{1}{M_A}+\frac{1}{M_B}\right)}}{P\sigma^2_{AB}\Omega_D} \tag{3.13}$$

where P = pressure in atmospheres

$$\sigma_{AB} = (\sigma_A + \sigma_B)/2 \tag{3.14}$$

To find Ω_D the value of the molecular energy parameter is found by

$$\left(\frac{\varepsilon}{k}\right)_{AB} = \sqrt{\left(\frac{\varepsilon}{k}\right)_A \left(\frac{\varepsilon}{k}\right)_B} \tag{3.15}$$

The multicomponent diffusion coefficient is approximated by the formula

$$D_{A-M} = \frac{1-x_a}{\sum_{j \neq A} \left(\frac{x_j}{D_{Aj}}\right)} \tag{3.16}$$

where D_{A-M} = diffusion coefficient between component "A" and the mixture.

3.4.4 Convection Rate

The following numerical calculation is used to approximate the convection rate formula given in Chapter 2.

$$G = \sum_{i=1}^{N} \frac{(R_{F_i} h_i)}{Y_0 (\alpha_{N+1} - \alpha_1)} \tag{3.17}$$

3.5 Solution Algorithm

The calculation procedure already outlined is used in this work to develop a computer code, which is detailed in Appendix F. The schematic of the procedure is shown in Fig. 3.2. This code uses the implicit matrices, the temperature matrix and the species matrix in turn, and solves them iteratively, while adjusting the convection rate and the reaction rate

profiles between each step of the iteration. However, this iteration is preceded by a procedure to initialize the profiles and furthermore this is preceded by a procedure to calculate (or input) the needed flame constants.

The input constants are:

1. E = activiation energy (cal/mode)
2. H_C = heat of combustion $(\frac{cal}{g\text{-}s\text{-}m^3})$
3. TIGN = cutoff temperature (°K)
4. Y_o = initial mass fuel fraction
5. F1; F2 = fraction of 1st and 2nd order reactions present respectively
6. ck_1;ck_2 = reaction rate constants
7. TROOM = Room Temperature (initial mixture temperature) (°K)
8. N_1;N_2;N_3;N_4;N_5;N_6 = No. of elements in each solution zone.
9. ALPHA (1) = initial species vector
10. XLE (1)... XLE (NELEM) = element sizes (cm)
11. F(1) ... F(NELEM) = Element weighting values.

The constants calculated are:

1. XLAMBDA = thermal conductivity
2. CP = specific heat at constant pressure
3. RHOO = initial mixture density
4. XLEWIS = Lewis no.

FIG. 3.2: SCHEMATIC OF COMPUTER PROGRAM

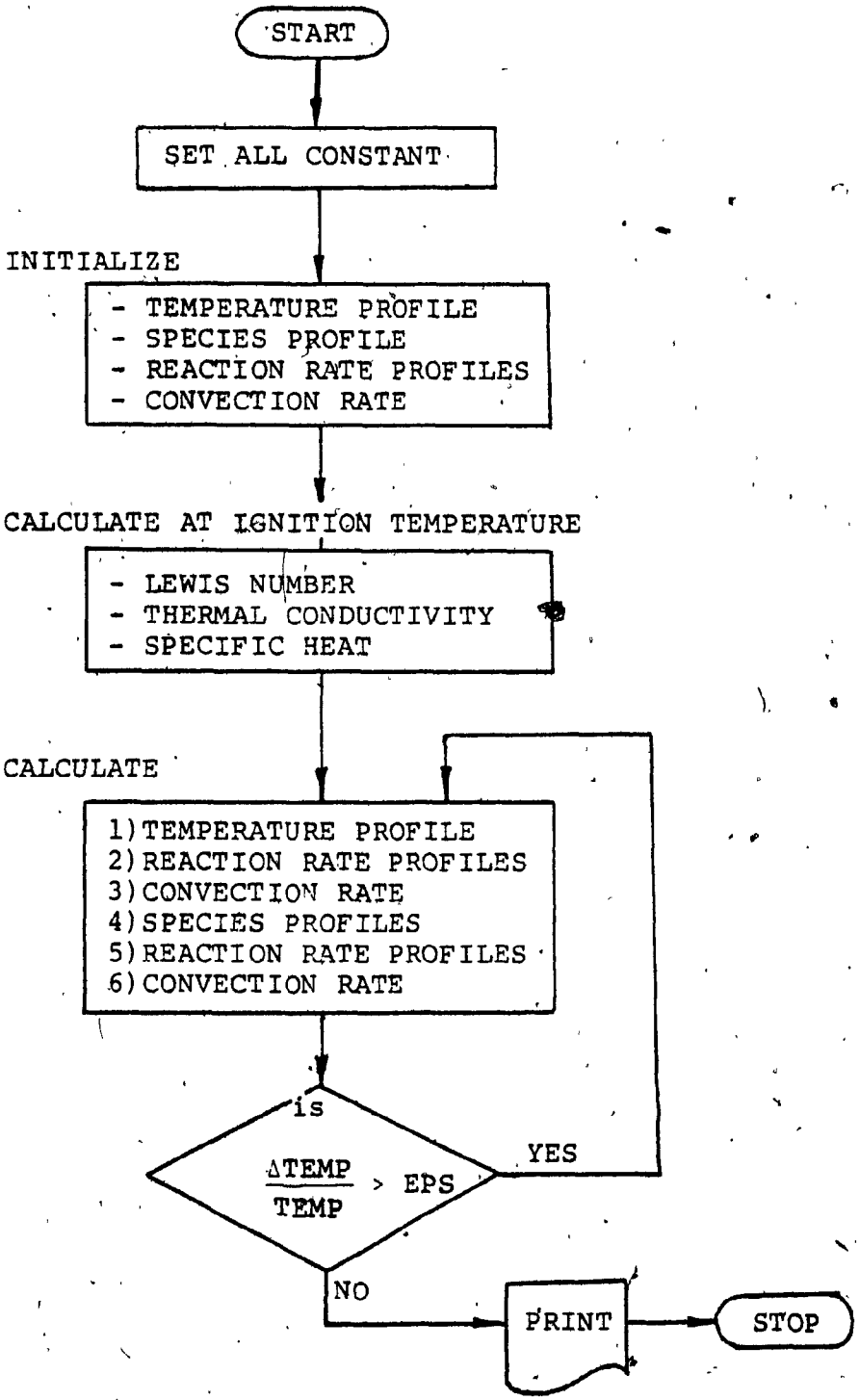

Using the above input, the calculations of the initial fuel vector profile and the reaction rate profile are provided by the code. The initial fuel vector is calculated from the formula derived in Appendix E.

$$\alpha_1 = \left[\frac{(G/h)}{\frac{G}{h} + \frac{k_1 \rho_0 T_0}{T_i \exp\ (E/RT_1)}} \right] \alpha_{i-1} \qquad (3.18)$$

The reaction rate is calculated using the formulas already derived.

CHAPTER 4

RESULTS

In Chapter two of this work the governing equations for a theory for a reacting flow system are presented. In chapter three, a general numerical procedure for solving these equations, in the form of a general computer code is developed. So that the code can subsequently confidently be applied to general engineering and scientific problems, tests are conducted in this chapter which activate different modules of the code independently.

The first section of this chapter is devoted to describing these tests and displaying the results together with data gathered from independent sources.

In the second section, the details of more general combustion problems are described and results are obtained from the code and displayed. The combustion problems discussed here involve gas flow systems consisting of fuel and air undergoing combustion to form products.

4.1 Characteristics of the Code

Testing the code consists of comparing the numerical solutions derived from it with exact solutions when they exist, and for non-analytical problems, with reliable, experimental data.

Using computer solutions which compare well with recommended data, and others which do not, many useful conclusions regarding the code can be drawn. This testing procedure demonstrates the power and versatility of this computing package, in application to transport and reacting flow problems in addition to combustion problems. The specific cases are detailed below.

4.1.1 Test #1: Heat and Mass Transfer Between Fixed Boundaries (convection-diffusion)

Consider two large tanks filled with different fluids at different temperatures and pressures (Fig. 4.1). Each fluid occupies a large well-stirred reservoir. Because these reservoirs are large, bulk changes in the occupying fluids will not take place, and because they are well-stirred, local changes in properties within the reservoirs are precluded.

Joining these reservoirs is a narrow pipe through which fluid is allowed to flow freely. Because the pressures in the reservoirs are different, constant convective flow between the reservoirs occurs, and because the fluids in the reservoirs are different, constant diffusion between the reservoirs results. Further, because the temperatures of the reservoirs differ, heat conduction will take place along the pipe from the high temperature reservoir to the low temperature reservoir.

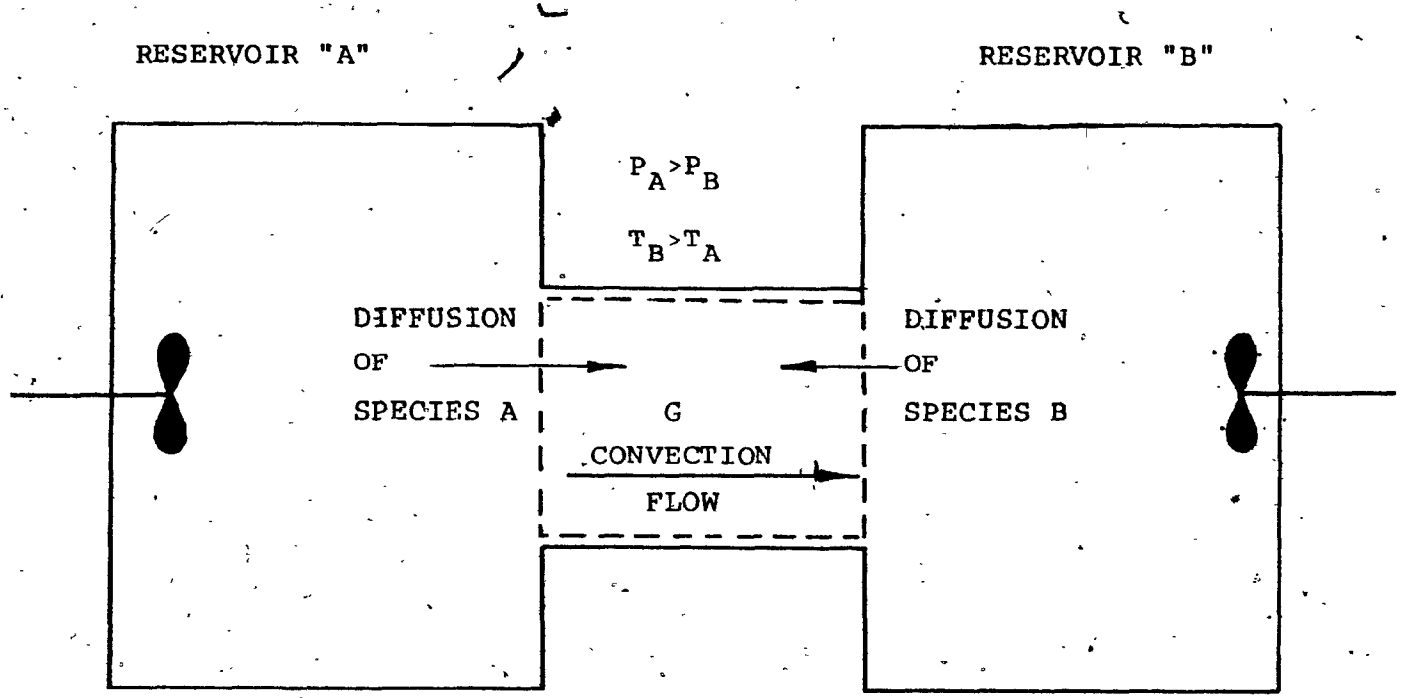

Fig. 4.1: Test #1 - Heat and Mass Transer Between Reservoirs

The governing equations for fluid movement, drawn from Appendix A without the reaction and heat loss terms are:

$$\frac{d^2T}{dx^2} - \frac{Gc_p}{k}\frac{dT}{dx} = 0 \qquad (4.1)$$

$$\frac{d^2\alpha}{dx^2} - \frac{Gc_p}{k}(L)\frac{d\alpha}{dx} = 0 \qquad (4.2)$$

For the case in which L =1, the two equations are identical and an exact solution for the entire system can be obtained. This exact solution is:

$$\alpha = \frac{(\exp(P\cdot x)-1)}{(\exp(P)-1)} \qquad (4.3)$$

(chung(1))

$$T = \frac{T_f(\exp(Px))-1}{(\exp(P)-1} \qquad (4.4)$$

where P = peclet no. $= \frac{cG}{k}$

T_f = temperature in hot reservoir (°K)

α = mass fraction of fluid in tank B.

4.1.1.1 Special Case

Here the following values are used in the governing equations

$P = 50$

$c_p = .32$ cal/g-°K

$k = 1.6E-4$ cal/cm-°K

$G = 2.5E-2$

The exact and the approximate solution to this case are

both illustrated in Fig. 4.2, so they can be compared. In this figure, the vertical axis represents the concentration of component B and the temperature at each point in the pipe joining the reservoirs and the horizontal axis represents the distance along the pipe from an origin located at the junction of the pipe with reservoir A.

4.1.1.2 Discussion

When 50 elements are used to represent the complete solution regime, the maximum error is about 7% and when 100 elements are used the maximum error is about 3%. Therefore the approximate numerical solution approaches the exact solution.

This problem is adapted from Chung (1). His observations concerning the finite element solution are not repeated here.

4.1.2 Test #2: Laminar Tube Flow with Convective Heat Loss

Consider the tube-flow situation portrayed in Fig. 4.3. An exact temperature profile along the length of the tube is desired under fully developed laminar flow conditions. The wall temperature of the tube is assumed to be constant and different from the bulk temperature of the flow and the pressure is assumed constant across any cross section. Furthermore, neglecting viscous loses and assuming a small flow

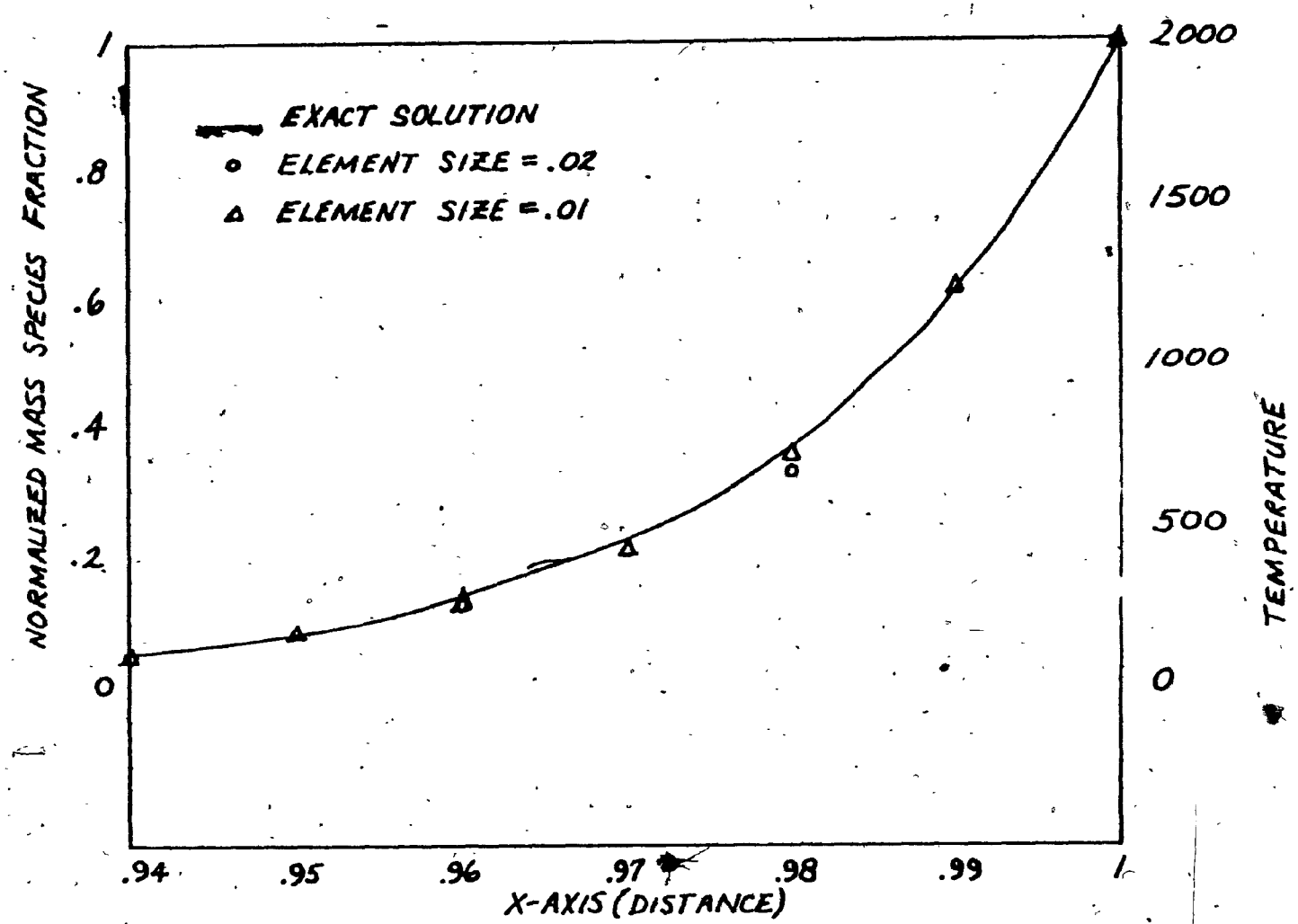

Fig. 4.2 - Test #1: Results - Heat Transfer and Diffusion with Convection

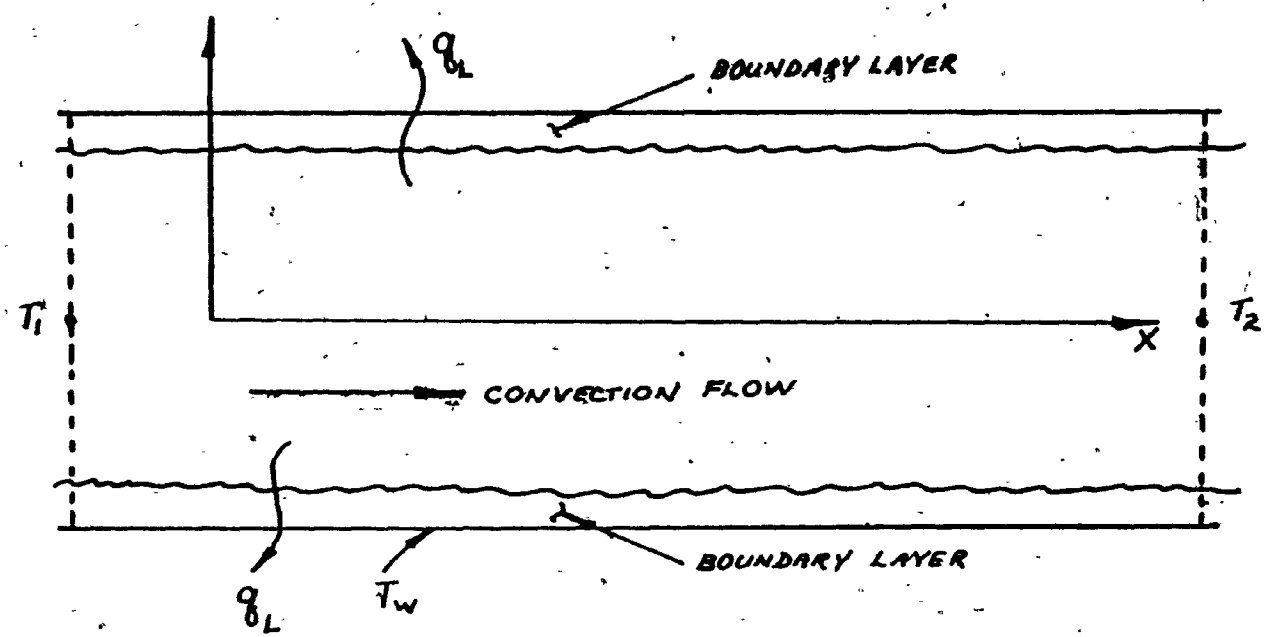

Fig. 4.3 - Test #2: Model - Laminar Tube Flow with Convecture Heat Loss

velocity makes the longitudinal pressure constant.

The governing equation for this situation is:

$$\frac{d^2T}{dx^2} - \frac{C_p G}{k}\frac{dT}{dx} - \frac{H}{k}T = -\frac{H}{k}T_w \qquad (4.5)$$

where T_w = wall temperature [°K]

H = convective heat transfer coefficient $\left[\frac{cal}{cm^2\text{-}s\text{-}°K}\right]$

An exact solution for this equation can be derived.

4.1.2.1 Special Case

The following information is given:

$T_w = 250°K$

$C_p = .3$ cal/g-°K

$k = 1.5(10^{-4})$ cal/g-°K-S

$H = \frac{48}{11}\frac{k}{d} = 6.2(10^{-4})$ cal/cm^2-s-°K*

hence P = Peclet no. $= \frac{Gc}{k} = 5$

The characteristic equation is:

$$(D^2\text{-}5D\text{-}13.737)T = 3434.25 \qquad (4.5.1)$$

To find the homogeneous solution:

---

* This value is arrived at by assuming a parabolic velocity profile and a constant heat flux at the wall along the full length. The exact value of Nusselt No. is found to be 4.364(2,3). This procedure gives a value of H correct in order of magnitude

$$D_{1,2} = \frac{5}{2} \pm \sqrt{\left(\frac{5}{2}\right)^2 + 13.737}$$

$$D_1 = 6.971; \; D_2 = -1.971 \qquad (4.5.2)$$

Thus, $$T_h = C_1 e^{6.971x} + C_2 e^{-1.971x} \qquad (4.5.3)$$

where C_1 and C_2 are determined from the boundary conditions.

From the specified wall temperature the particular solution is:

$$T_p = 250 \qquad (4.5.4)$$

To arrive at the complete solution, the particular and the homogeneous solutions are added:

$$T = T_h + T_p = C_1 e^{6.971x} + C_2 e^{-1.971x} + 250 \qquad (4.5.5)$$

When $x = 0$; $T = 300$

thus $$C_1 + C_2 = 50 \qquad (4.5.6)$$

and when $x = 1$; $T = 260$, so that,

$$1065.288C_1 + .1393C_2 = 10 \qquad (4.5.7)$$

Solving 4.5.6 and 4.5.7 simultaneously

$$C_1 = .002849$$

$$C_2 = 49.9972$$

and finally,

$$T = .002849e^{6.971x} + 49.9972e^{-1.971x} + 250 \qquad (4.6)$$

Figure 4.4 gives the exact temperature profile, plotted from equation 4.6, for this two point boundary value

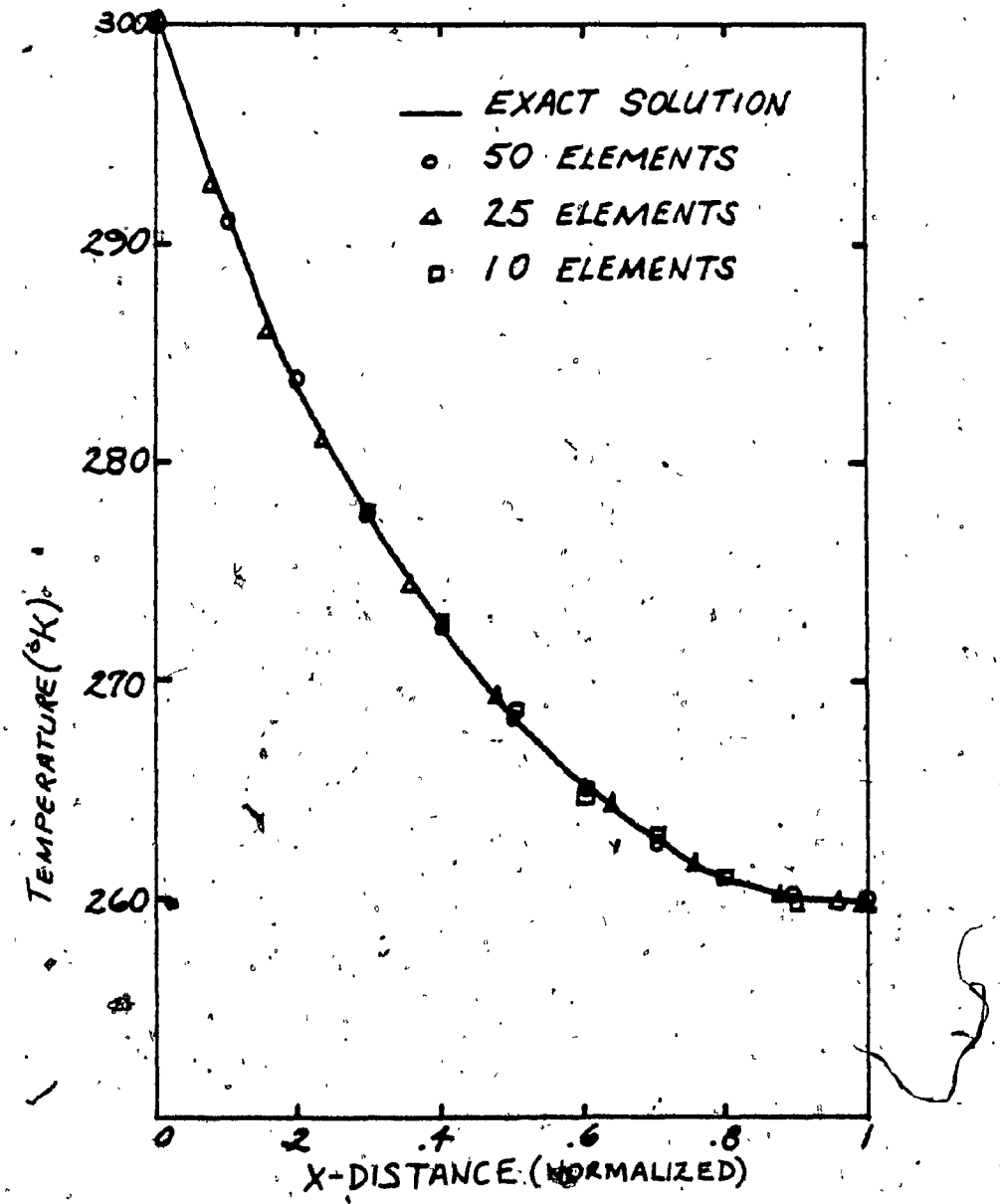

Fig. 4.4 - Test #2: Results - Laminar Tube Flow with Convecture Heat Loss.

problem and the solution of the same problem from the code. The vertical axis is the temperature in the fluid and the horizontal axis is the distance measured from the boundary where the temperature is at 300°K.

4.1.2.2 Discussion

In this case the convective heat loss term in the general energy equation is activated. With a grid containing ten elements, the maximum error is 2%. The maximum error for finer grids is less. Some oscillation of the nodal temperatures about the exact solution is observed.

4.1.3 Test #3: Tubular Reactive Flow

Consider another tubular flow problem; however, in addition to diffusion and convection, chemical reaction is involved. The chemical reaction is modelled as a simplex global reaction of the form

$$A \xrightarrow{k} B \tag{4.7}$$

By supposing that the temperature of the surroundings is the same as the initial temperature of the reacting fluid and that the chemical process does not involve any heat release, the energy equation is:

$$T = T_0 = \text{constant} \tag{4.8}$$

Further, the species equation is decoupled from the energy equation and becomes

$$LY_o \frac{d^2\alpha}{dx^2} - \frac{GY_o}{k} cp \frac{d\alpha}{dx} + C_1\alpha = 0 \qquad (4.9)$$

Because the equations are decoupled, the species equation can be solved independently from the energy equation when the reaction rate constant C_1 is established.

To solve the species equation exactly, the solution regime is divided into two regions as illustrated in Fig.4.5.

In the induction region, no chemical reaction occurs and the species profile is controlled by transport from the second region as a result of diffusion and convection. In the reaction region the transport and the reaction properties of the mixture together control the species profile. The origin of the coordinate frame is the boundary between these regions. The species equations in the two regions can now be solved exactly in compliance with the following boundary conditions.

$$x = -\infty \; ; \; \alpha^I = 1 \qquad (4.10.1)$$

$$x = 0 \; ; \; \frac{d\alpha^I}{dx} = \frac{d\alpha^{II}}{dx} \qquad (4.10.2)$$

$$\alpha^I = \alpha^{II} \qquad (4.10.3)$$

$$x = \infty \; ; \; \frac{d\alpha^{II}}{dx} = 0 \qquad (4.10.4)$$

4.1.3.1 Special Case

P = Peclet number = 10

L = Lewis number = 1

Y_o = 1

C_1 = 11 (REGION II)

C_1 = 0 (REGION I)

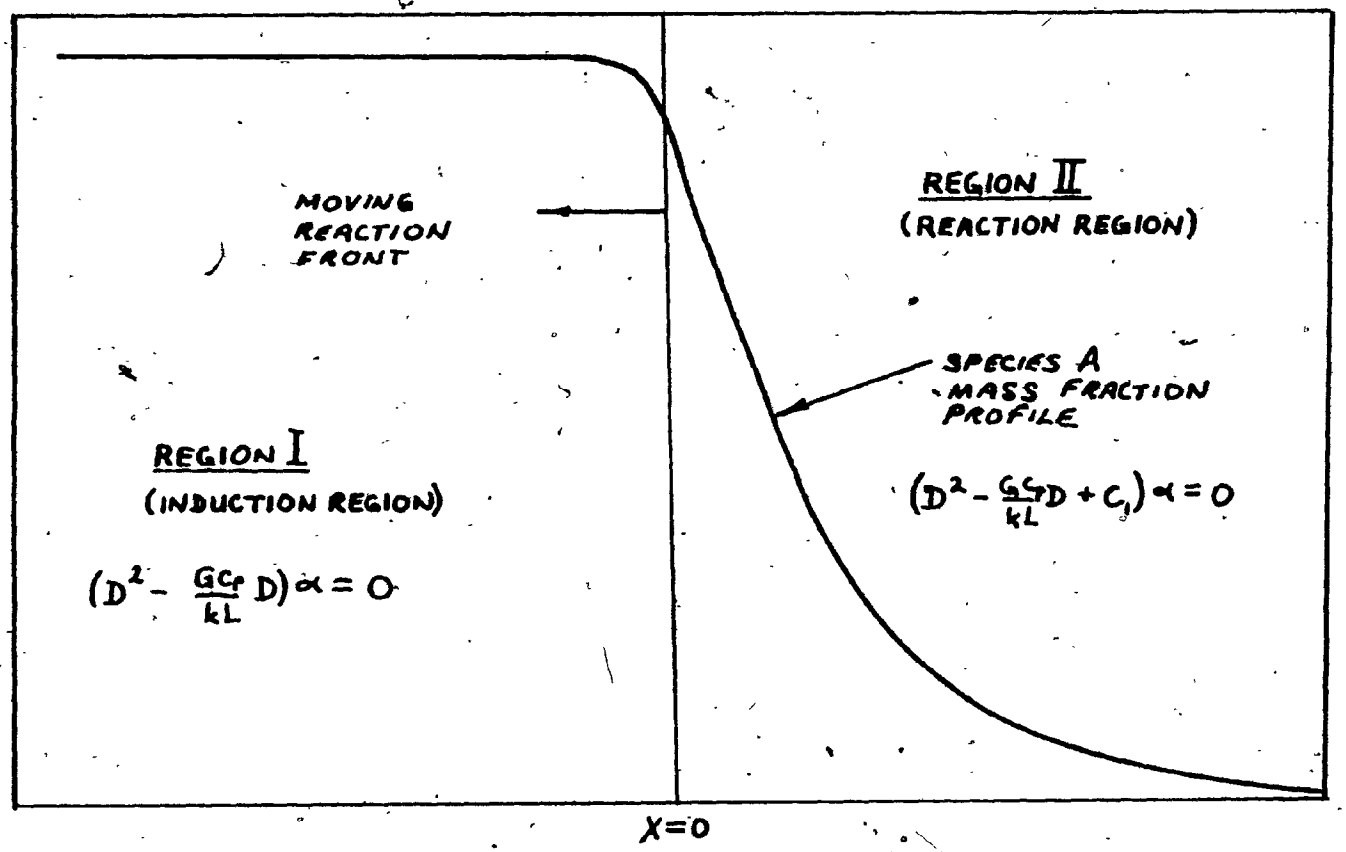

Fig. 4.5 - Test #3: Model - Tubular Reactive Flow

The characteristic equation is

$$(D^2-\frac{Gc}{kL}D + C_1)\alpha = 0 \qquad (4.11)$$

In region I

$$(D^2-10D)\alpha = 0 \qquad (4.11.1)$$

therefore

$$\alpha^I = A+B\exp(10x) \qquad (4.11.2)$$

In region II

$$(D^2-10D-11)\alpha = 0 \qquad (4.11.3)$$

$$\alpha^{II} = C\exp(11x) + E\exp(-x) \qquad (4.11.4)$$

where A, B, C and E are arbitrary constants which are found from the boundary conditions.

From equation 4.11.2, at $x = -\infty$

$$\alpha = 1 \text{ and } A = 1 \qquad (4.11.5)$$

From equation 4.11.2 and 4.11.3, at $x = 0$

$$\alpha^{II} = \alpha^I = 1+B = C+E \qquad (4.11.6)$$

From equation 4.11.3 at $x = L$;

$$\alpha_L^{II} = C\exp(11L) + E\exp(-L) \qquad (4.11.7)$$

$$\frac{\partial \alpha^{II}}{\partial x}\Big|_{x=L} = 11C\exp(11L)-E\exp(-L) \qquad (4.11.8)$$

From eqns. 4.11.8 and 4.10.4.

$$\lim_{L\to\infty}(11C\exp(11L)-E\exp(-L)) = \frac{d\alpha}{dx}\Big|^{II}_{L\to\infty} = 0$$

Therefore: $C = \frac{E}{11(\lim_{L\to\infty}(\exp(12L)))} = 0$

$$C = 0 \qquad (4.12)$$

Therefore at x = 0

$$\frac{d\alpha^I}{dx} = \frac{d\alpha^{II}}{dx} = 10B = -E \qquad (4.13.1)$$

and $$1+B = -10B \qquad (4.13.2)$$

This gives $$B = -1/11 \qquad (4.14)$$

and $$E = 10/11 \qquad (4.15)$$

Finally we get

$$\alpha^I = 1 - \frac{\exp(10x)}{11} \qquad (4.16)$$

$$\alpha^{II} = \frac{10}{11}\exp(-x) \qquad (4.17)$$

Equations 4.16 and 4.17 are the exact solutions to the governing equations in region I and region II respectively. The resulting solution curve is displayed graphically in figs. 4.6, 4.7 and 4.8. In these graphs the vertical axis represents the mass fraction of species A and the horizontal axis represents the distance measured from the previously selected origin.

The species equation solved here is similar in form to the species equation derived in Chapter 2 to describe flow combustion problems. Because of this similarity, this case is solved several times using the code with different element sizes: with upwinding and without upwinding. Hence, some

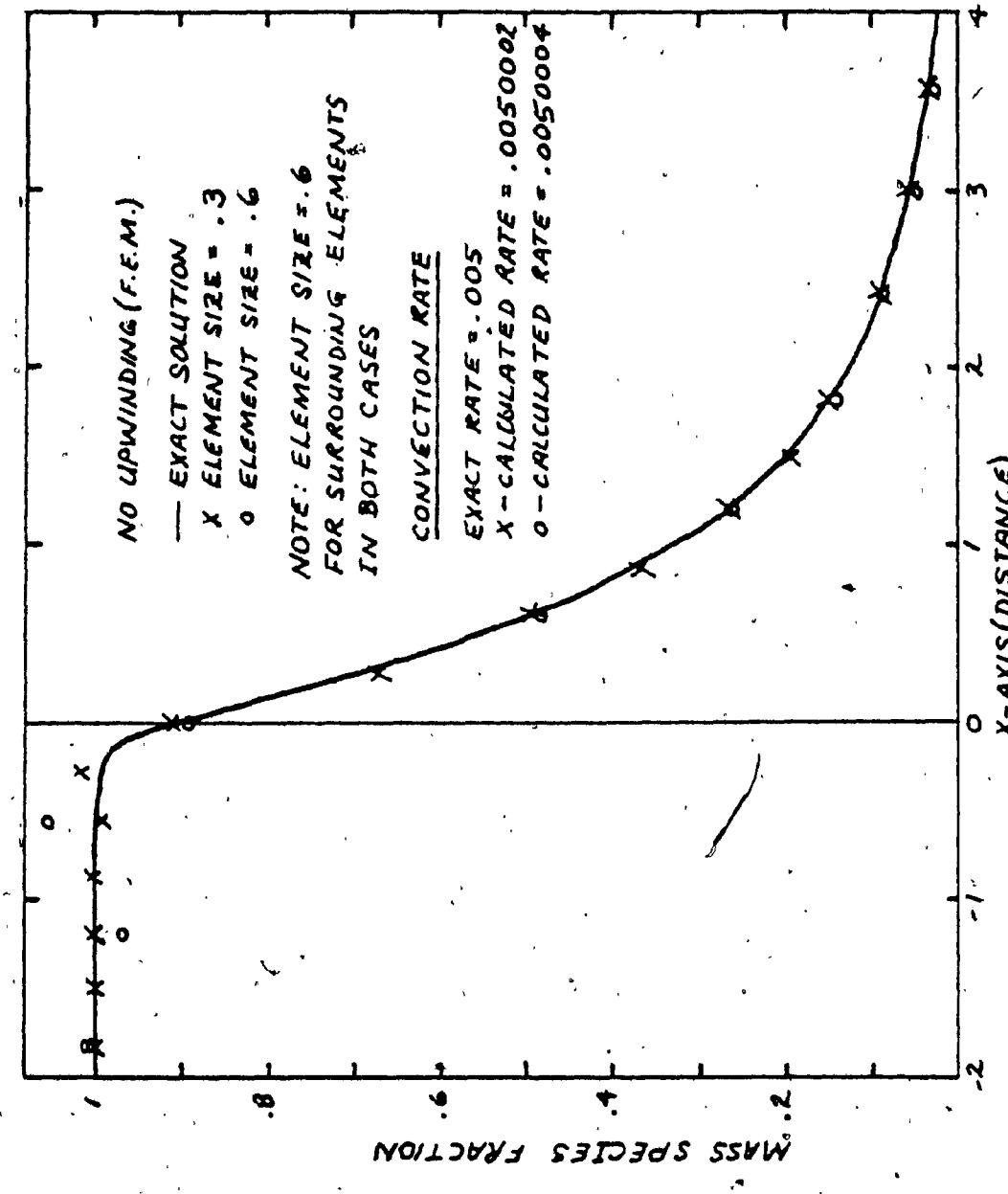

Fig. 4.6 - Test #3: Results - Tubular Reactive Flow
- Variable Element Size

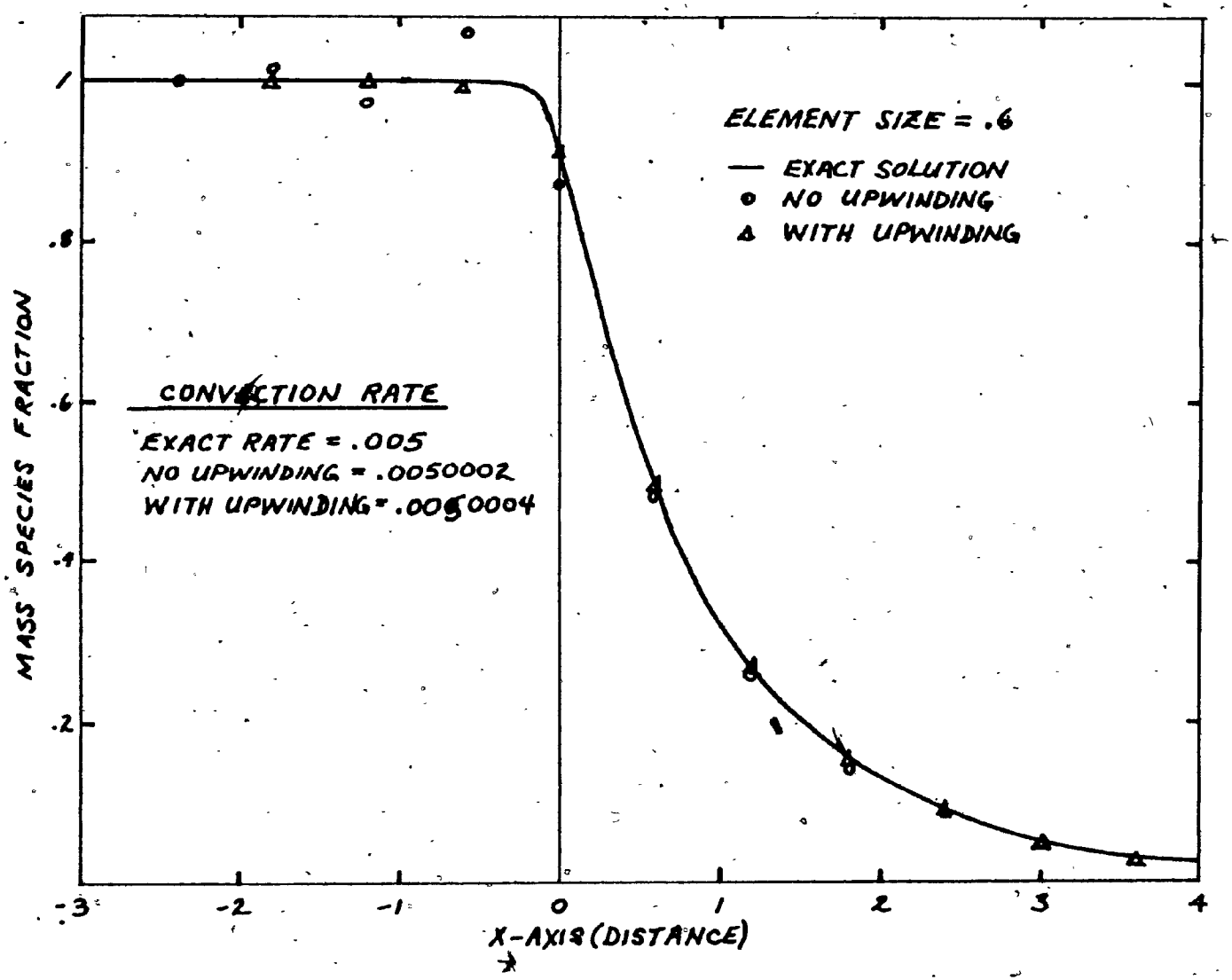

Fig. 4.7 - Test #3: Results - Tubular Reactive Flow
- Variable Element Weighting

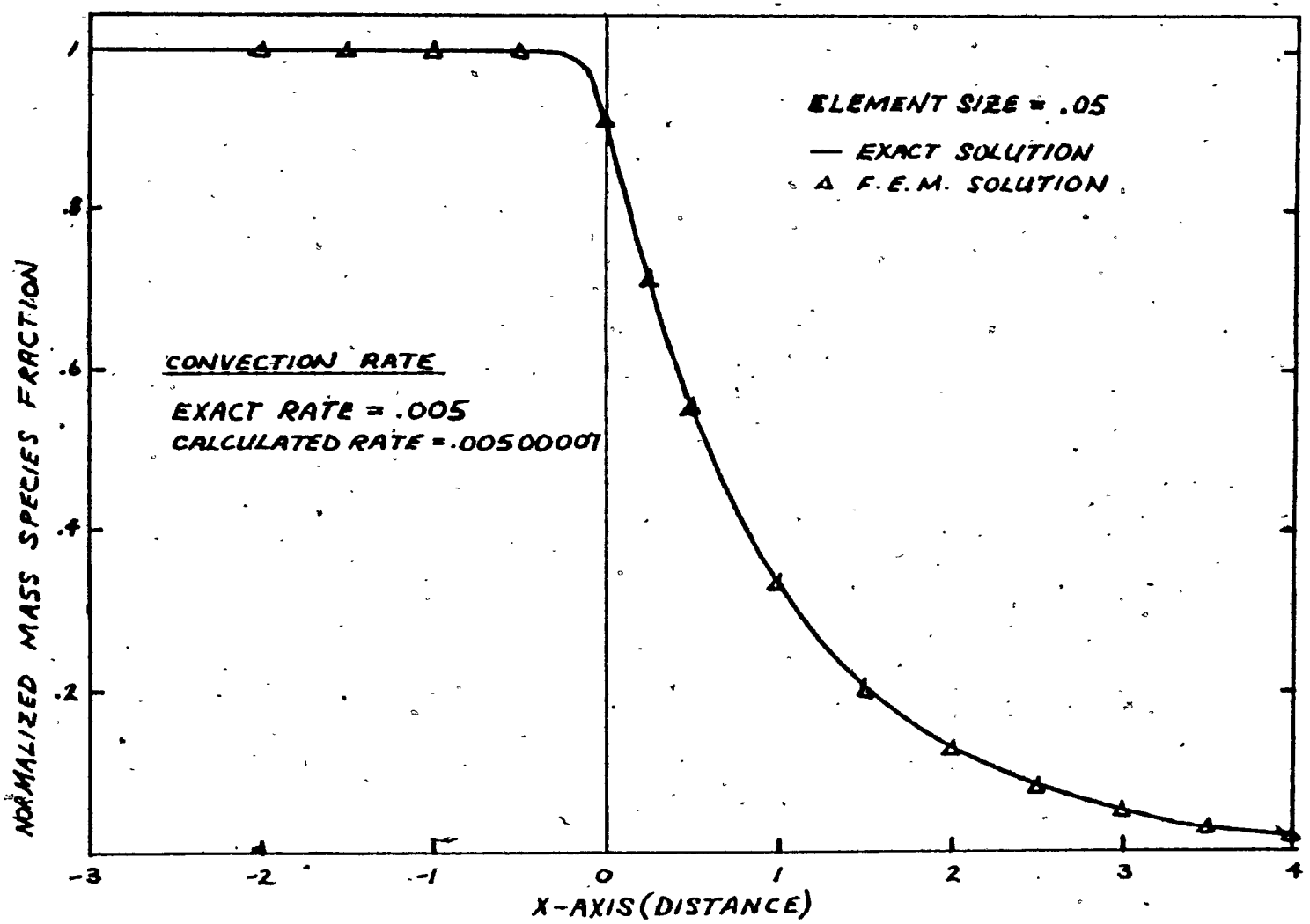

Fig. 4.8 -- Test #3: Results - Tubular Reactive Flow
- Accurate Solution

aspects of the problems related to the numerics can be studied.

As such, Fig. 4.6 displays the exact solution in conjunction with approximate solutions where the element size is 0.6 and 0.3 and no upwinding is used. Fig. 4.7 displays the exact solution in conjunction with approximate solutions where the element size is 0.6 with and without upwinding. Fig. 4.8 displays the exact solution in conjunction with the approximate solution where the element size is .05.

In all cases the computer code calculates the convection rate from the species profiles. These results are listed in the figures.

4.1.3.2 Discussion

Fig. 4.6 shows that the approximate solution oscillates about the exact solution with both coarse and fine grids. This oscillation produces a large maximum error in the profile shapes. In the former case a maximum error of 6% is observed and in the latter case a maximum error of 2% is observed, compared to the exact solution.

Using a constant upwinding factor of one throughout the solution regime, and the same coarse grid used formerly, the error of 6% is reduced to 1%. This can be seen in Fig. 4.7.

Because the convection rate is specified by the formulation of the problem, it is possible to compare the calculated convection rate with the exact convection rate. In every case, the comparison is good. In fact with a coarse

grid, where large oscillations are observed, the error is 0.005%. For the case in which oscillations are eliminated using an upwinding factor, the error is 0.01%. In both these cases, the error is negligible. With a fine grid the error is smaller (0.001%) with upwinding. This can be seen in Fig. 4.8.

The integration of the reaction rate over the solution regime, done to calculate the convection rate, involves choosing representative values for reaction rate within the individual elements. It is believed that this is the source of the small error that is found in the convection rate calculation.

4.1.4 Test#4: Heat Capacity and Transport Properties

To test the code for reliability, heat capacity and transport calculations must be considered. Here consideration is given to results yielded by the code over a range of temperatures, by comparing them with independently determined approximations or experimental values found in the literature. As such errors exist in the independent values as well as those calculated here. Wherever possible, both error values are quoted.

To study data which cannot be compared with exact information, the percent departure of the calculated values from the independent (recommended) values are plotted on departure plots. Such a departure plot consists of the independent variable scaled on the horizontal axis and the percent

departure scaled on the vertical axis. When the error bounds of the recommended data are known, they are plotted on the same display. This same type of display is useful in less restrictive applications and is made use of here whenever comparisons are made.

The departure plots presented below are discussed together at the end of the section.

4.1.4.1 Heat Capacity of Individual Gases

Some of the formulae used in this work to calculate heat capacity are drawn directly from other sources and their performance in the appropriate temperature range is well documented. In this work, however, some polynomial fitting of data for heat capacities is done and the polynomials are displayed below.

Figs. 4.9 and 4.10 show departure plots for heat capacity calculations. The temperature of the gas is the independent variable and is scaled on the horizontal axis.

4.1.4.2 Lennard-Jones Correction Factors

Figs. 4.11, 4.12, 4.13 and 4.14 display departure plots to the "fitted" Lennard-Jones correction factors derived from Hirschfelder's tables (6) and presented in Chapter 3. The non-dimensional parameter formed from temperature and the molecular energy parameter is the independent variable scaled on the abscissa. Figs. 4.11 and 4.12 are departure plots of the conductivity correction factor and Figs.4.13 and 4.14 are

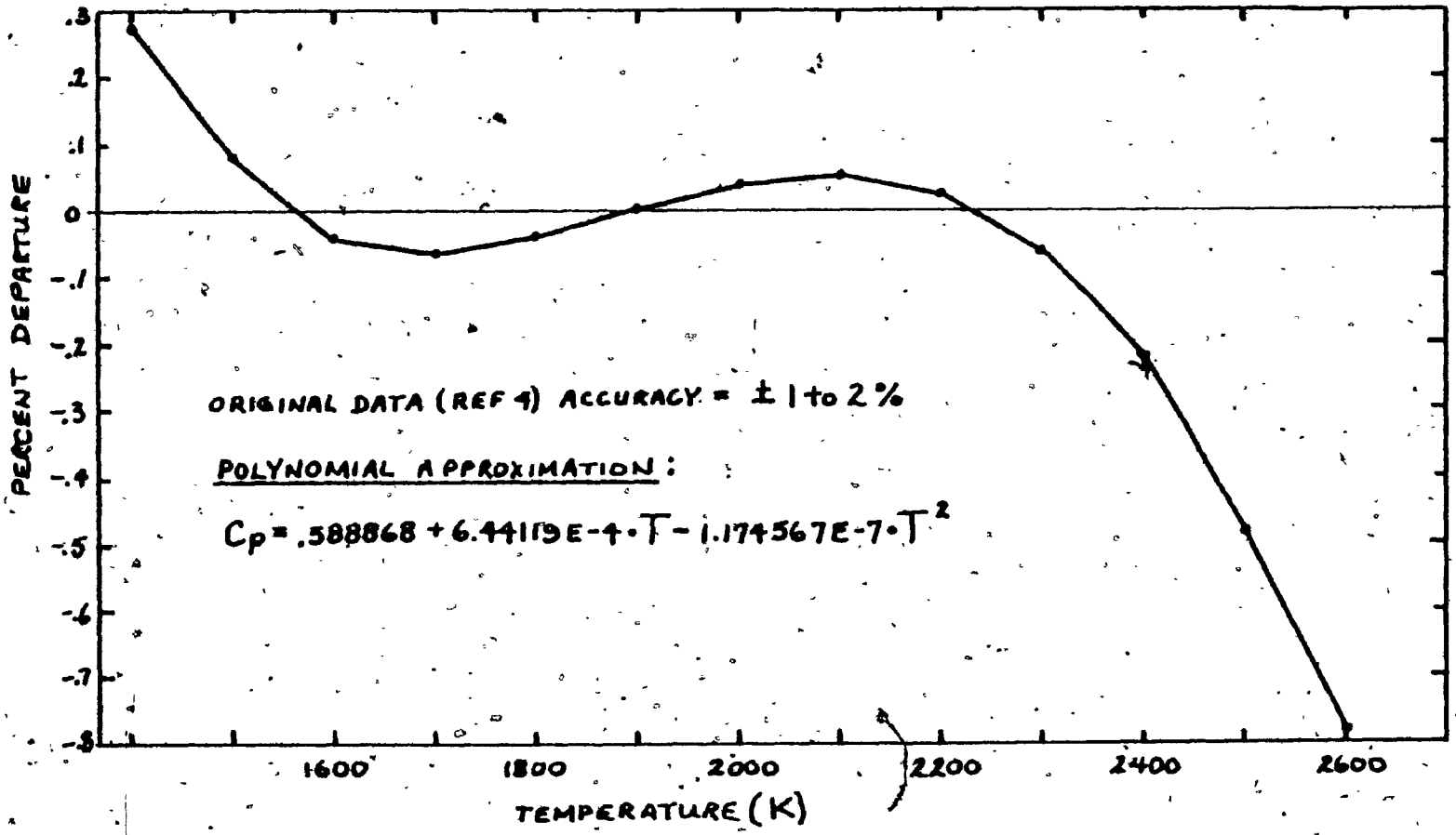

Fig. 4.9 - Departure Plot - Specific Heat of Methane vs Temperature

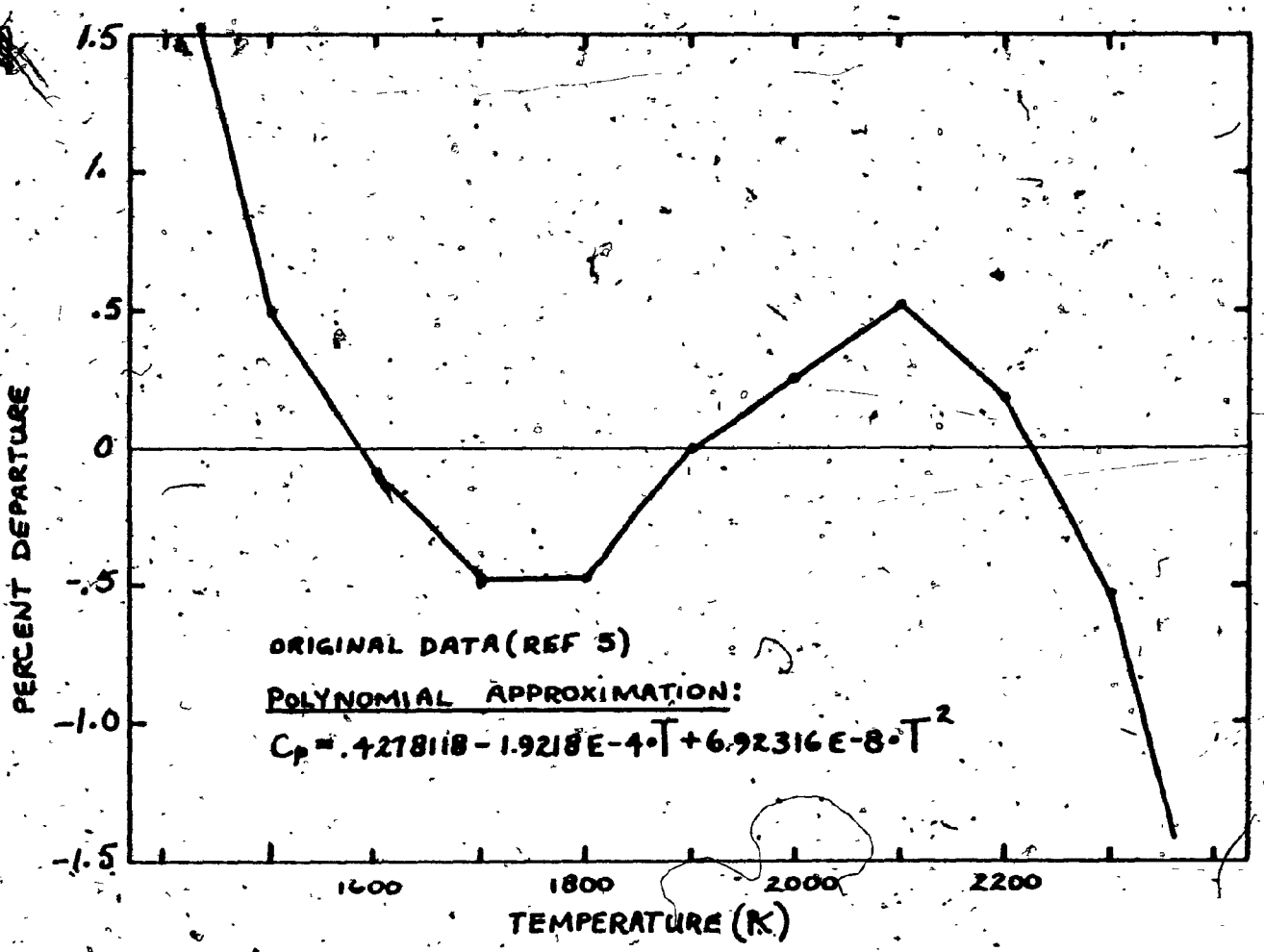

Fig. 4.10 - Departure Plot - Specific Heat of Air vs Temperature

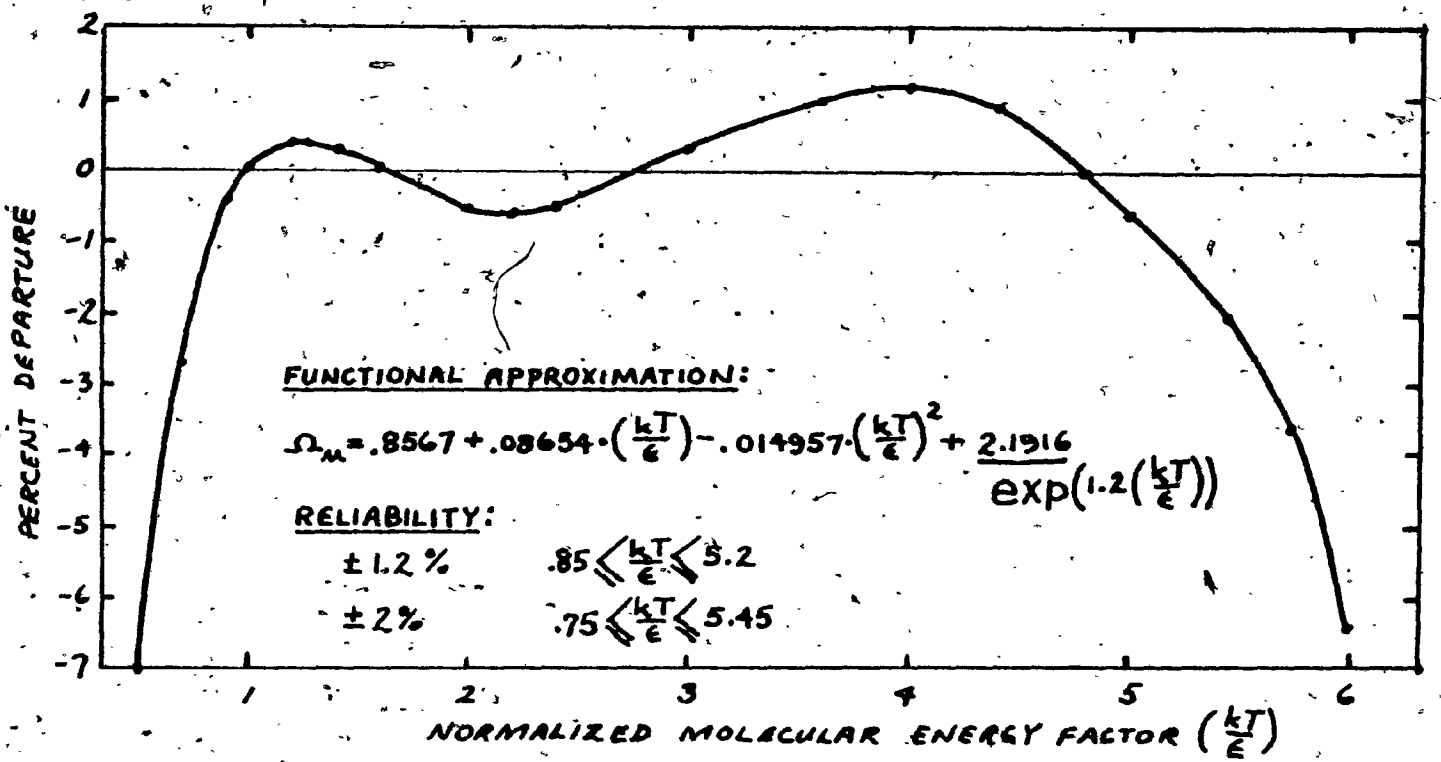

Fig. 4.11 - Departure Plot - Lennard-Jones Viscosity Factor vs Molecular Energy Parameter
$(.85 \leq \frac{kT}{\epsilon} \leq 5.2)$

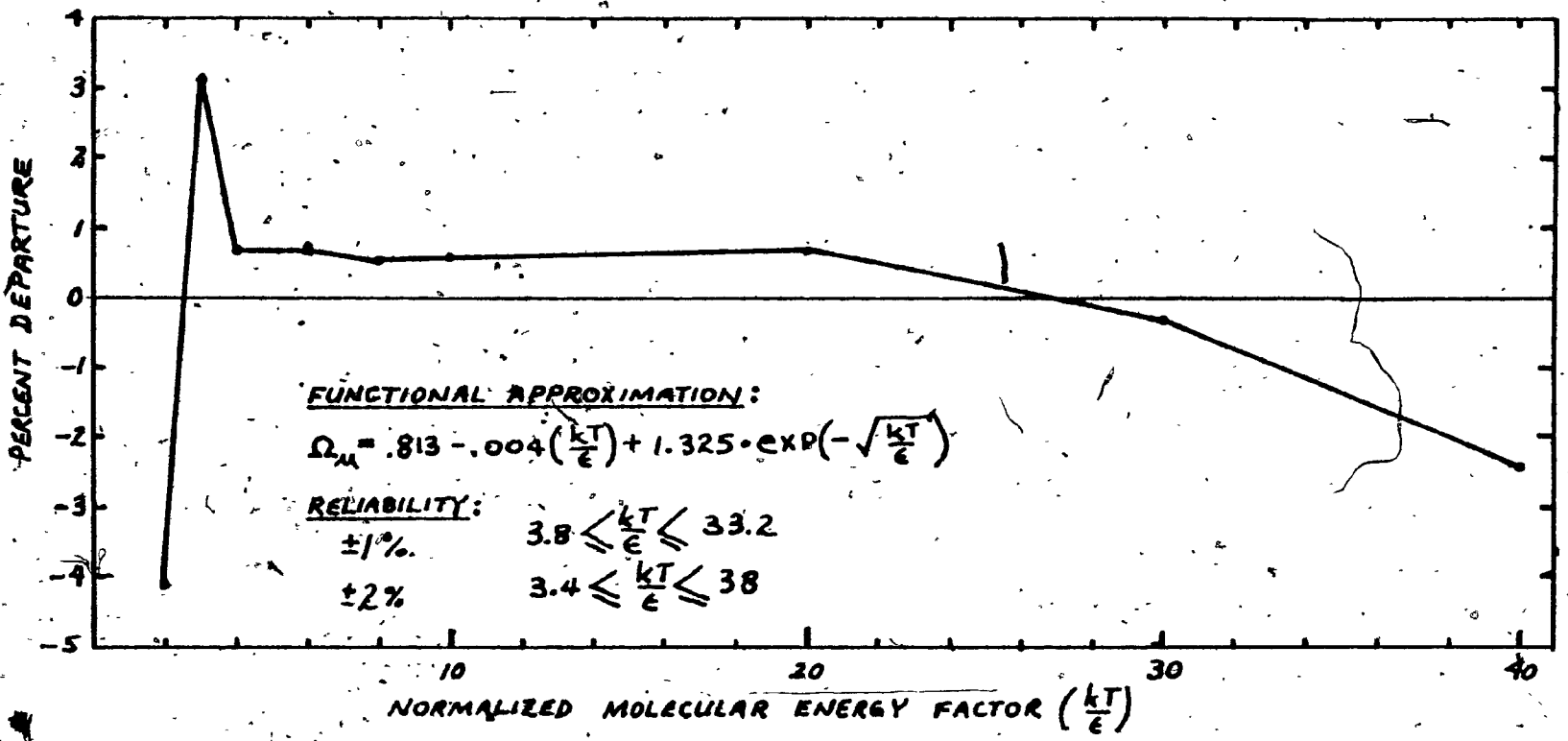

Fig. 4.12 - Departure Plot - Lennard-Jones Viscosity Factor vs Molecular Energy Parameter

$(3.8 \leq \frac{kT}{\epsilon} \leq 33.2)$

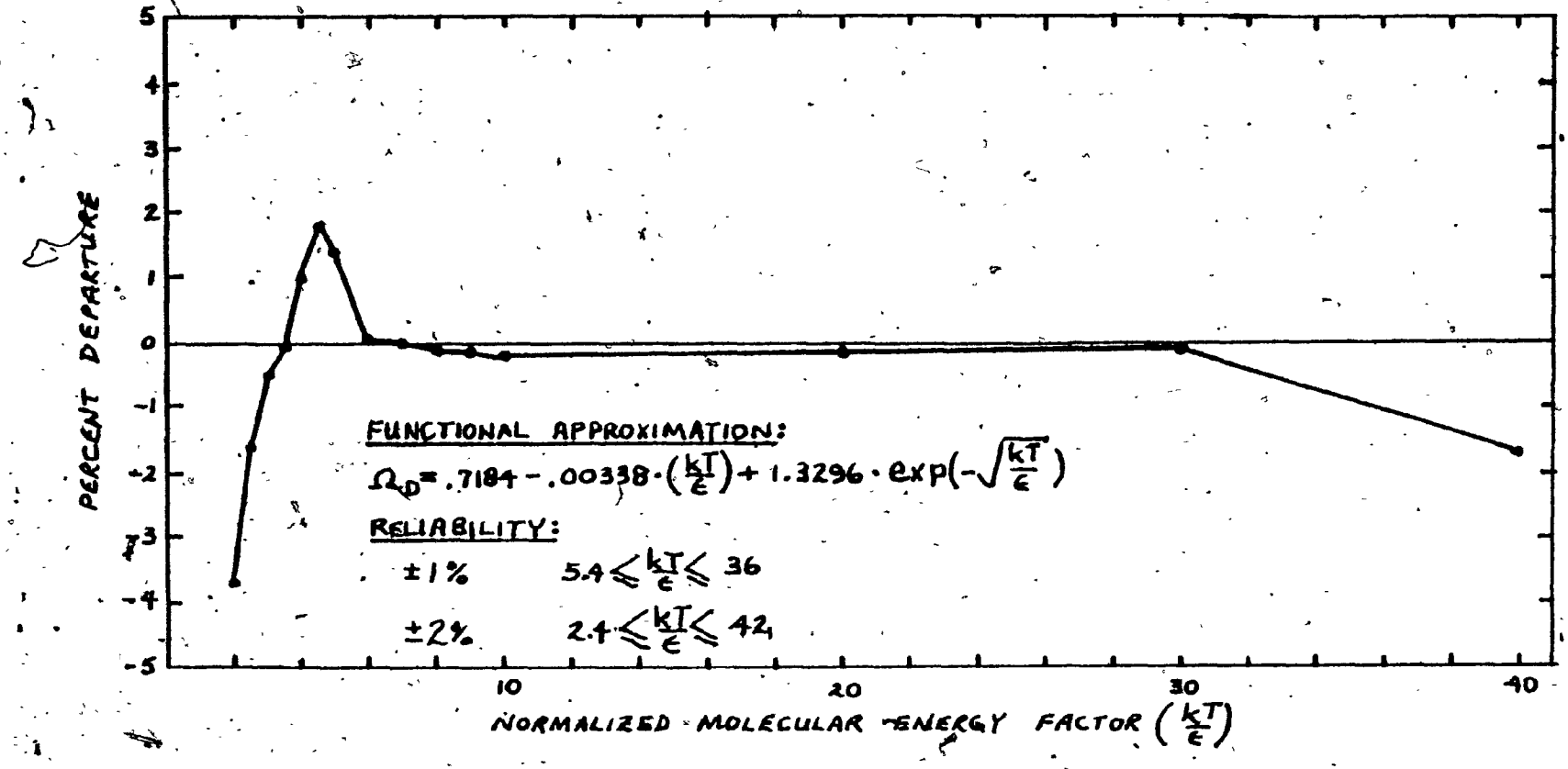

Fig. 4.13 - Departure Plot - Lennard-Jones Diffusivity Factor vs Molecular Energy Parameter

$(5.4 \leq \frac{kT}{\epsilon} \leq 36)$

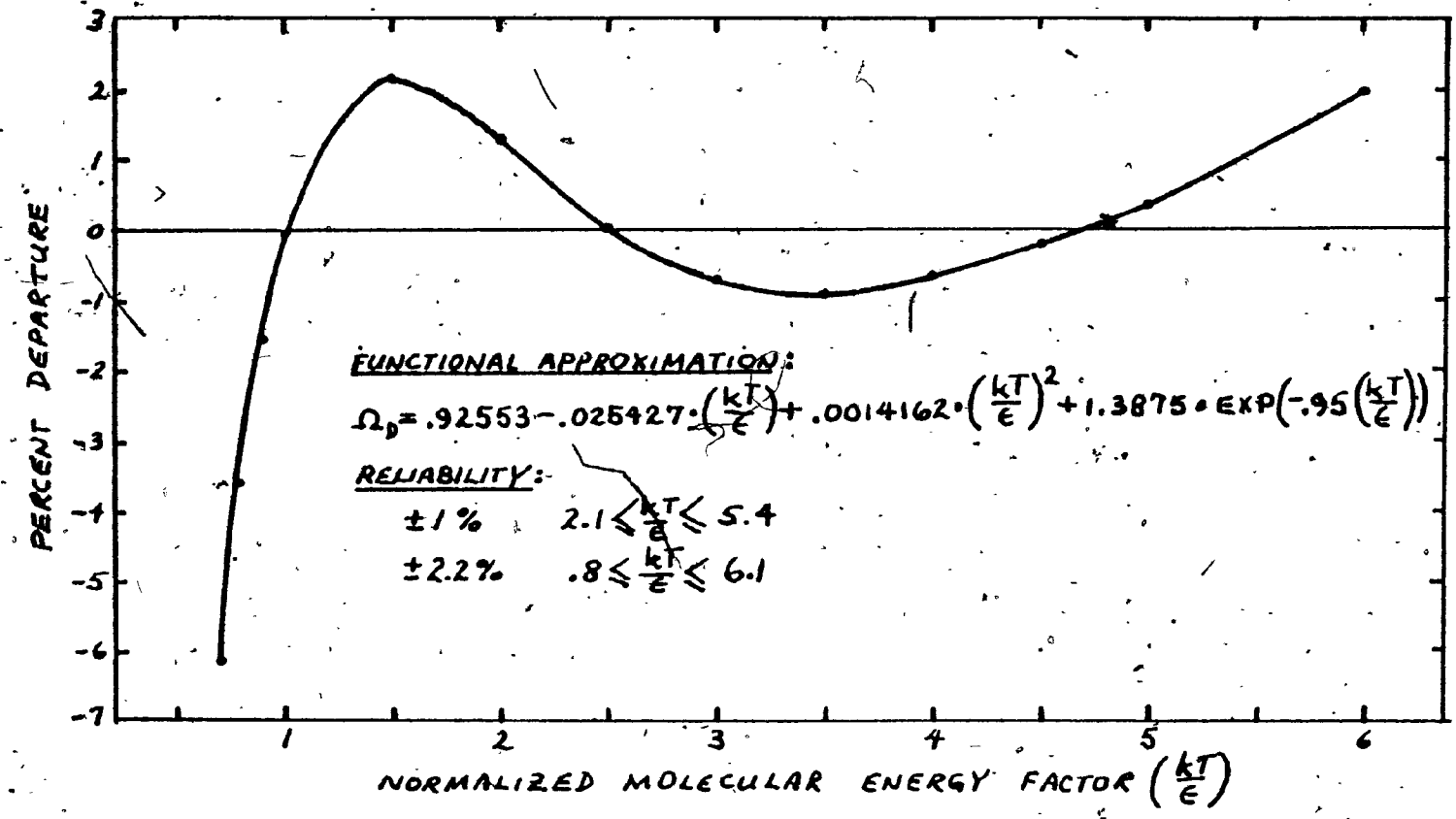

Fig. 4.14 - Departure Plot - Lennard-Jones
Diffusivity Factor vs Molecular Energy Parameter
$(2.1 \leq \frac{kT}{\epsilon} \leq 5.4)$

plots for the diffusivity (or viscosity) correction factor for different ranges of the independent variable.

4.1.4.3 Thermal Conductivity

Figs. 4.15 and 4.16 display departure plots for thermal conductivities calculated for the gas methane and the gas air from recommended data derived from experimental work over a range of temperatures (7,8). These plots are limited to temperature ranges where reliable data is available. Also included on the same displays are departure plots from the same recommended data using Hirschfelder's formula (9). The error bounds for the recommended data are included (7).

4.1.4.4 Viscosity

Viscosity is an important secondary parameter in this work. It is used to calculate the thermal conductivity of gases. Hence Figs. 4.17 and 4.18 are prepared to display departure of the calculations in this work from experimentally derived data (10). The independent variable scaled on the horizontal axis is temperature. The error bounds for the experimental data of 2% over the temperature range are displayed in the same figures.

4.1.4.5 Discussion

Specific heat formulas for methane and for air are readily available in temperature ranges below 1500°K. Hence, the departure plots in Figs. 4.9 and 4.10 are for curvefitted polynomials for specific heat of methane and of air respectively above this temperature. It can be seen that these

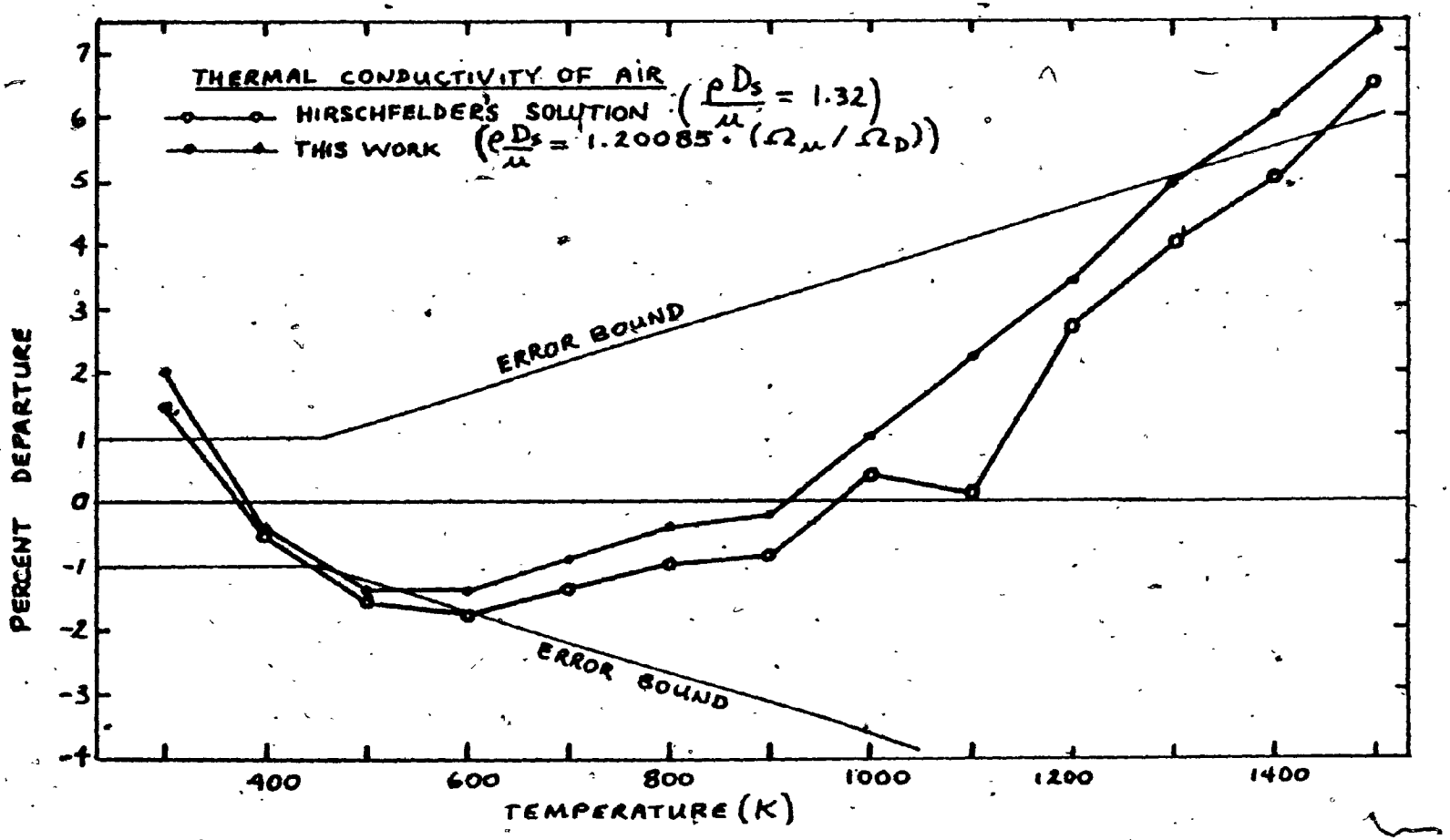

Fig. 4.15 - Departure Plot - Thermal Conductivity of Air vs Temperature

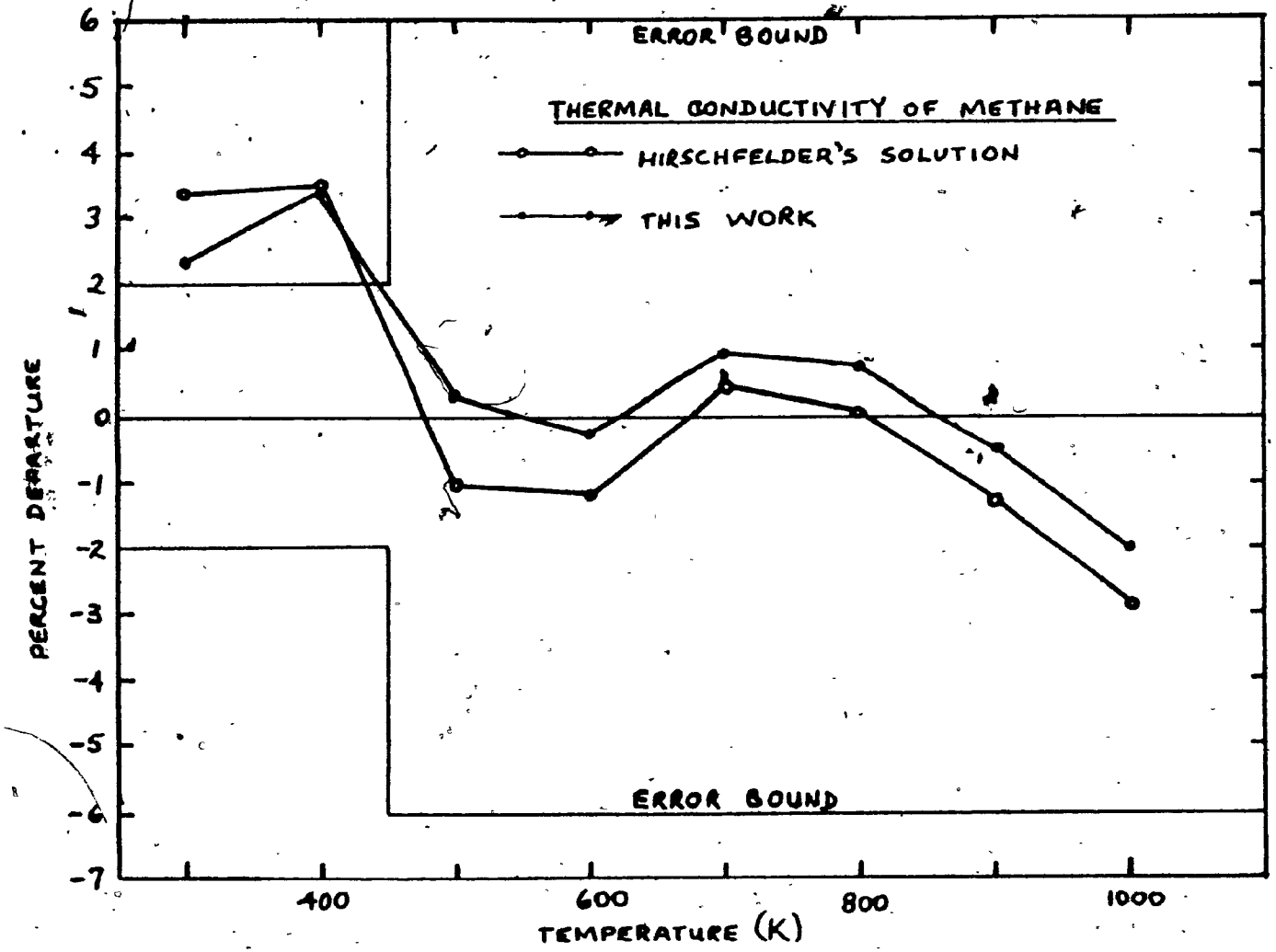

Fig. 4.16 - Departure Plot - Thermal Conductivity of-Methane vs Temperature

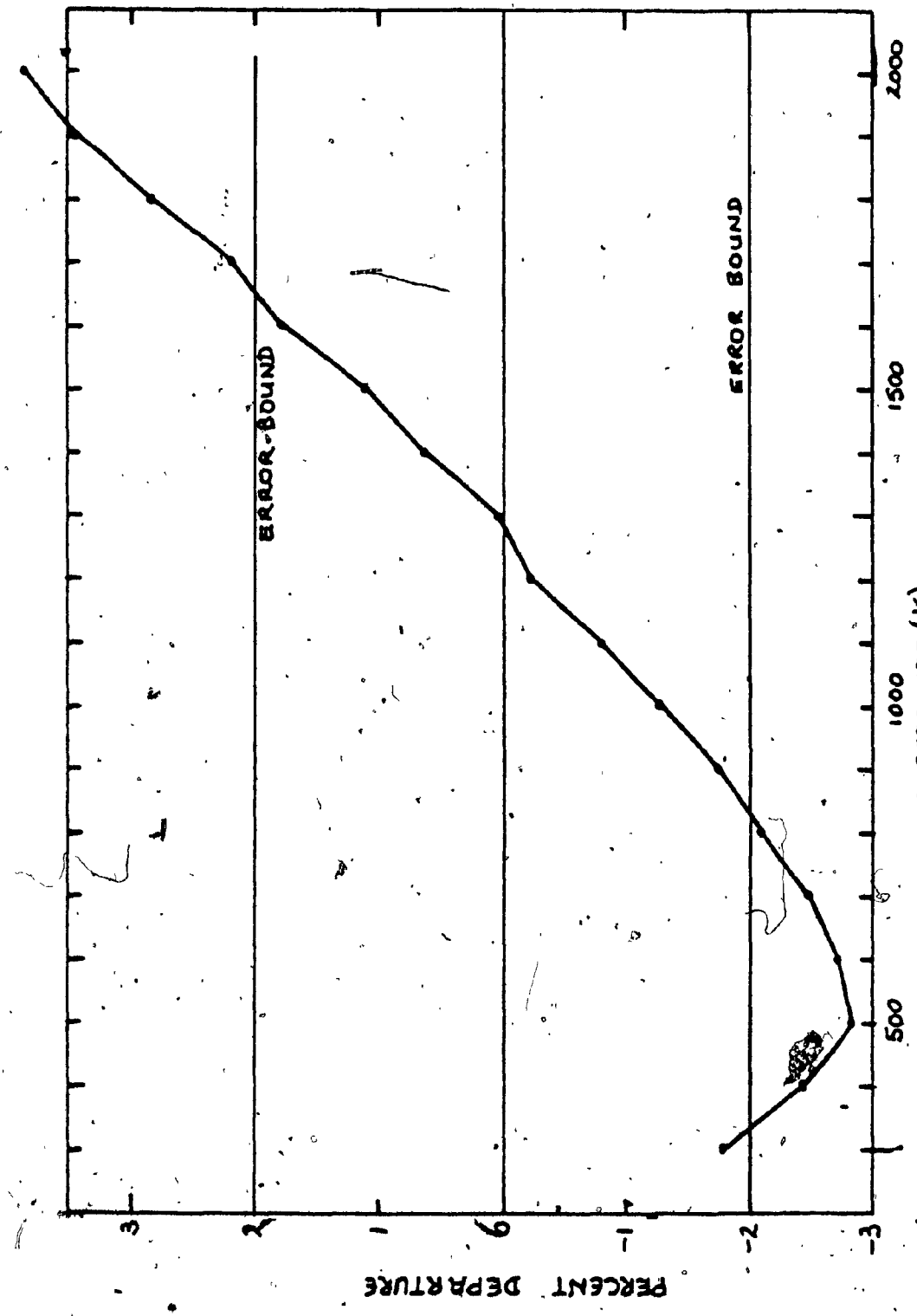

Fig. 4.17 - Departure Plot - Viscosity of Air vs Temperature

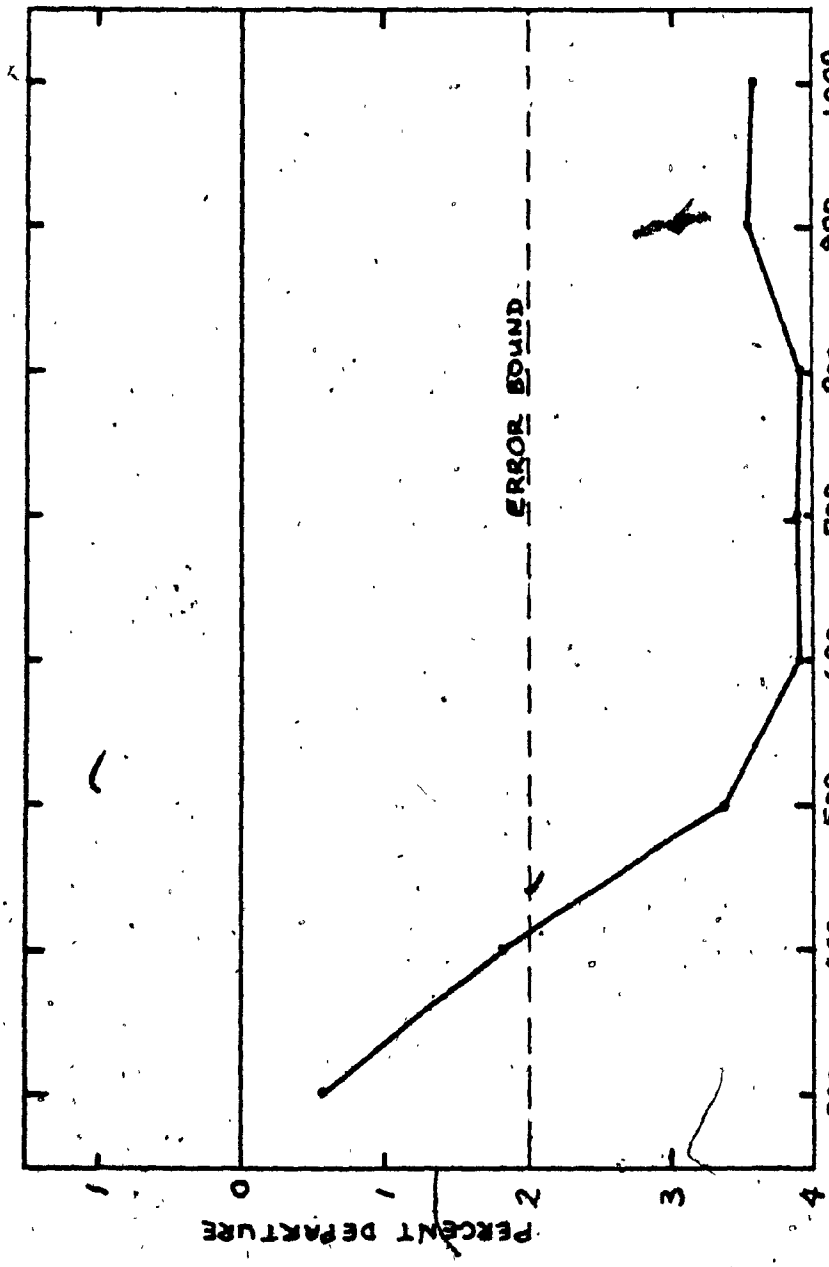

Fig. 4.18 - Departure Plot - Viscosity of Methane vs Temperature

polynomials produce reliable results up to 2300°K. Note, however, that the fitting error, which in both cases is less than .5%, is not the overall error, since the data has a maximum error of 1% to 2%.The maximum polynomial error is then 2% to 2.5%.

The viscosity formula, derived from standard Chapman-Enskog theory with Lennard-Jones correction factors resulted in the departure plots in Figs. 4.11, 4.12, 4.13 and 4.14. Between 300°K and 1000°K the maximum departure in the air viscosity plot is 3% and the maximum departure in the methane viscosity plot is 4%. The trends of these plots above 1000°K are not promising.

The thermal conductivity departure plots using Hirschfelder's formula and the modified formula developed here do not show a large difference. These departure plots for air show a maximum departure of 2% and for methane show a maximum departure of 3% between 300°K and 1000°K.

Figs. 4.16 and 4.17 show that the "fitted" Lennard-Jones correction formulas depart from the original data by a maximum of 1% over a wide range of values.

4.2 Steady Flow Laminar Combustion

Two combustion systems of the type described in Chapter 2 of this work are solved in this section. The first case is a laminar system using parameters from literature to represent a propane/air system. The purpose of this first case is a comparison between solutions derived by the F.E.M. and F.D.M. for similar problems. As such the flame

parameters are input to bypass the subroutines of the code that calculate these values. The second case, a more comprehensive study, is a laminar combustion flow field calculation in which the activation energy, heat of combustion and molecular weights are chosen to represent a methane/air system. The upwinding factor of one is used everywhere in this section.

4.2.1 Special Case #1: Propane-Air System

The data presented in Table 4.1 is taken directly from Aly (11). Aly, however, solves the propane-air combustion system in two dimensions, therefore his solution is not expected to correspond exactly with the one-dimensional solution obtained here from the same input data.

Aly finds a flame velocity of 45 cm/s. Using a convective heat transfer coefficient (H) of 6.25 $\left[\frac{cal}{s\text{-}m^2\text{-}°K}\right]$, corresponding to the flame velocity calculated here, Figs. 4.19a 4.19, 4.20 display the flame profiles of this calculation with the centerline flame profiles from Aly.

The origin on the abscissa can be placed arbitrarily. Here the choice is made to represent roughly the division between the flame region and the induction region of the solution regime. For the curves derived here, the point where the reaction rate first reaches 1/1000th of the peak reaction rate is used. Aly's profiles, however, are simply overlayed visually since precise information is not available. As such, no significance can be attached to the intersection of the

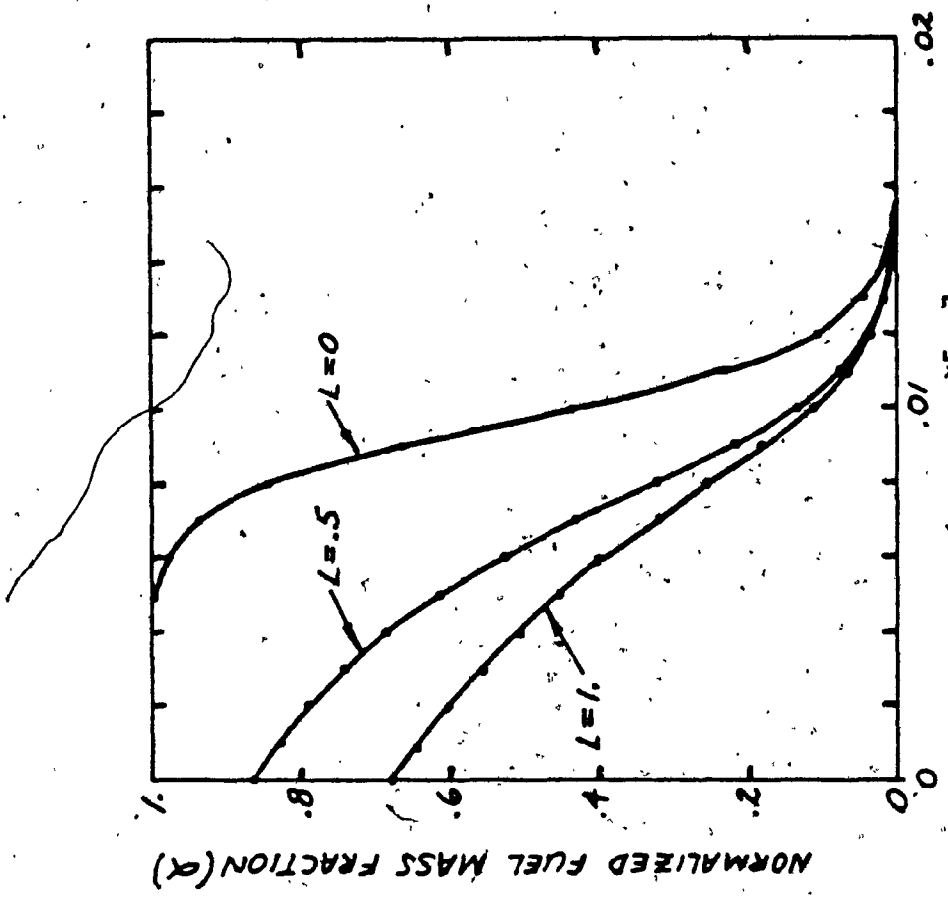

Fig. 4.23 - Fuel Species Profiles with Variable Lewis Number

rises, peaks and falls quickly. The end of the flame region and the beginning of the post flame region is chosen as the point where the reaction rate falls to the same value it has at the origin. The flame region is indicated in Fig. 4.21. It is seen that this region expands with increasing Lewis number, changing from .02cm when the Lewis number is zero to .024 cm when the lewis number is one. In this figure it can also be seen that the temperature profile changes little with the change in Lewis number. Fig. 4.22 shows the reaction rate profiles. It is seen that when the Lewis number is small and the flame zone is small, not surprisingly, the peak reaction rate is large. When Lewis number is zero, the peak reaction rate is .83 $\left(\frac{g}{s\text{-}cm^3}\right)$ and when the lewis number is one the peak reaction rate is .66 $\left(\frac{g}{s\text{-}cm^3}\right)$. Fig. 4.23 shows the fuel species profiles. When the Lewis number is zero, loss of fuel from the flame region is not observed. When $x = 0$, $\alpha \simeq 1$. When Lewis number is one, the loss of fuel from the flame region is large. When $x = 0$, $\alpha \simeq .68$.

Fig. 4.24 displays the effect of heat loss on the flame temperature profile. For convenience, this is done in the form of a departure plot from the flame temperature which would exist if heat loss was neglected. The magnitude of the departures are not realistic, because the heat loss parameters are not chosen in a realistic way. In fact, the heat loss parameters are chosen to exaggerate the heat loss so trends can be observed.

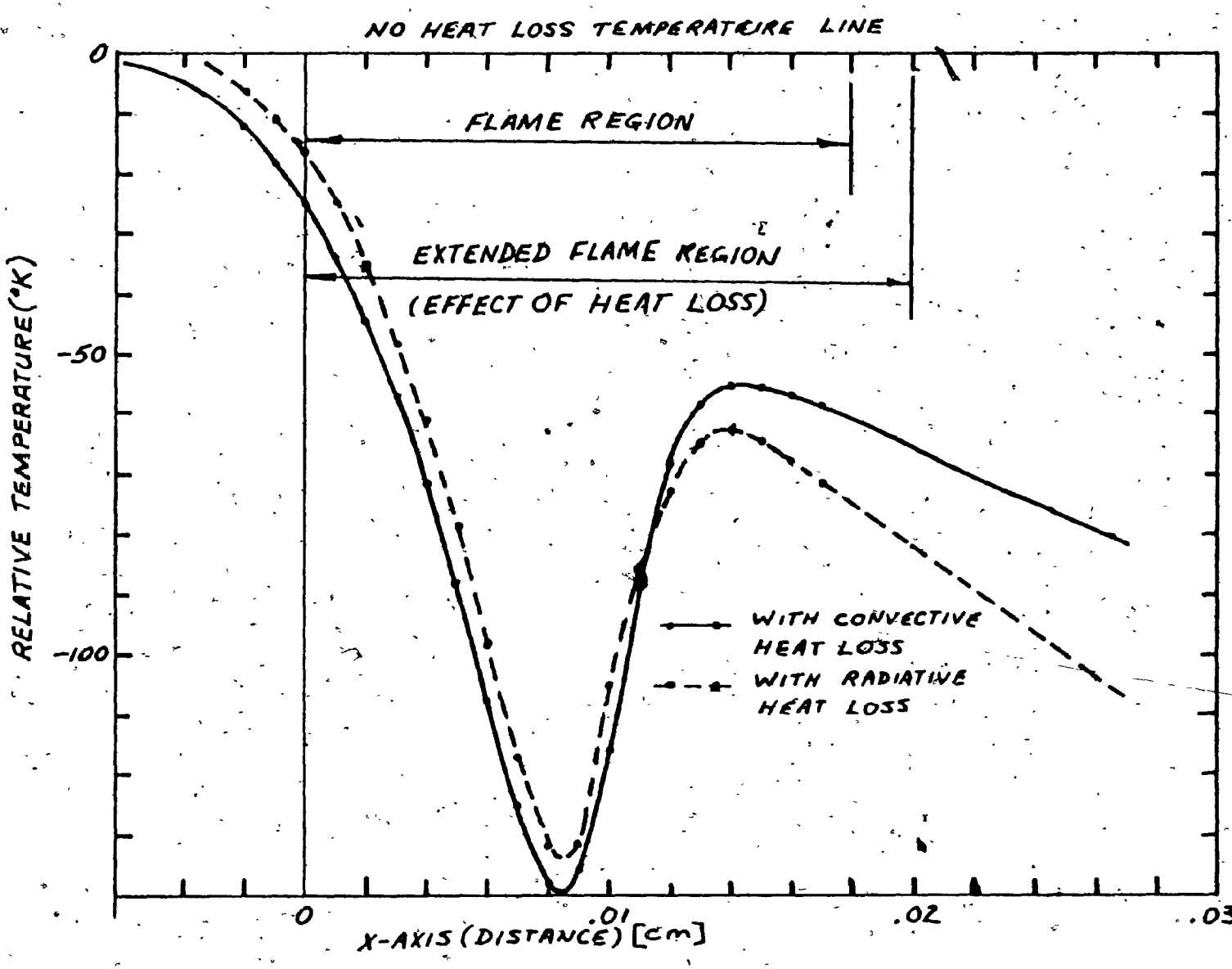

Fig. 4.24 - The Effect of Heat Loss on the Flame Temperature Profile

There are two relative temperature plots in this figure. The solid line represents relative temperature when only convective heat loss is considered. The broken line represents the relative temperature through the flame when only radiative heat loss is considered. In both cases, the heat loss parameter is chosen to yield a flame speed of 45 cm/s in compliance with Aly's solution. Without heat loss the flame speed is found to be 48.5cm/s, reflecting a connection between flame speed and available heat energy in the flame.

The departure plots are similar in that, from the beginning of the flame region, the departure plots drop abruptly to a maximum absolute departure before the middle of the flame region. After this, the plots rise abruptly to a peak near the end of the flame region, followed by a gradual decline of the relative temperatures in the post flame region. From this it is seen that the heat loss from the flame causes a delay in the temperature increase and a lowering of the final flame temperature. This, in turn, causes a widening of the flame region and a lowering of the flame speed.

4.2.2 Special Case #2: Methane/air

Using the data presented in Table 4.1 chosen from the literature to represent a methane-air system ( ), the code is used to calculate details of a flame. In all the calculations to follow, heat losses are neglected.

Before the problem can be solved, it is necessary to find a suitable cutoff temperature. The procedure for doing this is described using Fig. 4.25 to 4.35 for this methane-air flame.

Fig. 4.24 is a graphical display of flame speed as it is influenced by variations in the cutoff temperature for stoichiometric methane-air. The line is horizontal below a cutoff temperature of 900°K. This shows that flame speed is independent of cutoff temperature in this range. However, the variation of the flame speed with the cutoff temperature above 900°K is also seen in Fig. 4.25. Furthermore, because of the link between flame speed and reaction rate, 900°K is an effective ignition temperature for this stoichiometric mixture.

For confident use of the code it is only necessary to establish one cutoff temperature and this cutoff temperature must be below the ignition temperature: the exact value of ignition temperature need not generally be known. Given this advantage, a procedure for finding a suitable cutoff temperature is invented here. Two observations, noted here in turn, are made to derive this procedure.

First, it is observed from Fig. 4.25 that increasing the cutoff temperature in the vicinity of the ignition temperature results in a rapidly changing slope for the flame speed curve until the curve reaches a linear region where the slope is almost constant. Hence the overall curve

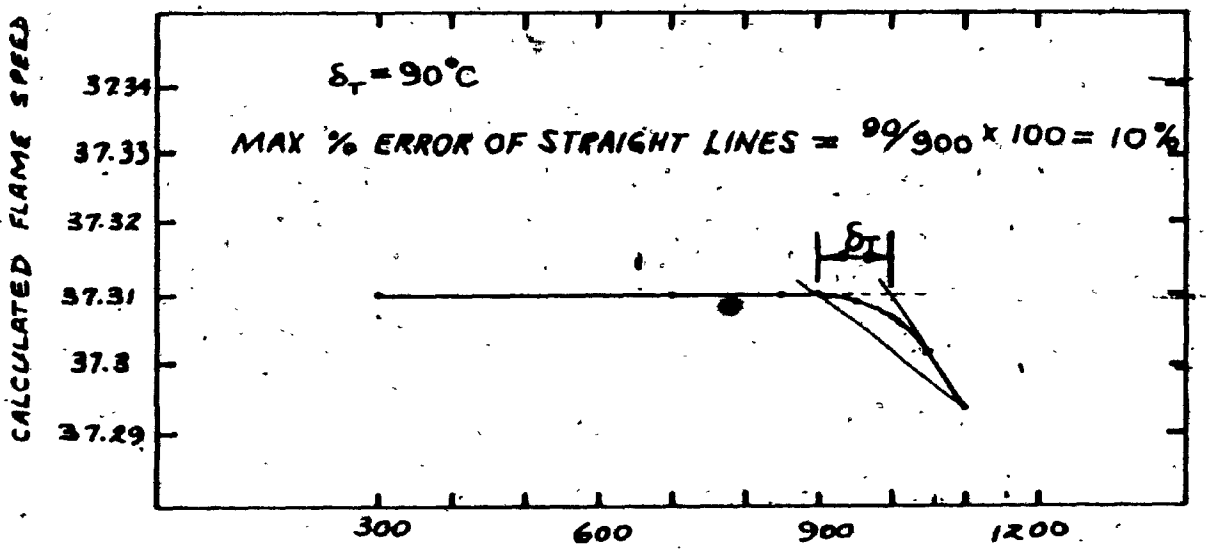

Fig. 4.25 - Detailed Ignition Temperature Calculation for Stoichiometric Methane (Y_o = .0581)

shape can be approximated by two straight lines (11). These two lines intersect near the ignition temperature. This procedure need be carried out with only four points as illustrated in Fig. 4.26. Based on maximum and on minimum slopes as Fig. 4.25 shows, the error of this procedure can be as high as 10% when the ignition temperature is wanted. However, since a minimum value of ignition temperature is sought, subtracting 100°K guarantees an acceptable value for cutoff temperature for use in this code for a given mixture.

By applying this procedure to several different initial mixtures as portrayed in Figs. 4.26, 4.27, 4.28, 4.29, 4.30, 4.31, 4.32 and 4.33 it is observed that the ignition temperature is a variable. The trend of this variability is plotted in Fig. 4.34 where the ignition temperature is displayed as a function of the initial fuel fraction. The upper line in this figure represents the intersection points of the lines from Figs. 4.26 - 4.33 and the lower line is the same value minus 100°K. Together these curves enclose a region in which the ignition temperature plot must fall. It is noticed from Fig. 4.34 that the ignition temperature declines with decreasing initial fuel concentration. Therefore only the ignition temperature of the lowest mixture strength is needed.

Here a cutoff temperature of 600°K is used in all calculations and no practical difficulties are encountered.

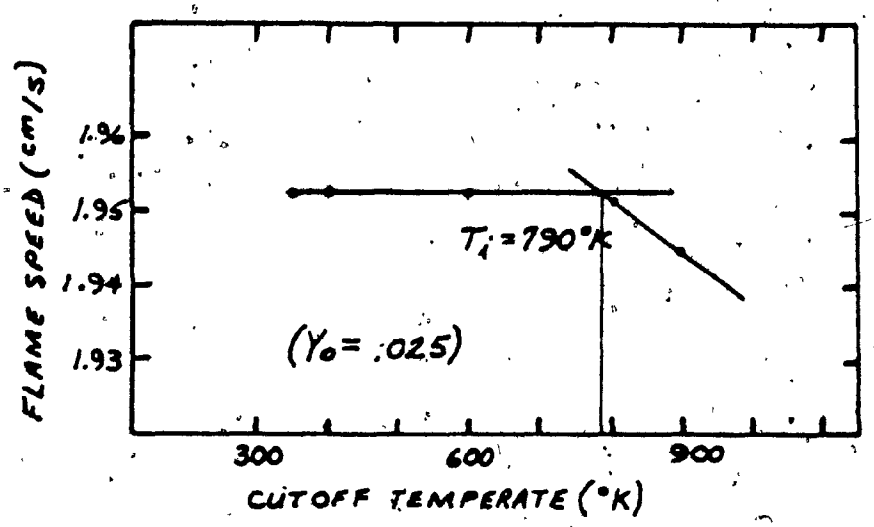

Fig. 4.26 - Ignition Temperature Analysis (Y_o = .025)

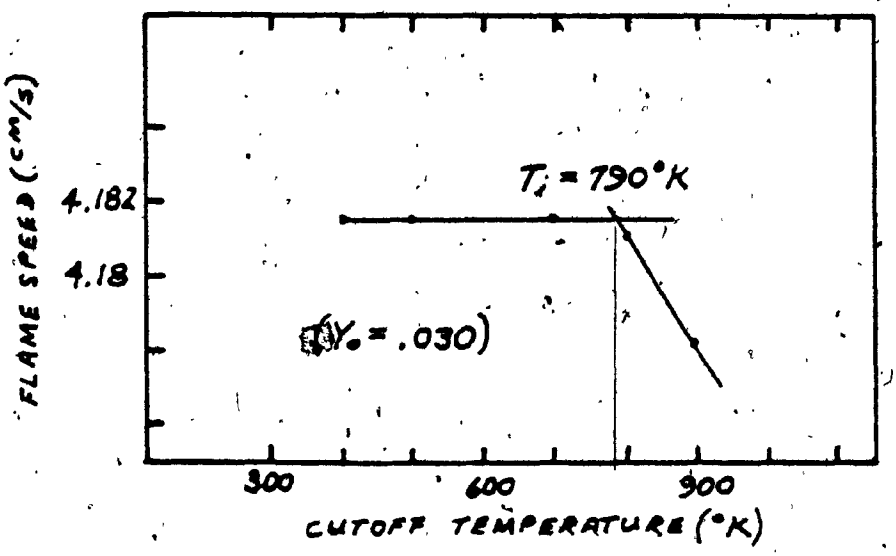

Fig. 4.27 - Ignition Temperature Analysis (Y_o = .030)

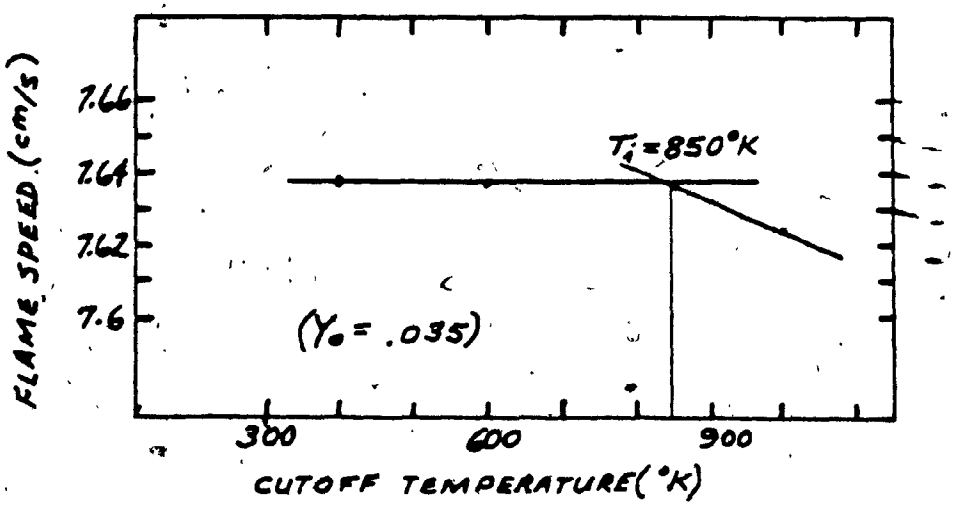

Fig. 4.28 - Ignition Temperature Analysis (Y_o = .035)

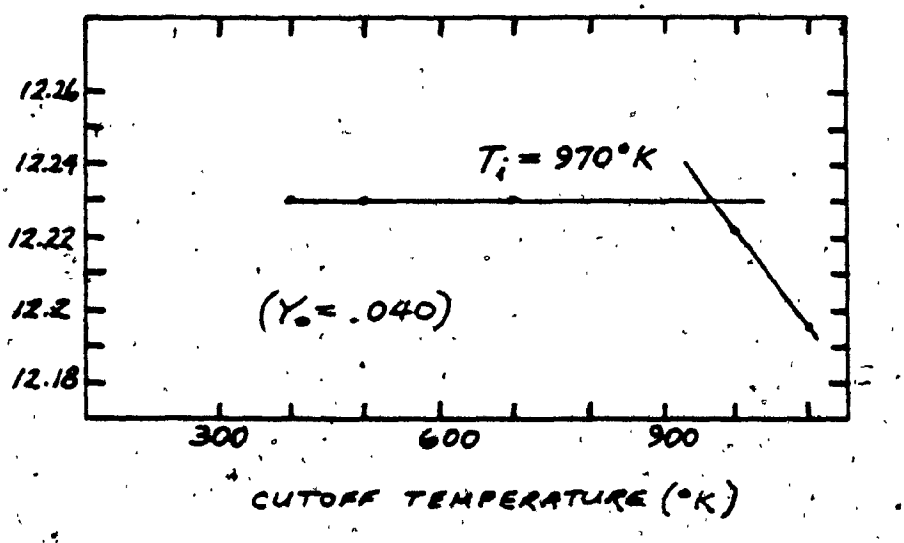

Fig. 4.29 - Ignition Temperature Analysis (Y_o = .040)

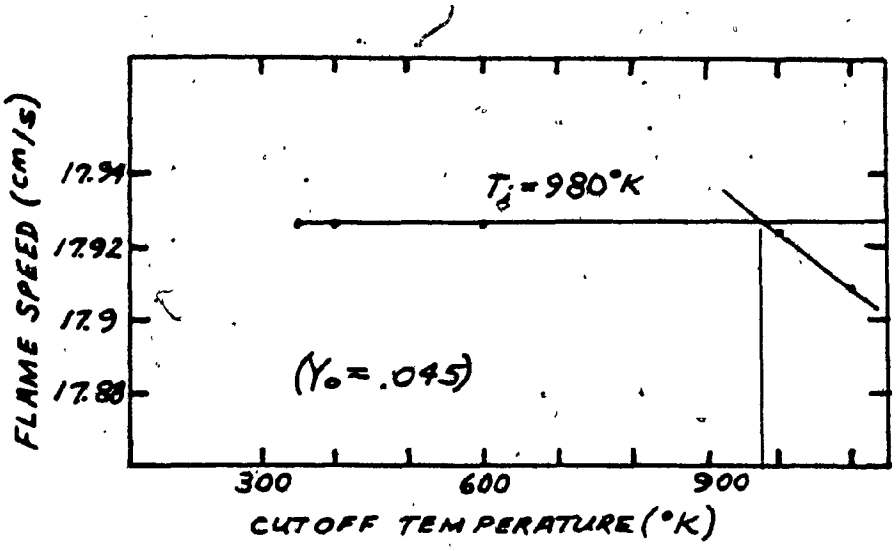

Fig. 4.30 - Ignition Temperature Analysis (Y_o = .045)

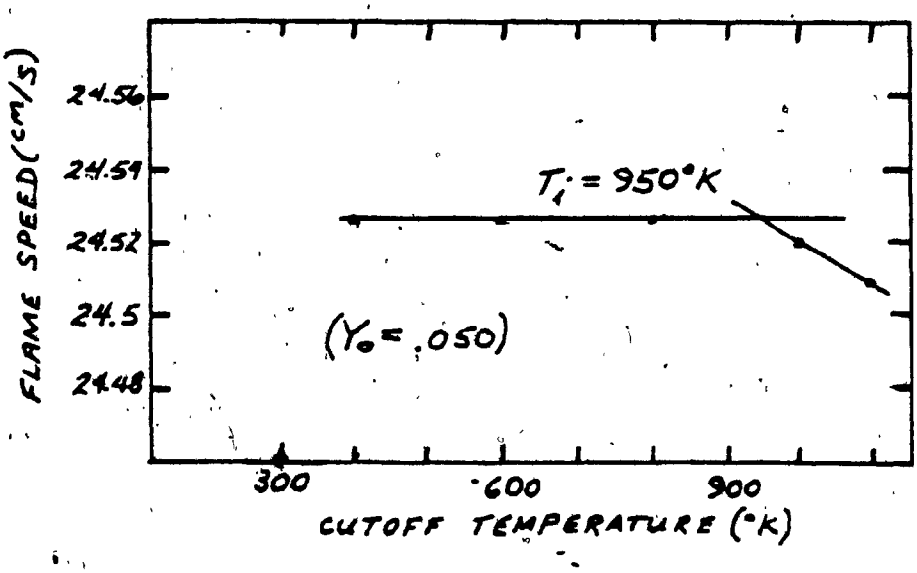

Fig. 4.31 - Ignition Temperature Analysis (Y_o = .050)

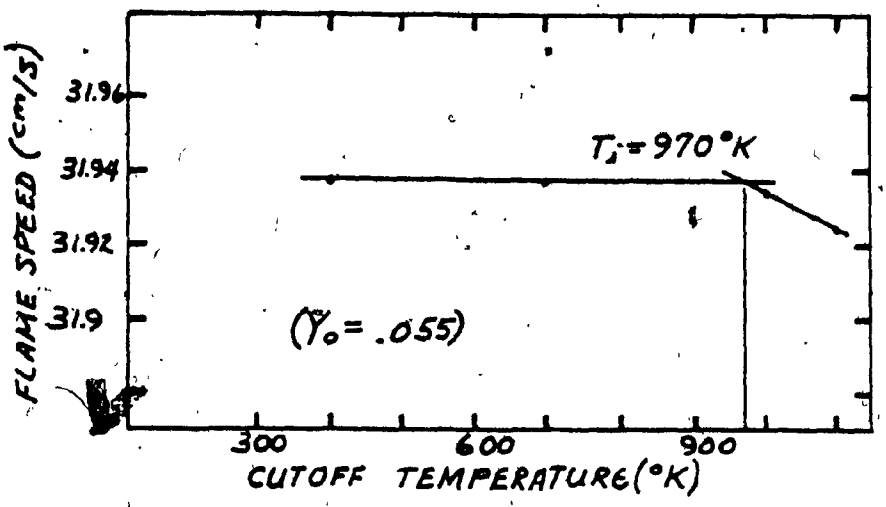

Fig. 4.32 - Ignition Temperature Analysis (Y_o = 0.55)

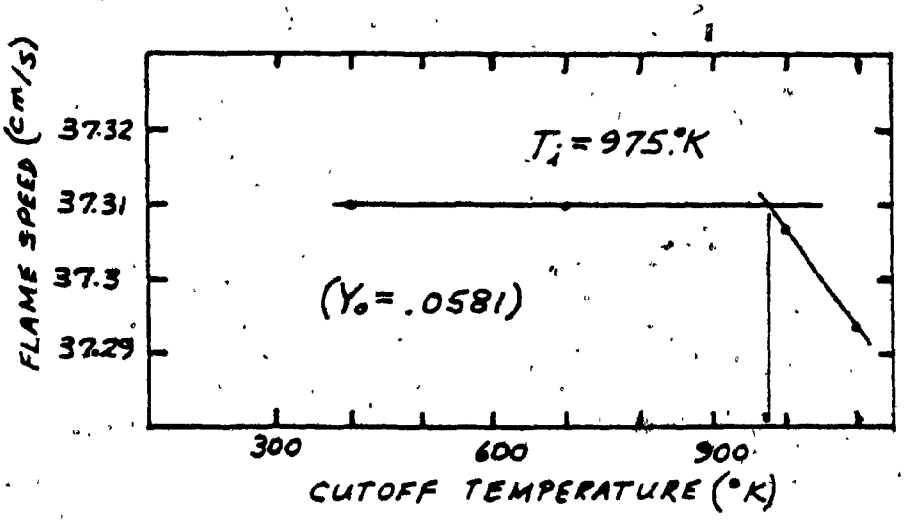

Fig. 4.33 - Ignition Temperature Analysis (Y_o = 0.581)

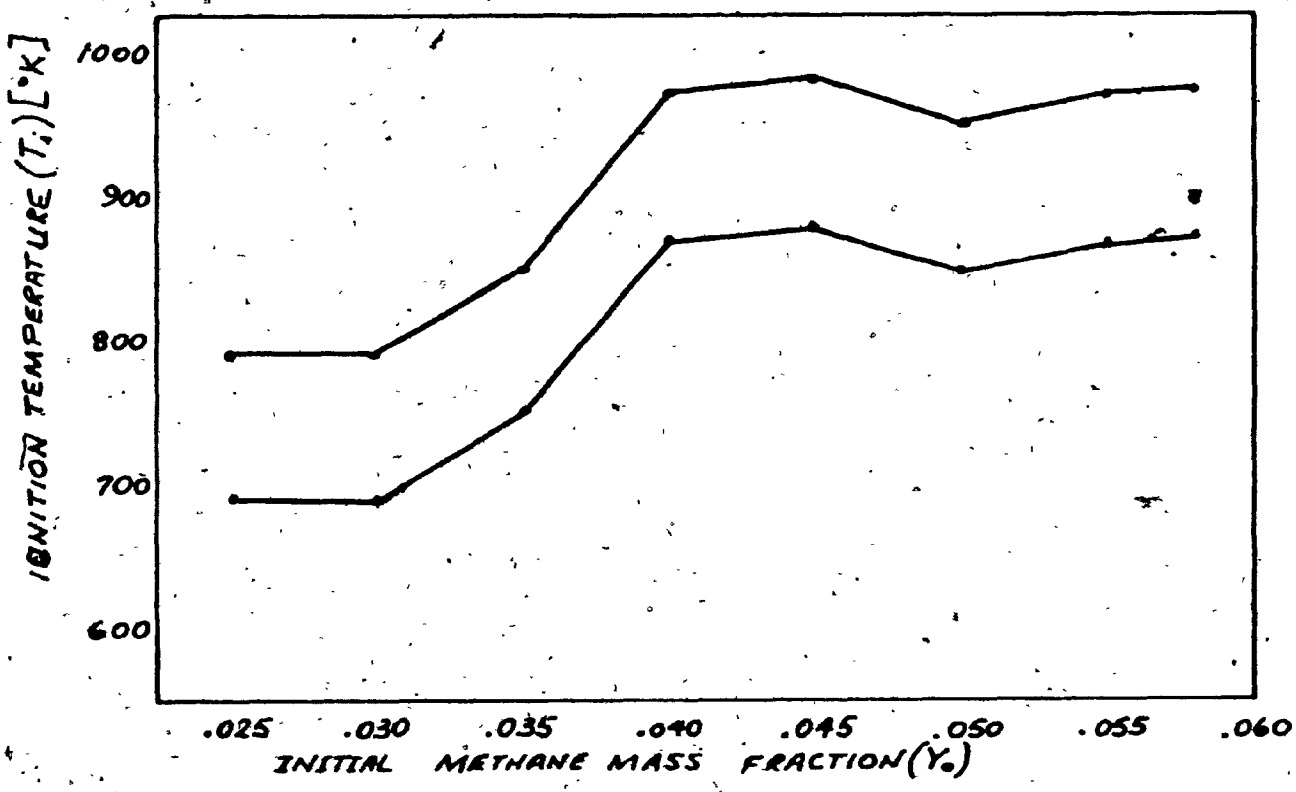

Fig. 4.34 - Ignition Temperature vs Initial Methane Mass Function

Fig. 4.35 illustrates the temperature, fuel species concentration and reaction rate profiles for a stoichiometric methane-air mixture. The shapes are "classical". Table 4.2 summarizes results for several lean fuel cases for which solutions are obtained. The flame speed found in each case on Table 4.2 is plotted against the methane mass fraction in Fig. 4.36 giving a flame speed profile, suitable for the flammability limit calculation which is discussed in Chapter 3. The procedure is included on this graph along with the results. Fig. 4.37 is a plot of the flame thickness vs methane mass fraction.

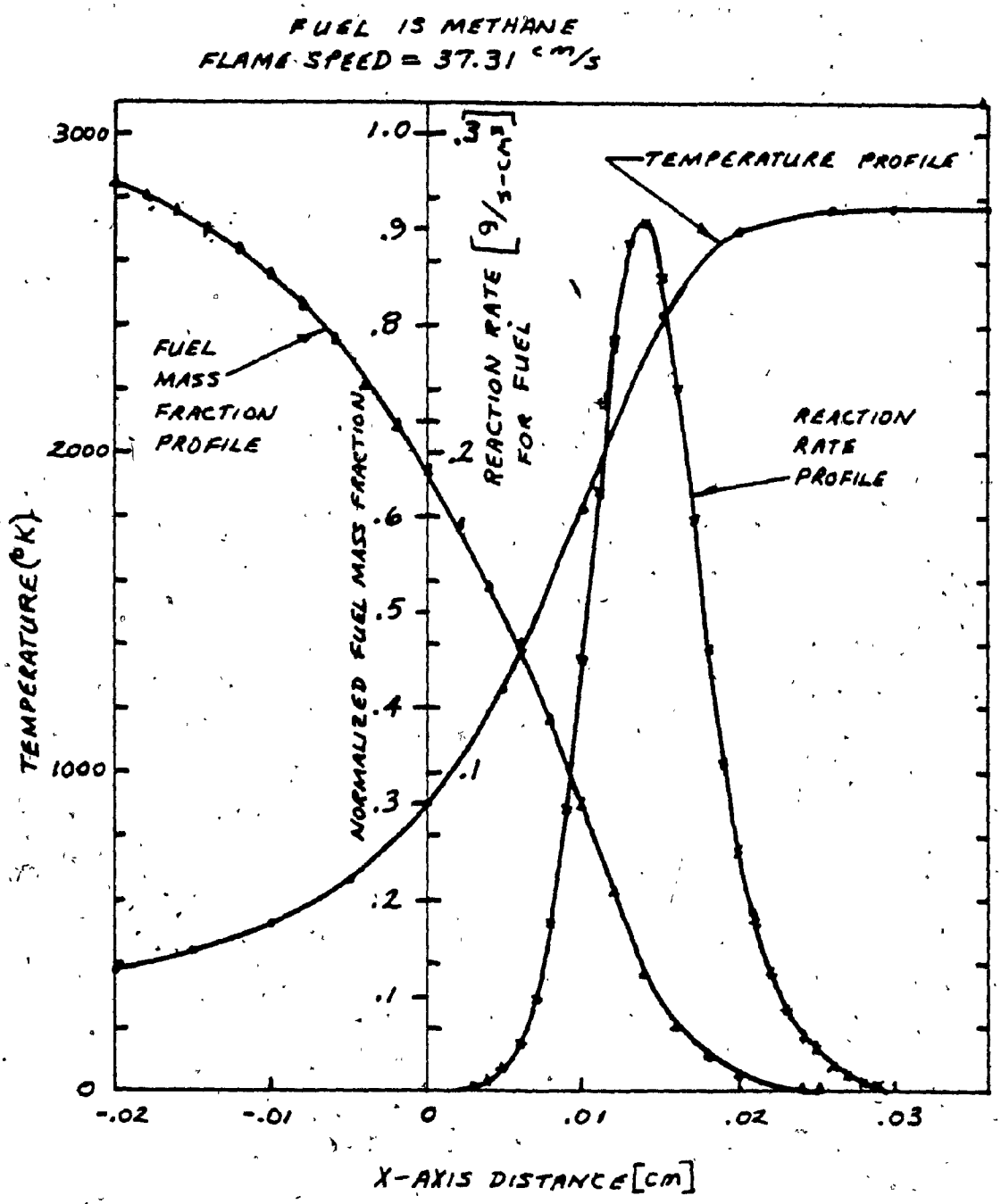

Fig. 4.35 - Solution Profiles for Stoichiometric Methane (Y_O = 0.581)

TABLE 4.2: METHANE/AIR FLAME CHARACTERISTICS

Yo	L	δ	k	c_p	T_i	V_o	AFT
.0581	1.404	.038	1.2E-4	.282	975°K	37.31	2772.17
.055	1.405	.042	1.2E-4	.280	9.70°K	31.94	2653.94
.050	1.407	.0525	1.2E-4	.278	950°K	24.526	2460.3
.045	1.409	.0675	1.1E-4	.275	980°K	17.934	2262.94
.040	1.411	.092	1.1E-4	.272	970°K	12.23	2061.75
.035	1.413	.138	1.1E-4	.270	850°K	7.64	1856.6°K
.030	1.415	.231	1.1E-4	.267	790°K	4.18	1647.44
.025	1.417	.459	1.1E-4	.265	790°K	1.95	1434.08

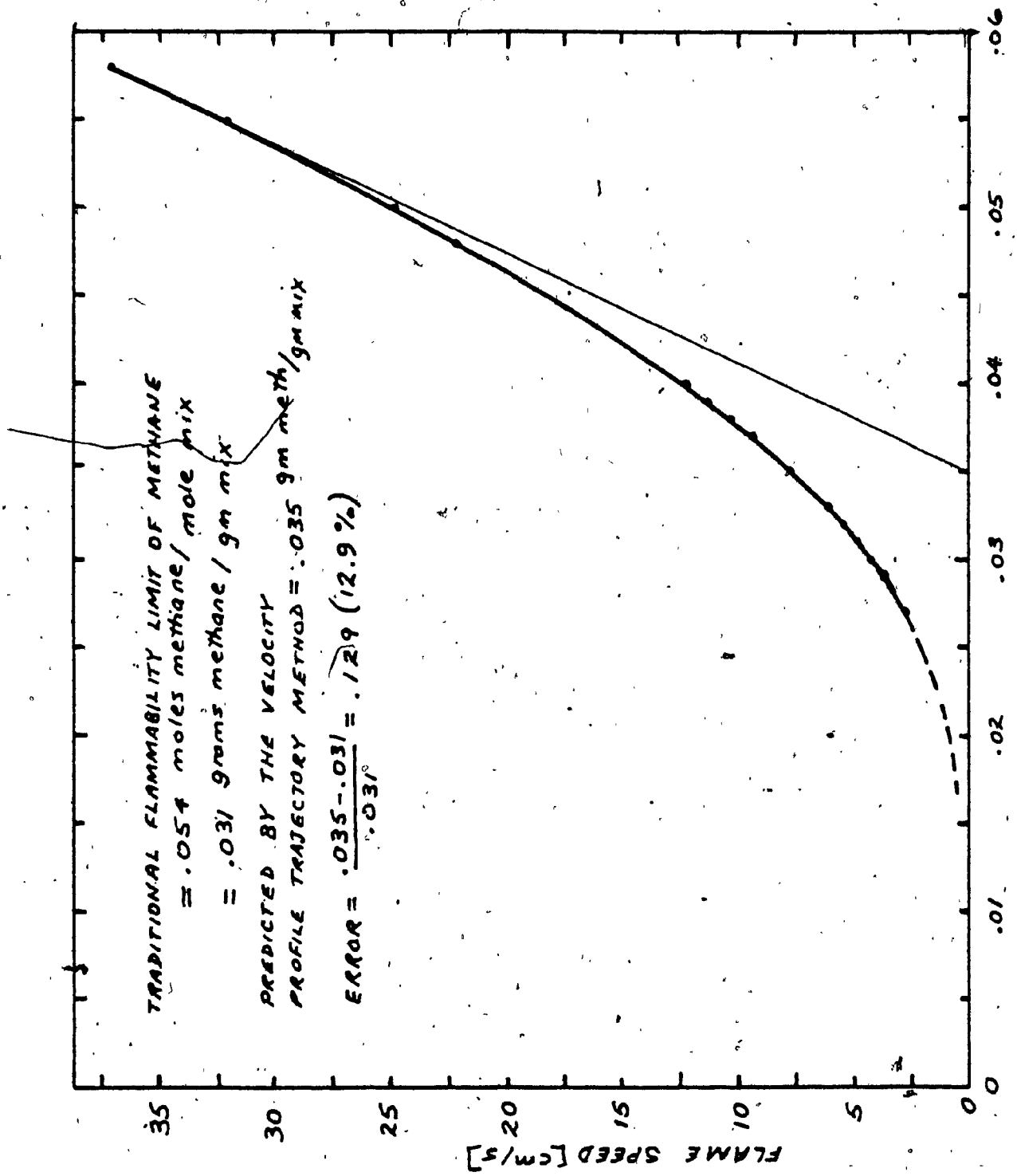

Fig. 4.36 - Flame Speed Profile and Flammability Limit for Methane-Air Flame

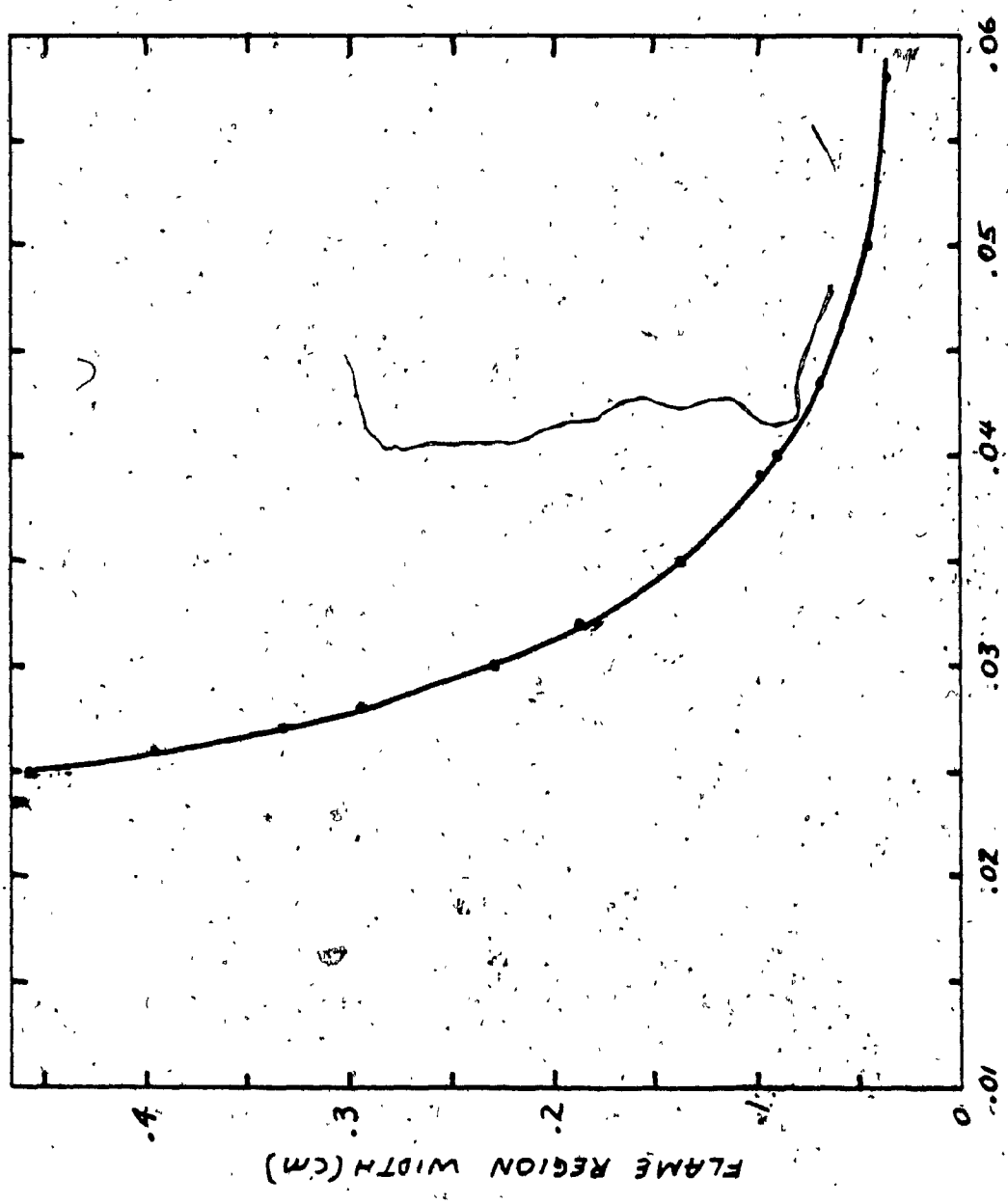

Fig. 4.37 - Initial Methane Mass Fraction vs Flame Region Thickness

CHAPTER 5

GENERAL DISCUSSION, CONCLUSIONS AND FUTURE WORK

The intention of this work is threefold: 1) to study the unique advantages the finite element method has when applied to flame problems, 2) to examine the details of applying it, 3) to achieve results for a laminar flame approximation and discuss the observed phenomena.

The mathematical equations that are presented in Chapter 2 have been derived with these goals in mind. In Chapter 3 a numerical model of these equations is developed which is tested extensively in Chapter 4. This chapter begins with remarks concerning the efficiency, accuracy and convenience of the numerical procedure.

As stated previously, it is the non-linearity of the equations which makes efficient solving of these equations difficult. As such, the linearization procedure is important. The linearization procedure used here is not theoretically or demonstrably the best procedure available. It is, however, found to be simple and efficient and the present problem is solved easily on the powerful contemporary computer system available.

The computer used in this work is the Concordia University CDC-CYBER 172/2. The execution times vary with the number of elements and the stiffness of the equations solved. For the methane-air model presented in section 4.2.2,

times vary from 4 seconds for a solution regime of 200 elements to 16 seconds for a solution regime of 1500 elements. A detailed comparison between this efficiency and the efficiency obtained using other codes is, however, difficult because of the many factors effecting the solution times, such as the compilation of the internal manipulations. Nevertheless, examination of Fig. 3.2 reveals that these solution times are reasonable. Future work using uniform models to compare solution times appears warranted, since it may be critical for multiple species, multiple dimension problems.

Picard linearization, which is used here, does not acknowledge the local non-linearity of the reaction rate terms. It is noted in Chapter 3 that the efficiency in solving similar "stiff" non-flow systems is greatly effected by such acknowledgement. Hence, this author believes the same is true in solving the laminar flow flame equations. Investigation in this area should be undertaken.

The many features of the finite element method which make it powerful and versatile, some of which are described in Chapter 3 can be harnessed to solve combustion problems. In this work the problems of general error reduction are addressed, in particular those errors associated with global quantities such as flame speed and convection rate.

The procedure adopted here, which couples a

conservation finite element scheme which is derived from Galerkin's concept of error minimization, affords a simple and effective approach to error control. Reexamination of Figs. 4.6, 4.7 and 4.8 substantiates this claim. It is seen that for all data sets derived from code test number 3, the maximum error in the convection rate calculation is .01%. Similar small global errors accrue in spite of large profile errors (as high as 6%). Furthermore, to achieve a reduced maximum profile error, upwinding is used. By using an upwinding factor of one throughout the flow regime, the maximum profile error reduction from 6% to 1% is observed in Fig. 4.7. This is, however, achieved with some sacrifice in the accuracy of the global calculations (.005% error in the convection rate increases to .01%).

In addition, it is noted that upwinding alters the nature of the error curve. In Fig. 4.7, for instance, it is observed that an oscillating error which exists without upwinding becomes a non-oscillating error with upwinding. Such observations have led some workers to suggest the existence of an optimum upwinding factor. Indeed, Chung (1) in studying the steady-state heat transfer equation, points out that no profile error occurs when linear elements are used with an upwinding factor of

$$f = (\coth \frac{P}{2}) - \frac{2}{P}$$

where $P = \frac{hC_p u}{k}$

It is unlikely such a simple formulation

of "f" exists for the laminar flame equations and no procedure appears to be available for approximating such a formulation. Such work would be valuable.

It is, however, now reiterated that the profile shapes in flames are generally less important than the global functions. Hence, such an upwinding factor is not necessarily desireable in the calculations, if a significantly less accurate convection rate or flame speed is achieved.

In view of the convection rate accuracy achieved here with an upwinding factor of one , this author uses this factor in all calculations.

The first laminar flame problem, solved in section 4.2.3 uses data to represent a propane-air flame (2). Figs.4.19a, 4.19 and 4.20 are a comparison of the solution profiles achieved here using the finite element method with a finite difference solution of a similar problem drawn from literature. It is apparent that the results are significantly different. Nevertheless, subsequent application of the code in 4.2.2 to the more completely formulated methane-air model is continued on the strength of the results of the previous testing in section 4.1.

The methane-air solutions harness the transport and specific heat routines of the code. Before studying the results of the full flame calculation, this feature of the code will be examined.

Curvefitting of data is used extensively in this

work, because it results in easily applied explicit functions by which the flame parameters may be described. In this way, for instance, data for the specific heat of methane and the specific heat of air are "functionalized" in the temperature range between 1500°K and 2400°K. Figures 4.9 and 4.10 illustrate that the polynomial functions fit the data satisfactorily in this temperature range. Similarly, curvefitting is used to invent a functional expression between the normalized molecular energy term "$\frac{Tk}{\varepsilon}$", and the Lennard-Jones correction factors Ω_u and Ω_D. Figures 4.11, 4.12, 4.13 and 4.14 illustrate that the data fitting is successful over a wide range of values.

Using the specific heat and Lennard-Jones correction factors calculated this way, acceptable results are achieved for thermal conductivity, viscosity and diffusivity. Examination of Figs. 4.15, 4.16, 4.17 and 4.18 substantiate this.

In particular, Figs. 4.15 and 4.16 which are departure plots for the thermal conductivity calculation from recommended data reveals a maximum departure of 3% in the range of interest. Figs. 4.17 and 4.18, departure plots of viscosity calculations, show a larger maximum error of about 4%. The calculated values transgress the error bounds of the recommended data only marginally.

Figs. 4.15 and 4.16 also compare departure plots calculated using Hirschfelder's formula $\left(\frac{\rho D_s}{u} = 1.32\right)$

and the formula used in this work (Eq'n. D.5) to calculate thermal conductivity. A significant improvement in the results is not found. Nevertheless, the modification is retained because the theoretical improvement could sometimes be significant and implementation presents no computational problems.

An interesting fact is seen by comparing the viscosity plot for air (Fig. 4.17) with the thermal conductivity plot for air (Fig. 4.15) and the viscosity plot for methane (Fig. 4.18) with the thermal conductivity plot for methane (Fig. 4.16). In both cases the shape of the departure plot for thermal conductivity is similar to the departure plot for viscosity. Because the viscosity is calculated independently of the thermal conductivity while it is employed directly in the calculation of thermal conductivity, the viscosity error propagates into the conductivity calculation. The similar departure plots suggests that the viscosity calculation is a primary source of error in the conductivity calculated.

These calculation problems coupled with the simplifications in the numerical approach and the mathematical model limit, but do not preclude, observing important trends within the framework already outlined and concrete conclusions regarding the laminar flame problem are possible.

For stoichiometric methane the code derived flame

profiles, which are presented in Fig. 4.35 are classical in shape. Furthermore, it is seen from Table 4.3 that the flame thickness for a stoichiometric methane flame found in the code is .038cm. This represents the thickness of the reaction zone, whereas, traditionally the flame thickness is calculated to include the preheat zone, which is roughly the same size as the reaction zone. The experimentally observed flame thickness is around .2 cm,giving a reaction zone thickness around .1 cm. This is within an order of magnitidue of the calculated value.

That the flame thickness is predicted accurately for stoichiometric methane-air does not mean that equivalent accuracy will result when the mixture ratio is changed. Flame thickness, like flame speed, is related to the reaction rate which has been modelled as a simplex global reaction.

Nevertheless, Fig. 4.37, where flame thickness is graphed against mixture strength reveals a general thickening of the flame as the mixture strength is weakened and the general trend of flame speed reduction with mixture dilution is observed in both speed profiles presented in Fig. 4.36. Here, these trends in the flame structure are interpreted as a tendency towards susceptibility to extinction.

Because susceptibility to extinction is not precisely defined, a distinct extinction point is likewise strictly unattainable. This same arguement holds as well

for the self-extinction associated with the flammability limit.

A review of Figs. 4.34, 4.36 and 4.37 where different flame properties are plotted against initial fuel mass fraction reveals curves which undergo interesting changes near the flammability limit. In Fig. 4.37 the flame width doubles as the fuel mass fraction decreases from .032 cm to .029 cm, which is an interval containing the traditional flammability limit. Also, the calculated flame speed profile, intersects the experimental profile in Fig. 4.36 near the flammability limit. This is because the calculated flame speed curve falls slower at this point than the experimental curve. Finally, in Fig. 4.34, it is noticed that the ignition temperature near stoichiometric methane-air is nearly constant as the mixture strength weakens at a value near 950°K. In the interval between Y_O = .04 and Y_O = .03 the ignition temperature drops to around 750°K where it again levels out.

To predict a point where flame extinction susceptibility is so great that self-extinction is expected for the methane-air mixture, the flame speed profile trajectory method, already described is used in Fig. 4.36. The traditional flammability limit is predicted with an error of less than 13%.

This result is promising, considering the use of simplex global reaction kinetics. In the future this method

should be applied to a more sophisticated model.

Experiments suggest that buoyancy and multidimensional effects raise the lean flammability limit. As such, a numerical model developed to include these effects would expand the theoretical base for studying flammability limits. It is suggested that such development be pursued.

REFERENCES

CHAPTER 1

1. An Energy Strategy for Canada: Policies for Self-Reliance, Dept. of Energy, Mines and Resources Canada, Minister of Supply and Services Canada, Ottawa, 1976, pp. 52-53.
2. Barnea, Joseph, The Energy Crisis and the Future, Unitar Research Report No. 21, Unitar, New York, 1975, pp. 5.
3. Les Options Energetiques du Canada, Rapport no. 23, Science Council of Canada, Mars 1975 (SS22-1975/23F Canada) pp. 26.
4. Lichty, L.C., Combustion Engine Processes, McGraw-Hill Book Company, New York, 1967, p. 158.
5. Ibid, p. 62B.
6. Barnea, Joseph, op. cit.
7. Saber, A.J., Coal Conversion Project, Proprietary Report, Lignasco Resources Ltd., Toronto, Ontario, 14 Oct. 1980, p. 6.
8. Knelman, F.H., Energy Conservation, Science Council of Canada, Backgrounder Study no. 33, July 1975, p. 21.
9. Canada as a Conserver Society, Report no. 27, Science Council of Canada, September, 1977, p. 10.
10. Porter, F.C., Design for Fuel Economy - The New G.M. Front Drive Cars, SAE Paper, no. 790721.
11. Automotive Fuel Economy - Part 2, Progress in Technology Series, No. 18, S.A.E., 1979.

12. Spalding, D.B., Combustion and Mass Transfer, Pergamon Press, New York, 1979, pp. 1-24.

13. Strehlow, R.A., Fundamentals of Combustion, International Textbook Company, Scranton, Penn., 1968, chapt. 7.

14. Ibid, p. 206.

15. Kanury, A.M., Introduction to Combustion Phenomena (For Fire Incineration, Pollution, and Energy Applications), Gordon and Breach Science Publishers, N.Y., pp. 8-79, 1975.

16. Evans, M.J., Current Theoretical Concepts of Steady-State Flame Propagation, Chemical Reviews, 51, 363 (1952).

17. Tsatsaronis, G., Prediction of Propagating Laminar Flames in Methane, Oxygen, Nitrogen Mixtures, Combustion and Flame, 33, 217ff, (1978).

18. Bittker, D.A., and Scullin, V.J., General Chemical Kinetic Computer Program for Static and Flow Reactions with Application to Combustion and Shock-Tube Kinetics, NASA, TND-6586, 1972.

19. Moretti, G., A New Technique for the Numerical Analysis of Non-Equilibrium Flows, AIAA Journal, vol. 3, no. 2, p. 223, 1965.

20. Spalding, D.B., Stephenson, P.L., and Taylor, R.G., A Calculation Procedure for the Prediction of Laminar Flame Speeds, Combustion and Flame, 17, 55-64, (1971).

21. Lovachev, Babkin, Burev, V'Yun, Krivulin, Baratov, "Flammability Limits, An Invited Review", Combustion and Flame, 20, 259 (1973).

22. Sorenson, S.C., Savage, L.D., and Strehlow, R.A., "Flammability Limits - A New Technique," Combustion and

Flame, 24, 347 (1975).

23. Coward, H.F., Jones, G.W., "Limits of Flammability of Gases and Vapors," U.S. Bureau of Mines Bulletin, 1952.

24. Barnea, Joseph, op. cit., p. 75 and p. 47.

CHAPTER 2

1. Evans, M.J., Current Theoretical Concepts of Steady-State Flame Propagation, Chemical Reviews, 51, 363 (1952)

2. Williams, F.A., Combustion Theory, Addison-Wesley Publishing Co. Inc., Reading, Mass, 1965, p. 420.

3. Strehlow, R.A., Fundamentals of Combustion, International Textbook Co., Scranton, Penn., 1968, p. 196.

4. Bradley, J.N., Flame and Combustion Phenomena, Chapman and Hall Ltd., London, 1972, Chapter 5.

5. Mahan, B., College Chemistry, Addison-Wesley (Canada) Limited, Don Mills, Ont., 1966, p. 320.

6. Aly, S.L., Simpson, R.B., and Hermance, C.E., "Numerical Solution of the Two-Dimensional Premixed Laminar Flame Equations," AIAA Journal, 17, 1(1979).

7. Mahan, B., op. cit., p. 322.

8. Maron, S.H., and Lando, J.B., Fundamentals of Physical Chemistry, Macmillan Publishing Co. Inc., New York, N.Y. p. 676.

9. Bledjian, L., "Computation of Time Dependent Laminar Flame Structure", Combustion and Flame, 20, 5-17 (1973).

10. Badami, G.N., and Egerton, A., "The Determination of Burning Velocities in Slow Flames," Proc. Roy. Soc. A228,

297 (1955).

11. Williams, F.A., op. cit., p. 192.
12. Aly, S.L., Simpson, R.B., and Hermane, C.F., op. cit.
13. Lovachev, Babkin, Bunev, V'Yun, Krivilin, Baratov, "Flammability Limits: An Invited Review," Combustion and Flame, 20, 259, (1973).
14. Coward, J.F., and Jones, G.W., "Limits of Flammability of Gases and Vapours," U.S. Bureau of Mines Bulletin, 1952.
15. Lewis, B., and Von Elbe, G., Combustion Flames and Explosions of Gases, Academic Press, 1961, p. 310.
16. Spalding, D.B.," A Theory of Inflammability Limits and Flame Quenching," Proc. Roy. Soc., A240, 83 (1957).
17. Egerton, A.C., and Powling, J., Proc. Roy. Soc., A193, pp.172 and 190 (1948).
18. Lewis, B., and Von Elbe, op. cit., p. 310ff.
19. Lovachev et al, op cit. (1973).
20. Lewis, B., and Von Elbe, G.," Theory of Flame Propagation," Second Symposium (Int.) on Combustion, Combustion Institute, Pitts., Penn., 1954.
21. Aly, S.L., et al, op. cit.
22. Lovachev et al, op. cit. (1973).
23. Egerton, A.C., Fourth Symposium (Int.) on Combustion, Wiliams and Wilkins, Baltimore, p. 4, 1953.
24. Powling, J., Fuel, 28, 25 (1949).
25. Egerton, A.C. and Thabet, S.K., Proc. Roy. Soc. (London) A211, 445 (1952).
26. Badami, G.N., and Egerton, A., op. cit., (1955).

27. Dixon-Lewis, G., and Isles, G.L., Seventh Symposium (Int.) on Combustion, Butterworths, London, p. 475, 1959.

28. Badami, G.N., and Egerton, A., op. cit., (1955).

29. Sorenson, S.C., Savage, L.D., and Strehlow, R.A., "Flammability Limits - A New Technique," Combustion and Flame, 24, 347 (1975).

30. Penner, S.S., and Mullins, B.P., Explosions, Detonations, Flammability and Ignition, Pergamon Press, New York, N.Y., 1959, Chapter 6.

CHAPTER 3

1. Evans, M.J., "Current Theoretical Concepts of Steady-State Flame Propagation," Chemical Reviews, 51, 363 (1952).

2. Pierson, B.L., and Kutler, P., "Optimal Nodal Point Distribution for Improved Accuracy in Computation Fluid Dynamics," AIAA Journal, vol. 18, no. 1, 49 (1980).

3. Roache, Patrick J., Computation Fluid Dynamics, Hermosa Publishers, Albuquerque, N.M. , 1972, p. 16.

4. Chung, T.J., Finite Element Analysis in Fluid Dynamics, McGraw-Hill Int. Book Co., New York, N.Y. 1978, p. 1.

5. Hornbeck, R.W. Numerical Methods, Quantum Publishers Inc., New York, N.Y. 1975, p. 29.

6. Chung, T.J., op. cit., p. 133.

7. Roache, P.J., op. cit., p. 289.

8. Tang, J.W., and Turcke, D.J., "Characteristics of Variable Grids," Computer Methods in Applied Mechanics and Engineering, Vol. 11, pp. 31-37, (1977).

9. Felippa, C.A.,"Numerical Experiments in Finite Element Optimization by Direct Energy Search," Applied Numerical Modelling, Vol. 1, pp. 239-244 (1977).

10. Chung, T.J., op. cit., p. 50.

11. ibid, p. 41"

12. Milne, W.E., Numerical Solution of Differential Equations, Dover Publications, Inc., New York, N.Y., 1970, p. 114.

13. Roache, P.J., op. cit., pp. 28-33.

14. Chung, T.J., op. cit., p. 264.

15. Heinrich, J.C., Huyakorn, P.S., Zienkiewicz, O.C., and Mitchell, A.R.,"An Upwind Finite-Element Scheme for Two-Dimensional Convective Transport Equation," Intl. J. Num. Meth. Engng., 11, pp. 131-144 (1977).

16. Roache, P.J., op. cit., p. 191.

17. Moretti, G.,"Analysis of Two-Dimensional Problems of Supersonic Combustion Controlled by Mixing,"AIAA paper, 64-96, (Jan. 1964).

18. Moretti, G.,"A New Technique for the Numerical Analysis of Non-Equilibrium Flows,"AIAA Journal, Vol. 3, No. 2, p. 223 (1965).

19. Treanor, C.E.,"A Method for the Numerical Integrating of Coupled First Order Differential Equations with Greatly Different Time Constants,"Math. Comp., Vol. 20, p. 39, (1966).

20. Lilley, D.G.,"Methods for Rapid Solution of Stiff Systems of Diffusion/Reaction Equations," Presented at Combustion

Institute (Canadian Section) Meeting, held in Ottawa, Canada, May 4-5, 1978.

21. Tyson, T.J.,"An Implicit Integration Method for Chemical Kinetics," Report No. 9840-6002-R000, TRW Space Tech, Lab., Redondo Beach, California, Spet. 1964.

22. Kligel, J.R., Tyson, T.J. ,"Discussion of Chemical Kinetics Integration Techniques", Paper 45-68, Combustion Institute, Oct. 1968.

23. Bittker, D.A., Scullin, V.J.,"General Chemical Kinetic Computer Program for Static and Flow Reactions with Application to Combustion and Shock-Tube Kinetics," NASA, TND-6586, 1972.

24. Hirschfelder, J.O., Curtiss, C.F. and Campbell, D.F., "The Theory of Flame Propagation IV," Journal of Physical Chemistry, Vol. 57, pp. 403-414, (1953).

25. Dixon-Lewis, G.,"Flame Structure and Flame Reaction Kinetics I: Solution of Conservation Equations and Application to Rich Hydrogen-Oxygen Flames", Proceedings of the Royal Society of London, Vol. A298, pp. 495-513 (1967).

26. Spalding, D.B., Aircraft Engrg., 25, 264 (1953).

27. Spalding, D.B., Stephenson, P.L., Taylor, R.C., A "Calculation Procedure for the Prediction of Laminar Flame Speeds", Combustion and Flame, 17, pp. 55-64 (1971).

28. Spalding, D.B.,"The Theory of Flame Phenomena with a Chain Reaction,"Phil. Trans. Roy. Soc. London, A249, pp. 1-25 (1956).

29. Howarth, L., Proc. Roy. Soc., A194, p. 16 (1948).

30. Patankar, S.V. and Spalding, D.B., "Heat and Mass Transfer in Boundary Layers", 2nd Ed., Intertext Books, London, 1970.

31. Tsatsaronis, G., "Prediction of Propagating Laminar Flames in Methane, Oxygen, Nitrogen Mixtures," Combustion and Flame, 33, p. 217 (1978).

32. Aly, S.L., Simpson, R.B., and Hermance, C.E., "Numerical Solution of the Two-Dimensional Premixed Laminar Flame Equations," AIAA Journal, 17, 1 (1979).

33. Butler, T.D., O'Rourke, P.J., "A Numerical Method for Two-Dimensional Unsteady Reacting Flows," Sixteenth Symposium (int.) on Combustion, The Combustion Institute, p. 1503, (1976).

34. Wilde, K.A., "Boundary-Value Solutions of the One-Dimensional Laminar Flame Propagation Equations," Combustion and Flame, 18, pp. 43-52 (1972).

35. Bledjian, L., "Computation of Time-Dependent Laminar Flame Structure," Combustion and Flame, 20, 5-17 (1973).

36. Huebner, K.H., The Finite Element Method for Engineers, John Wiley and Sons, New York, N.Y., 1975.

37. Wilkins, R.L., Theoretical Evaluation of Chemical Propellants, Prentice-Hall Inc., Englewood Cliffs, N.J., 1963, Chap. 1.

38. Touloukian, Y.S., Liley, P.E., Saxena, S.C., Thermal Conductivity-Nonmetallic Liquids and Gases, The TPRC Data Series, Vol. 3, IFI/Plenum, New York, N.Y., 1970, pp. 35a-37a.

39. Strehlow, R.A., Fundamentals of Combustion, International Textbook Co., Scranton, Penn., 1968, p. 71.

40. Wilke, C.R., J. Chem. Phys., 18, 517 (1950).

41. Touloukian, Y.S., Makita, T., Specific Heat, The TPRC Data Series, Vol. 6, IFI/Plenum, New York, N.Y., 1970, p. 293.

42. Holman, J.P., Heat Transfer, McGraw-Hill Book Co., New York, 1963, p. 503.

43. Touloukian, Y.S., Makita, T., op. cit., p. 246.

44. Wilkins, R.L., op. cit., p. 411.

CHAPTER 4

1. Chung, T.J., Finite Element Analysis in Fluid Dynamics, McGraw-Hill Book Co., New York, 1978, p. 315.

2. Holman, J.P., Heat Transfer, McGraw-Hill Book Co., New York, 1963, p. 187.

3. Sellars, J.R., Tribus, M., Klein, J.S., "Heat Transfer to Laminar Flows in a Round Tube or Flat Conduit: The Graetz Problem Extended," Trans. ASME, Vol. 78, p. 441 (1956).

4. Wilkins, R.L., Theoretical Evaluation of Chemical Propellants, Prentice-Hall Inc., Englewood Cliffs, N.J., 1963.

5. Holman, J.P., op. cit., p. 503.

6. Hirschfelder, J.O., Curtiss, C.F. and Bird, R.B., Molecular Theory of Gases and Liquids, Wiley, New York, 1954.

7. Touloukian, Y.S., Liley, P.E., Saxena, S.C., Thermal Conductivity-Nonmetallic Liquids and Gases, The TPRC Data Series, Vol. 3, IFI/Plenum, New York, 1970, p. 218.

8. ibid, p. 512.

9. ibid, p. 37a.

10. Touloukian, Y.S., Saxena, S.C., Hestermans, P., Viscosity, The TPRC Data Series, Vol. 11, IFI/Plenum, New York, 1970.

11. Aly, S.L., Simpson, R.B., Hermance, C.E.," Numerical Solution of the Two-Dimensional Premixed Laminar Flame Equations," AIAA Journal, 17, 56 (1979).

APPENDIX D

1. Kanury, A.M., Introduction to Combustion Phenomena, Gordon and Breach Science Publishers, New York, N.Y., 1975, p. 51.

2. Touloukian, Y.S., Liley, P.E., Saxena, S.C., Thermal Conductivity-Nonmetallic Liquids and Gases, IFI/Plenum, New York, N.Y., 1970, p. 35aff

APPENDIX E

1. Aly, S.L., Simpson, R.B., Hermance, C.E.,"Numerical Solution of the Two-Dimensional Premixed Laminar Flame Equations," AIAA Journal, 17, 1 (1979).

APPENDIX A

A. Mathematical Formulation of the Laminar Flame Equations

A-1: Overall Continuity Equation

From Figure A.1

$$G_x - G_1 = -Gacc \qquad (A.1.1)$$

and $$G_1 = \rho_1 u_1 \; ; \; G_x = \rho_x u_x \qquad (A.1.1.1)$$

where $$Gacc = \frac{d}{dt} \int_1^x \rho dx \qquad (A.1.1.2)$$

Hence

$$\rho_1 u_1 - \rho_x u_x = \frac{d}{dt} \int_1^x \rho dx \qquad (A.1.2)$$

Differentiating gives

$$\frac{d}{dt}(\rho) + \frac{d}{dx}(\rho u) = 0 \qquad (A.1.4)$$

and for steady state $$\frac{d}{dt}(\rho) = 0 \qquad (A.1.3)$$

$$\therefore G = \text{constant} \qquad (A.1)$$

A.2: Momentum Equation

From Figure A.1

$$\frac{d}{dt} \int_1^x (\rho u) dx = \sum F + u_1 (\rho u)_1 - u_x (\rho u)_x \qquad (A.2.1)$$

Differentiating gives

$$\frac{d}{dt}(\rho u) + \frac{d}{dx}(\rho u^2) = -\frac{d}{dx}(\rho) \qquad (A.2.2)$$

For steady-state and constant pressure

$$\frac{d}{dx}(\rho u^2) = 0 \qquad \text{(A.2.3)}$$

$$p = \text{constant} \qquad \text{(A.2)}$$

A.3: Species Equation

From Figure A.1

with

$$\dot{m}_{i_1} = G_{i_1} A \qquad \text{(A.3.1.1)}$$

$$\dot{m}_{i_x} = G_{i_x} A \qquad \text{(A.3.1.2)}$$

$$\dot{m}_{iacc} = \frac{d}{dt} \int_1^x (\rho_i A)\, dx \qquad \text{(A.3.1.3)}$$

$$\dot{m}_{i_{gen}} = \int_1^x R_i A dx \qquad \text{(A.3.1.4)}$$

$$\frac{d}{dx}(\dot{m}_{i_1} - \dot{m}_{i_x}) = \frac{d}{dx}(\dot{m}_{iacc} - \dot{m}_{i_{gen}}) \qquad \text{(A.3.1)}$$

$$\frac{dG_i}{dx} = R_i - \frac{d}{dt}(\rho_i) \qquad \text{(A.3.2)}$$

For a steady state flame front

$$\frac{d\rho_i}{dt} = 0$$

and

$$\frac{dG_i}{dx} = R_i \qquad \text{(A.3.3)}$$

By definition, $G_{convi} + G_{diffi} = Gi$ (A.3.4)

where G_{convi} = movement of species i because of convection

G_{diffi} = movement of species i because of diffusion

G_i = movement of species i

$$G_{convi} = \rho_i u \quad \text{(A.3.5)}$$

$$G_{diffi} = \rho D_i \frac{dY_i}{dx} \quad \text{- Ficks Law -} \quad \text{(A.3.6)}$$

Using equations A.3.5 and A.3.6, equation A.3.2 can be rewritten

$$\frac{d}{dx}(\rho Y_i u - \rho D_i \frac{dY_i}{dx}) = R_i \quad \text{(A.3.7)}$$

To simplify A.3.7 the following non-essential assumptions are now made

c_p = constant and uniform (A.3.8.1)

ρD = constant (A.3.8.2)

k = constant (A.3.8.3)

This allows the equation A.3.7 to be rewritten as

$$G\frac{dY_i}{dx} - \rho D\frac{d^2Y_i}{dx^2} = R_i \quad \text{(A.3.8)}$$

If the variables are now normalized so

$$\alpha_i = \frac{Y_i}{Y_0} \quad \rightarrow Y_i = Y_0\alpha_i \quad \text{(A.3.9.1)}$$

$$\frac{dY_i}{dx} = Y_0\frac{d\alpha_i}{dx} \quad \text{(A.3.9.2)}$$

$$\frac{d^2Y_i}{dx^2} = Y_0 \frac{d^2\alpha_i}{dx^2} \qquad (A.3.9.3)$$

and L = lewis number = $\frac{\rho c_p D}{k}$ (A.3.9.4)

Hence the equation is

$$\frac{C_p G}{k} Y_0 \frac{d\alpha_i}{dx} - \frac{\rho Dc}{k} \frac{d^2\alpha_i}{dx^2} = \frac{R_i C_p}{k} \qquad (A.3.9)$$

In this work interest is in the special case when only a single global reaction is involved. Hence

$$LY_0 \frac{d^2\alpha}{dx^2} - \frac{GY_0}{k} C_p \frac{d\alpha}{dx} = -\frac{R_F C_p}{k} \qquad (A.3)$$

A.4: The Energy Equation

From Figure A.1, the energy equation can be written by knowing that the energy crossing a flow boundary of the control volume is

$$E = \sum_{i=1}^{n} G_i h_i + Q_{cond} + \frac{Gu^2}{2} + W_s \qquad (A.4.1)$$

where E = energy crossing boundary

h_i = enthalpy of species i

n = number of species present

W_s = shaft work

Q_{cond} = heat conduction in the flow direction

and the energy accumulation is

$$E_{acc} = \frac{d}{dt} \int_1^x \sum^1 (\rho_i E_i) dx \qquad (A.4.2)$$

and the energy loss to surroundings through heat transfer is

$$E_L = \int_1^x q_2 dx \qquad (A.4.3)$$

For steady-state $E_{acc}=0$.

$$\therefore \quad \frac{dE}{dx} + \frac{dE_L}{dx} = 0 \qquad (A.4.4)$$

Hence

$$\frac{d}{dx}(\sum G_i h_i + Q_{cond}) + q_L = 0 \qquad (A.4.5)$$

Looking at the first term in equation A.4.5

$$\frac{d}{dx}(\sum G_i h_i) = \sum \frac{d}{dx}(G_i h_i)$$

$$= \sum G_i \frac{dh_i}{dx} + \sum h_i \frac{dG_i}{dx}$$

$$\frac{d}{dx}(\sum G_i h_i) = \sum G_i \frac{d}{dx}(C_p T + h_{oi}) + \sum h_i \frac{dG_i}{dx} \qquad (A.4.6)$$

Where h_{oi} = chemical enthalpy content on species i

Rearranging and substituting in the species equation A.3.3 into A.4.6 gives

$$\frac{d}{dx}(\sum G_i h_i) = C_p \frac{dT}{dx}(\sum G_i) + \frac{dh_{oi}}{dx}(\sum G_i) + \sum h_i R_i$$

which gives

$$\frac{d}{dx}(\sum G_i h_i) = C_p G \frac{dT}{dx} - \sum h_i W_i \qquad (A.4.7)$$

Substituting A.4.7 into A.4.5 gives

$$c_p G \frac{dT}{dx} + \sum h_i R_i + \frac{d}{dx}(Q_{cond}) + q_L = 0 \qquad (A.4.8)$$

Noting that Fourier's Law of heat transfer is

$$\frac{d}{dx}(Q_{cond}) = -\frac{d}{dx}(k \frac{dT}{dx}) \qquad (A.4.9.1)$$

Hence A.4.8 becomes A.4.9.1

$$c_p G\frac{dT}{dx} + \sum h_i R_i - \frac{d}{dx}\left(k\frac{dT}{dx}\right) + q_L = 0 \qquad \text{(A.4.9)}$$

Rearranging and noting that a single reaction is involved yields

$$-\frac{d^2T}{dx^2} - c_p G\frac{dT}{dx} = \frac{H_C R_F}{k} + \frac{q_L}{k} \qquad \text{(A.4)}$$

APPENDIX B

B. Finite Element Formulation

B.1: Species Equation

Writing the species equation A.3.10 so that its linearity becomes apparent gives

$$LY_o\frac{d^2\alpha}{dx^2} - \frac{c_pG}{k}Y_o\frac{d\alpha}{dx} - F(T)\alpha = 0 \qquad (B.1.1)$$

By Galerkin's method with upwinding

$$\xi = LY_o\frac{d^2\tilde{\alpha}}{dx^2} - \frac{c_pG}{k}Y_o\frac{d\tilde{\alpha}}{dx} - F(T)\tilde{\alpha} \qquad (B.1.2)$$

where

$$\tilde{\alpha} = \sum_{j=1}^{N}\phi_j\alpha_j \simeq \alpha \qquad (B.1.3)$$

N = no. of nodes in discretized solution regime.

Now

$$(\xi, W) = \int_D (\xi \cdot W)\,dD = 0 \qquad (B.1.4)$$

where W = weighting function

Substituting B.1.2 into B.1.4 gives

$$\int_D \left(LY_o\frac{d^2\tilde{\alpha}}{dx^2} - \frac{GY_oc_p}{k}\frac{d\tilde{\alpha}}{dx} - F(T)\tilde{\alpha}\right)W_i\,dx = 0 \qquad (B.1.5)$$

If the second order term of B.1.5 is integrated by parts

$$\int_D LY_o\frac{d^2\tilde{\alpha}}{dx^2}W_i\,dx = LY_oW_i\frac{d\tilde{\alpha}}{dx}\Big|_\Gamma - LY_o\int_D \frac{d\tilde{\alpha}}{dx}\frac{dW_i}{dx}\,dx \qquad (B.1.6)$$

Substituting B.1.6 into B.1.5 gives

$$LY_o \int_D \frac{d\tilde{\alpha}}{dx} \frac{dW_i}{dx} dx + \frac{GY_o c_p}{k} \int_D \frac{d\tilde{\alpha}}{dx} W_i dx$$

$$+F(T) \int_D (\tilde{\alpha} W_i) dx - LY_o W_i \frac{d\tilde{\alpha}}{dx}\Big|_\Gamma = 0 \qquad \text{(B.1.7)}$$

Transforming the finite element equation from global to local coordinates, the boundary conditions may be dropped from the formula and applied separately to the global matrix to be constructed later. Hence

$$\int_o^h \left(LY_o \frac{d\phi_M}{dx} \frac{dW_N}{dx} + \frac{c_p G}{k} Y_o \frac{d\phi_M}{dx} W_N + F(T) \phi_M W_N\right) dx \{\alpha\}_M = 0 \qquad \text{(B.1.8)}$$

where $N = 1,2$ and $M = 1,2$

for linear 1-D elements and

ϕ = elemental functions.

Introducing the following symbols

$$A_{NM} = \int_o^h [LY_o \frac{d\phi_M}{dx} \frac{dW_N}{dx}] dx \qquad \text{(B.1.9.1)}$$

$$B_{NM} = \int_o^h \frac{c_p G}{k} Y_o \frac{d\phi_M}{dx} W_N \, dx \qquad \text{(B.1.9.2)}$$

$$C_{NM} = \int_o^h (F(T) \phi_M W_N) dx \qquad \text{(B.1.9.3)}$$

The following equation results

$$(A_{NM} + B_{NM} + C_{NM})\{\alpha\} = 0 \qquad \text{(B.1.9)}$$

Giving the matrix

$$\begin{bmatrix} A_{11} + B_{11} + C_{11} & A_{12} + B_{12} + C_{12} \\ A_{21} + B_{21} + C_{21} & A_{22} + B_{22} + C_{22} \end{bmatrix} \begin{Bmatrix} \alpha_1 \\ \alpha_2 \end{Bmatrix} = 0 \quad \text{(B.1.10)}$$

Now the elemental functions are defined:

$$\phi_1 = 1 - \frac{x}{h} \; ; \; \frac{d\phi_1}{dx} = -\frac{1}{h} \quad \text{(B.1.11.1)}$$

$$\phi_2 = \frac{x}{h} \; ; \; \frac{d\phi_2}{dx} = \frac{1}{h} \quad \text{(B.1.11.2)}$$

For upwinding the weighting functions are different from the elemental functions

$$W_N = \phi_N + \zeta_N \quad \text{(B.1.11.3)}$$

where

$$\zeta_1 = \frac{3f}{h^2}(x^2 - hx) \; ; \; \frac{d\zeta_1}{dx} = \frac{3f}{h^2}(2x-h)$$

$$\zeta_2 = -\frac{3f}{h^2}(x^2 - hx) \; ; \; \frac{d\zeta_2}{dx} = -\frac{3f}{h^2}(2x-h)$$

and therefore

$$W_1 = 1 - \frac{1+3f}{h} x + \frac{3fx^2}{h} \quad \text{(B.1.11.4)}$$

$$\frac{dW_1}{dx} = -\frac{1+3f}{h} + \frac{6fx}{h^2} \quad \text{(B.1.11.5)}$$

$$W_2 = \left(\frac{1}{h} + \frac{3f}{h}\right)x - \frac{3fx^2}{h^2} \quad \text{(B.1.11.6)}$$

$$\frac{dW_2}{dx} = \left(\frac{1}{h} + \frac{3f}{h}\right) - \frac{6fx}{h^2} \quad \text{(B.1.11.7)}$$

Now by substituting B.1.11.1; B.1.11.2, B.1.11.4, B.1.11.5, B.1.11.6 and B.1.11.7 into B.1.9.1, B.1.9.2, B.1.9.3 and

B.1.9.4 the integrals can be evaluated to give

$$A_{11} = A_{22} = \frac{LY_o}{h} \qquad \text{(B.1.12.1)}$$

$$A_{12} = A_{21} = -\frac{LY_o}{h} \qquad \text{(B.1.12.2)}$$

$$B_{11} = \frac{Gc_p}{k} Y_o\left(-\frac{1}{2} + \frac{f}{2}\right) \qquad \text{(B.1.12.3)}$$

$$B_{22} = \frac{Gc_p}{k} Y_o\left(\frac{1}{2} + \frac{f}{2}\right) \qquad \text{(B.1.12.4)}$$

$$B_{12} = \frac{Gc_p}{k} Y_o\left(\frac{1}{2} - \frac{f}{2}\right) \qquad \text{(B.1.12.5)}$$

$$B_{21} = \frac{Gc_p}{k} Y_o\left(-\frac{1}{2} - \frac{f}{2}\right) \qquad \text{(B.1.12.6)}$$

$$C_{11} = F(T)\left(\frac{h}{3} - \frac{fh}{4}\right) \qquad \text{(B.1.12.7)}$$

$$C_{22} = F(T)\left(\frac{h}{3} + \frac{fh}{4}\right) \qquad \text{(B.1.12.8)}$$

$$C_{12} = F(T)\left(\frac{h}{6} - \frac{fh}{4}\right) \qquad \text{(B.1.12.9)}$$

$$C_{21} = F(T)\left(\frac{h}{6} + \frac{fh}{4}\right) \qquad \text{(B.1.12.10)}$$

Substituting B.1.12.1 to B.1.12.10 into B.1.10 yields the elemental species matrix given in Fig. B.1.

B.2: Energy Equation

The energy equation is strongly non-linear in the reaction rate terms. With the second and first order derivatives

$$\left[\begin{array}{c|c} \frac{LY_o}{h}+\frac{GC_f}{k}Y_o\left[-\frac{1}{2}+\frac{f}{2}\right]+ & -\frac{LY_o}{h}+\frac{GC_f}{k}Y_k\left[\frac{1}{2}-\frac{f}{2}\right]+ \\ CONST\cdot\left(\frac{h}{3}+\frac{fh}{4}\right) & CONST\cdot\left(\frac{h}{6}-\frac{fh}{4}\right) \\ \hline -\frac{LY_o}{h}+\frac{GC_f}{k}Y_o\left[-\frac{1}{2}-\frac{f}{2}\right]+ & \frac{LY_o}{h}+\frac{GC_f}{k}Y_o\left[\frac{1}{2}+\frac{f}{2}\right]+ \\ CONST\cdot\left(\frac{h}{6}+\frac{fh}{4}\right) & CONST\cdot\left(\frac{h}{3}+\frac{fh}{4}\right) \end{array}\right] \left\{\begin{array}{c}\alpha_1\\ \alpha_2\end{array}\right\} = \left[\begin{array}{c} 0 \\ 0 \end{array}\right]$$

Table B.1 - Evaluated Species Matrix (Elemental)

on the left hand side, the reaction rate term is viewed as a forcing function in this formulation.

Writing the energy equation A.4

$$\frac{d^2T}{dx^2} - \frac{c_p G}{k}\frac{dT}{dx} = \frac{H_c R_F}{k} + \frac{q_L}{k} \qquad (B.2.1)$$

Applying Galerkin's method

$$-q_2 + \frac{d^2T}{dx^2} - \frac{c_p G}{k}\frac{d\tilde{T}}{dx} - \frac{H_c R_F}{k} = \xi \qquad (B.2.2)$$

$$(\xi, W) = \int_D (\xi \cdot W)\, dD = 0 \qquad (B.2.3.1)$$

This gives

$$\int_D \left[\frac{d^2T}{dx^2} - \frac{c_p G}{k}\frac{dT}{dx} - \frac{H_c R_F}{k} - \frac{q_L}{k}\right] \cdot W dD = 0 \qquad (B.2.3)$$

Integrating the second order term of B.2.3 by parts and substituting back into B.2.3 gives

$$\int_D \left(\frac{d\tilde{T}}{dx}\frac{dW_i}{dx} + \frac{c_p G}{k}\frac{dT}{dx}W_i + \frac{H_c R_F}{k}W_i + \frac{q_L}{k}W_i\right) dD - W_i \frac{d\tilde{T}}{dx}\bigg|_\Gamma = 0 \qquad (B.2.4)$$

Where the last term represents the heat transfer at the flow boundary and q_L is the heat lost to the surrroundings:

$$q_L = q_r + q_c$$

where q_r = heat loss due to radiation

$$= \sigma_r \varepsilon_r A_r (T^4 - T_\infty^4) \qquad (B.2.5.1)$$

q_c = heat loss across a convection sheet

$$= H A_r (T - T_\infty) \qquad (B.2.5.2)$$

where A_r = heat loss area

σ_r = Stefan-Boltzmann constant

ε_r = surface emissivity

T_∞ = ambient temperature

Hence

$$\frac{q_L}{k} = \frac{\sigma_r \varepsilon_r A_r}{k} (T^4 - T_\infty^4) + \frac{HA_r}{k} (T - T_\infty) \qquad (B.2.5.3)$$

Substituting B.2.5.3 into B.2.4 gives

$$\int_D \left[\frac{d\tilde{T}}{dx} \frac{dW_i}{dx} + \frac{c_p G}{k} \frac{d\tilde{T}}{dx} W_i + \frac{H_C R_F}{k} W_i + \frac{\sigma_r \varepsilon_r A_r}{k} (\tilde{T}^4 - T_\infty^4) + \frac{HA_r}{k} (\tilde{T} - T_\infty) \right] dD - W_i \frac{d\tilde{T}}{dx}\Big|_\Gamma = 0 \qquad (B.2.5)$$

and changing to local coordinates

$$\int_o^h \left[\frac{d\phi_M}{dx} \frac{dW_N}{dx} + \frac{c_o G}{k} \frac{d\phi_M}{dx} W_N + \frac{\sigma_r \varepsilon_r A_r}{k} T(e)^3 + \frac{A_r H}{k} \phi_M W_N \right] dx$$

$$= \int_o^h \left[\frac{A_r \sigma_r \varepsilon_r}{k} T_\infty^4 + \frac{A_r H}{k} T_\infty + \frac{H_C R_F}{k} \right] W_N \, dx \qquad (B.2.6)$$

In this formulation, the same elemental functions and weighting function are used as in the species equation. Now introducing convenient symbols

$$A_{NM} = \int_o^h \left(\frac{d\phi_M}{dx} \cdot \frac{dW_N}{dx} \right) dx \qquad (B.2.7.1)$$

$$B_{NM} = \int_o^h \left(\frac{c_p G}{k} \cdot \frac{d\phi_M}{dx} \right) W_N \, dx \qquad (B.2.7.2)$$

$$C_{NM} = \int_o^h \left(\frac{\sigma_r \varepsilon_r A_r}{k} T(e)^3 + \frac{A_r H}{k} \right) \phi_M W_N dx \qquad (B.2.7.3)$$

$$D_N = \int_o^h \left(\frac{A_r \sigma_r \varepsilon_r}{k} T_\infty^4 + \frac{A_r H}{k} T_\infty + \frac{H_C R_F}{k} \right) W_N dx \qquad (B.2.7.4)$$

Gives

$$(A_{NM} + B_{NM} + C_{NM})\{T\} = D_N \qquad (B.2.7)$$

and the following elemental matrix results

$$\begin{bmatrix} A_{11} + B_{11} + C_{11} & A_{12} + B_{12} + C_{12} \\ A_{21} + B_{21} + C_{21} & A_{22} + B_{22} + C_{22} \end{bmatrix} \begin{Bmatrix} T_1 \\ T_2 \end{Bmatrix} = \begin{bmatrix} D_1 \\ D_2 \end{bmatrix} \qquad (B.2.8)$$

Introducing the elemental functions and weighting functions into B.2.7.1, B.2.7.2, B.2.7.3 and B.2.7.4 allows the following integral evaluations

$$A_{11} = A_{22} = \frac{1}{h} \qquad (B.2.9.1)$$

$$A_{12} = A_{21} = -\frac{1}{h} \qquad (B.2.9.2)$$

$$B_{11} = \frac{c_p G}{k}\left(-\frac{1}{2} + \frac{f}{2}\right) \qquad (B.2.9.3)$$

$$B_{22} = \frac{c_p G}{k}\left(\frac{1}{2} + \frac{f}{2}\right) \qquad (B.2.9.4)$$

$$B_{12} = \frac{c_p G}{k}\left(\frac{1}{2} - \frac{f}{2}\right) \qquad (B.2.9.5)$$

$$B_{21} = \frac{c_p G}{k}\left(-\frac{1}{2} - \frac{f}{2}\right) \qquad (B.2.9.6)$$

$$C_{11} = \left(\frac{\sigma_r \varepsilon_r A_r}{k} T_{(e)}^3 + \frac{A_r H}{k}\right) \frac{h}{3} - \frac{fh}{4} \qquad (B.2.9.7)$$

$$C_{22} = \left(\frac{\sigma_r \varepsilon_r A_r}{k} T_{(e)}^3 + \frac{A_r H}{k}\right) \frac{h}{3} + \frac{fh}{4} \qquad (3.2.9.8)$$

$$C_{12} = \left(\frac{\sigma_r \varepsilon_r A_r}{k} T_{(e)}^3 + \frac{A_r H}{k} \right) \frac{h}{6} + \frac{fh}{4} \qquad \text{(B.2.9.10)}$$

$$C_{21} = \left(\frac{\sigma_r \varepsilon_r A_r}{k} T_{(e)}^3 + \frac{A_r H}{k} \right) \frac{h}{6} - \frac{fh}{4} \qquad \text{(B.2.9.11)}$$

$$D_1 = \left(\frac{A_r \sigma_r \varepsilon_r}{k} T_\infty^4 + \frac{A_r H}{k} T_\infty + \frac{H_C R_F}{k} \right) \frac{h}{2} - \frac{fh}{2} \qquad \text{(B.2.9.12)}$$

$$D_2 = \left(\frac{A_r \sigma_r \varepsilon_r}{k} T_\infty^4 + \frac{A_r H}{k} T_\infty + \frac{H_C R_F}{k} \right) \frac{h}{2} - \frac{fh}{2} \qquad \text{(B.2.9.13)}$$

Substituting these evaluated integrals into B.2.8 results in the element matrix shown in Fig. B.2.

$$\left[\begin{array}{c|c} \frac{1}{h}+\frac{GC_p}{k}\left[-\frac{1}{2}+\frac{f}{2}\right]+ & -\frac{1}{h}+\frac{GC_p}{k}\left[\frac{1}{2}+\frac{f}{2}\right]+ \\ \left[\frac{\sigma_r \epsilon_r A_r}{k} T_e^3+\frac{A_r H}{k}\right]\left(\frac{h}{3}-\frac{fh}{4}\right) & \left[\frac{\sigma_r \epsilon_r A_r}{k} T_e^3+\frac{A_r H}{k}\right]\left(\frac{h}{6}-\frac{fh}{4}\right) \\ \hline -\frac{1}{h}+\frac{GC_p}{k}\left[\frac{1}{2}-\frac{f}{2}\right]+ & \frac{1}{h}+\frac{GC_p}{k}\left[\frac{1}{2}+\frac{f}{2}\right]+ \\ \left[\frac{\sigma_r \epsilon_r A_r}{k} T_e^3+\frac{AH}{k}\right]\left(\frac{h}{6}+\frac{fh}{4}\right) & \left[\frac{\sigma_r \epsilon_r A_r}{k} T_e^3+\frac{A_r H}{k}\right]\left(\frac{h}{3}+\frac{fh}{4}\right) \end{array}\right] \left\{\begin{array}{c} T_1 \\ T_2 \end{array}\right\} = \left[\begin{array}{c} \left[\frac{\sigma_r A_r \epsilon_r}{k} T_\infty^4+\frac{A_r H}{k} T_\infty+\frac{H_c R_c}{k}\right]\left(\frac{h}{2}-\frac{fh}{2}\right) \\ \hline \left[\frac{\sigma_r A_r \epsilon_r}{k} T_\infty^4+\frac{A_r H}{k} T_\infty+\frac{H_c R_c}{k}\right]\left(\frac{h}{2}-\frac{fh}{2}\right) \end{array}\right]$$

Table B-2: Evaluated Energy Matrix (Elemental)

APPENDIX C

C. Calculation of Convection Rate

From Appendix A, the species equation for a control volume is

$$LY_o \frac{d^2\alpha}{dx^2} - \frac{GY_o c_p}{k} \frac{d\alpha}{dx} = -\frac{R_F c_p}{k} \qquad (C.1)$$

If the boundaries of the control volume are located a long distance from the flame front, the second order diffusion term becomes negligible. Hence the equation reduces to

$$G\frac{d\alpha}{dx} = R_F \qquad (C.2)$$

and

$$G = \frac{\int_{-\infty}^{\infty} R_F dx}{(\alpha_\infty - \alpha_{-\infty})} \qquad (C.3)$$

APPENDIX D

D. Calculation of Thermal Conductivity

From modified Chapman-Enskog theory the self diffusion coefficient can be calculated by (1).

$$D_S = 2.662.821 \frac{\sqrt{T^3/M}}{p\sigma^2 \Omega_D} \ cm^2/s \qquad (D.1)$$

and viscosity can be calculated by (1)

$$u = 2.669(10^{-5}) \frac{\sqrt{TM}}{\sigma^2 \Omega_u} \ \frac{g}{cm-s} \qquad (D.2)$$

Also, the ideal gas law is

$$\rho = \frac{pM}{RT} \ \frac{g}{cm^3} \qquad (D.3)$$

Hence the ratio

$$\frac{\rho D_s}{u} = 9.98459(10^7) \ \frac{p}{R} \frac{\Omega_u}{\Omega_D} \qquad (D.4)$$

Substituting in consistent values for $\bar{R}$ and P gives

$$\frac{\rho D_S}{u} = 1.2008506 \ \frac{\Omega_u}{\Omega_D} \qquad (D.5)$$

Now, by Euchens formula (2)

$$k = \eta u C_v$$

where η = correction factor

To calculate η (2)

$$\eta = \frac{\rho D_S}{u C_v} \ C_p - \frac{5}{2}R + \frac{15}{4} \frac{R}{C_v} + \text{CORRECTION} \qquad (D.6)$$

where; correction = a correction factor to account for the time required for translational - internal energy equilibration.

CORRECTION is calculated by

$$\text{CORRECTION} = -\frac{3}{2}\frac{R}{(C_v)^2}\left(\frac{5}{2} - \frac{\rho D}{u}\right)C_p - \frac{5}{2}R\left(1-\exp\left(-\frac{2}{3}\frac{C_v}{RZ}\right)\right) \tag{D.7}$$

where Z = number of collisions required for translational-internal energy equilibration

If Z is very large, this whole correction factor approaches zero.

Adding all these terms and manipulating them algebraicly, the following formulation for thermal conductivity is derived:

$$k = \left[\frac{\rho D_s}{u} + \frac{3}{2}\frac{R}{C_v}\left(\frac{5}{2} - \frac{\rho D_s}{u}\right) - \frac{2}{3}\frac{R}{C_v}\left(\frac{5}{2} - \frac{\rho D_s}{u}\right)\left(1 - \frac{3}{2}\frac{R}{C_v}\right) \times\left(1-\exp\left(-\frac{2}{3}\frac{C_v}{RZ}\right)\right)\right]\mu C_v \tag{D.8}$$

APPENDIX E

E. Forward Stepping Finite Difference Solution of Species Equation (with Lewis No. equal to zero)

Using equation A.3 describing species transport

$$LY_o \frac{d^2\alpha}{dx} - \frac{Gc_p}{k} Y_o \frac{d\alpha}{dx} - \text{CONST.}\left(\frac{\alpha}{T} \exp\left(-\frac{E}{RT}\right)\right) \qquad (E.1)$$

Assuming L = 0 and expressing the equation discretely using finite differences gives

$$\frac{-c_p G}{k} Y_o \left[\frac{\alpha_i - \alpha_{i-1}}{h}\right] = \text{const.} \frac{\alpha_i}{T_i} \exp\left(-\frac{E}{RT_i}\right) \qquad (E.2)$$

Rearranging this equation gives

$$\alpha_i = \left[\frac{1}{1 + \text{const} \frac{h}{GT_i} \exp\left(-\frac{E}{RT_i}\right)}\right] \alpha_{i-1} \qquad (E.3)$$

This equation is exactly the same as Aly's who solved the case when L = 0 (1).

APPENDIX F- COMPUTER CODE LISTING

```
      PROGRAM STREAK(INPUT,OUTPUT)
C THIS PROGRAM SOLVES THE LAMINAR FLAME  EQUATIONS
C THE CHEMICAL KINETICS ARE GOVERNED BY A SIMPLEX REACTION.
C THE LEWIS NUMBER IS VARIABLE.
C THE DISCRETIZED EQUATIONS ARE FORMULATED USING FINITE ELEMENT
C THEORY.  THE CONVECTION TERMS ARE DEALT WITH BY STRAIGHT
C SUBSTITUTION. PICARD LINEARIZATION IS USED..
C
C*****************************************************************
C.............i....LEGEND.....................r.....
C*****************************************************************
C
C     NELEM=NO. OF ONE DIMENSIONAL ELEMENTS OVER SOLUTION FIELD
C     X=NO. OF NODES
C     XLEWIS=LEWIS NO.
C     YO=MASS FRACTION OF FUEL IN UNBURNT MIXTURE
C     CP=SPECIFIC HEAT OF MIXTURE
C     E=ACTIVATION ENERGY
C     RHOO=DENSITY OF UNBURNT MIXTURE AT AMBIENT TEMPERATURE
C     HC=HEAT OF COMBUSTION OF THE FUEL
C     TFLAME=ADIABATIC FLAME TEMPERATURE
C     ALPHA=Y/YO
C     XLAMBDA=THERMAL CONDUCTIVITY OF GAS MIXTURE
C     G=MASS FLOW RATE PER UNIT AREA
C     XLE= ELEMENT SIZE
C     X=DISTANCE VECTOR ZEROED AT THE FRONT OF THE FLAME
C
C*****************************************************************
C
      COMMON X(1380),XLE(1380),TEMP(1380),NX,NELEM,G
      COMMON/TRI/ D(1380),A(1380),B(1380),ET(1380)
      COMMON/KK/CK1,CK2,F1,F2
      COMMON/PR/XLEWIS,XLAMBDA,CP,YO,HC,E,RHOO,TROOM
      COMMON/PRRR/F(1380)
      COMMON/RR/XRR,ALPHA(1380),ESR,TIGN
      COMMON/DDD/RR(1380),CPX,HCX
      COMMON/RAR/TFLAME
      COMMON/NC/N1,N2,N3,N4,N5,N6
C     ASSIGN VALUES TO BASIC PROPERTIES OF THE FLAME
      NELEM=600
      NX=NELEM+1
      XLEWIS=1.
      YO=.0581
      READ*,YO
      CP=.32
      XLAMBDA=1.6E-4
      G=5.4E-2*1.
      R=1.9859
      HC=1.2E4
      E=32500.
      X(1)=0.
```

```
      F1=1.
      F2=1.-F1
      CK2=0.
      CK1=2.769795E8
      RHOO=1.3E-3
      TROOM=300.
      N1=20
      N2=50
      N3=200
      N4=150
      N5=100
      NX1=N1+1
      NE2=N1+N2
      NX2=NE2+1
      NE3=NE2+N3
      NX3=NE3+1
      NE4=NE3+N4
      NX4=NE4+1
      NE5=NE4+N5
      NX5=NE5+1
      N6=NELEM-NE5
      TIGN=600.
      TEMP(1)=TROOM
      ALPHA(1)=1.
      ESR=E/R
      TFLAME=AFT(XX)
      TT=600
      BOLTS=5.669E-12/4.1864
      EPS=0.
      HT1=EPS*3.14*BOLTS
      CONSTT=0.
      HT2=.0005*3.14*CONSTT
      CALL LEWIS(TT,P)
      PRINT 10, TFLAME
   10 FORMAT(///,T10,*ADIABATIC FLAME TEMPERATURE.....*,F10.4///)
      XRR=YO*RHOO*TROOM
      PRINT 102
  102 FORMAT(T20,*THE FOLLOWING NUMBERS ARE A SEQUENTIAL LIST*,
     .* OF THE NUMBER OF ELEMNTS ASSIGNED TO EACH REGION*//)
      PRINT*,N1,N2,N3,N4,N5,N6
      CPX=CP/XLAMBDA
      YX=CPX*YO
      RXL=(R/29.)/XLAMBDA
      HCX=HC/XLAMBDA
C     INITIAL GUESS FOR THE TEMPERATURE PROFILE
C     ASSIGN ELEMENT SIZES THROUGHOUT FIELD
      DO 1 I=1,N1
      II=I+1
      XLE(I)=.02
      F(I)=1.
      TEMP(II)=TIGN
    1 CONTINUE
      DO 2 I=NX1,NE2
      XLE(I)=.002
```

```
      F(I)=1.
      II=I+1
      TEMP(II)=TEMP(I)+(TFLAME-TIGN)/(10*NX)
    2 CONTINUE
      DO 3 I=NX2,NE3
      XLE(I)=.002
      F(I)=1.
      II=I+1
      TEMP(II)=TEMP(I)+(TFLAME-TEMP(NE2))/(N3*1.2)
    3 CONTINUE
      DO 14 I=NX3,NE4
      XLE(I)=.002
      F(I)=1.
      II=I+1
      TEMP(II)=TEMP(I)+(TFLAME-TEMP(NE3))/N4
   14 CONTINUE
      DO 15 I=NX4,NE5
      XLE(I)=.002
      F(I)=1.
      II=I+1
      TEMP(II)=TFLAME
   15 CONTINUE
      DO 16 I=NX5,NELEM
      XLE(I)=.02
      F(I)=1.
      II=I+1
      TEMP(II)=TFLAME
   16 CONTINUE
      XMU=.9
      CALL SPECIES(1.)
    C     SOLUTION ITERATION
      DO 4 IT=1,50
      DO 5 NNN=1,50
      DO 55 NN=1,3
      BIG=0.
      ET(1)=0.
      D(1)=0.
      A(1)=0.
      B(1)=0.
      DO 6 I=1,NELEM
      RR(I)=ABS(RRATE(I))
    6 CONTINUE
      G=SPEED(UU)
      DO 9 I=1,NELEM
      II=I+1
      AAAAA=(ALPHA(I)+ALPHA(II))/2
      TTTTT=(TEMP(I)+TEMP(II))/2.
      XK1=1./XLE(I)
      XK3=CPX*G/2
      XK3P=CPX*G*F(I)/2.
      XXK=HT1*TTTTT**3+HT2
      XXK1=XXK*(XLE(I))
      XXK2=XXK*F(I)*XLE(I)/4.
```

```
      XK9=(HCX*(AAAAA)*RR(I)+HT1*TROOM**4+HT2*TROOM)*XLE(I)/2.
      XK10=(HCX*AAAAA*RR(I)+HT1*TROOM**4+HT2*TROOM)*XLE(I)*F(I)/2.
      D(I)=D(I)+XK1-XK3+XK3P+XXK1/3-XXK2
      A(I)=-XK1+XK3-XK3P+XXK1/6.-XXK2
      B(II)=-XK1-XK3-XK3P+XXK1/6.+XXK2
      D(II)=XK1+XK3+XK3P+XXK1/3+XXK2
      ET(I)=ET(I)+XK9-XK10
      ET(II)=XK10+XK9
    9 CONTINUE
      D(1)=1.E100
      ET(1)=300.E100
      CALL TRIDIAG(NX)
      TEMP(NX+1)=TEMP(NX)
      DO 111 I=1,NX
      CHANGE=ET(I)-TEMP(I)
      IF(ABS(CHANGE)/TEMP(I).GT.BIG)BIG=ABS(CHANGE)/TEMP(I)
      TEMP(I)=TEMP(I)+XMU*CHANGE
      RR(I)=ABS(RRATE(I))
  111 CONTINUE
      GG=G
      G=SPEED(UU)
      IF(ABS(GG-G).GT.DG)DG=ABS(GG-G)
      D(1)=0.
      DO 222 I=1,NELEM
      II=I+1
      XK3=CPX*G/2.*YO
      XK3P=CPX*G*YO*F(I)/2.
      XK5=XLEWIS*YO/XLE(I)
      XK7=XLE(I)*CPX*RR(I)/3.
      XK7P=XK7*3.*F(I)/4.
      XK8=XK7/2.
      D(I)=D(I)+XK5-XK3+XK3P+XK7-XK7P
      D(II)=XK5+XK3+XK3P+XK7+XK7P
      A(I)=-XK5+XK3-XK3P-XK7P+XK8
      B(II)=-XK5-XK3-XK3P+XK7P+XK8
      ET(II)=0.
  222 CONTINUE
      D(1)=1.E100
      ET(1)=1.E100
      CALL TRIDIAG(NX)
      DO   221 I=1,NX
      CHANGE=ET(I)-ALPHA(I)
      IF(ABS(CHANGE).GT.BIG)BIG=ABS(CHANGE)
      ALPHA(I)=ALPHA(I)+XMU*CHANGE
  221 CONTINUE
      IF(BIG.LT..00001)GO TO 999
   55 CONTINUE
    5 CONTINUE
    4 CONTINUE
  999 CONTINUE
      CALL PRINT(CK)
      STOP
      END
```

```
      SUBROUTINE LEWIS(T,P)
     C      ......LEGEND.......
      C**************************************************
     C                                                    *
     C     LE=LEWIS NO.                                   *
     C     CPMIX=SPECIFIC HEAT OF THE MIXTURE             *
     C     CKMIX=THERMAL CONDUCTIVITY OF THE MIXTURE      *
     C     XN= NO. OF MOLES OF COMPONENT (%) IN THE MIXTURE *
     C     XM=MOLECULAR WEIGHT OF THE COMPONENT           *
     C                                                    *
      C**************************************************
     C
     C
     C
     C THE LEWIS NO IS CALCULATED IN A SUBROUTINE OF THIS PROGRAM
      REAL LE
      DIMENSION XM(2),CP(2),XN(2)
      COMMON/PR/LE,CKMIX,CPMIX,YO,HC,E,RHOO,TROOM
      COMMON/RAR/TFLAME
      COMMON/DDDX/EPKD,SIGMAD
      XM(1)=28.97
      XM(2)=16.0
      RU=1.9859
      P=1.
      XN(2)=YO*XM(1)*100./(XM(2)+YO*(XM(1)-XM(2)))
      XN(1)=100.-XN(2)
    1 CALL SPHEAT(CP(1),CP(2),T)
      CALL THERMK(P,XN,T,XM,RU,CP,CKMIX)
      EPKT=T/EPKD
      CALL COEFFD(T,XM(1),XM(2),P,CKDA,EPKT,SIGMAD)
      CALL LEWISNO(T,P,XM,RU,CKDA,LE,XN,CP)
      TFLAME=AFT(XX)
      CALL IGNTEM(TFLAME,E,N,TROOM,LE,TX)
      PRINT 23,TROOM,E
   23 FORMAT(1H1,/////////10X,
     2/10X*ROOM TEMPERATURE BEFORE THE FLAME (KELVIN)=      *,F12.7,
     4/10X*ACTIVATION ENERGY OF THE CONTROLLING REACTION=*,F15.7,//)
      RETURN
      END
```

```
      SUBROUTINE SPHEAT(CPA,CPB,AFT)
      AA=AFT-600.
      BB=AFT-790.
      CC=AFT-1500.
      IF(AA) 1,1,2
    1 CPA=.249679-7.55179E-5*AFT+1.69194E-7*AFT**2-6.46128E-11*AFT**3
      GO TO 3
    2 IF(CC.GT.0.)GO TO 7
      CPA=.208831+7.71027E-5*AFT-8.56726E-9*AFT**2+4.75772E-12*AFT**3
    3 CONTINUE
      IF(BB) 4,4,5
    4 CPB=.458066-2.61341E-4*AFT+2.07904E-6*AFT**2-1.25017E-9*AFT**3
      GO TO 6
    5 CPB=.0258866+1.60802E-3*AFT-6.67069E-7*AFT**2+1.06432E-10*AFT**3
      GO TO 6
    7 CPA=.4278118-1.9218E-4*AFT+6.92316E-8*AFT**2
      CPB=.588868+6.44119E-4*AFT-1.174567E-7*AFT**2
    6 CONTINUE
      RETURN
      END
```

```
      SUBROUTINE COEFFD(T,XMA,XMB,P,CKDA,TEP,SIGMA)
      COMMON/DDX/OMEGAD
      XX=TEP-5.4
      IF(XX) 1,1,2
    1 OMEGAD=.92553-.025427*TEP+.0014162*TEP**2+1.3875/EXP(.95*TEP)
      GO TO 3
    2 OMEGAD=.7184-.00338*TEP+1.3296/EXP(SQRT(TEP))
    3 CONTINUE
      X=1/XMA+1/XMB
      CKDA=2.628E-3*SQRT(T**3*X)/SIGMA**2/OMEGAD/P
      RETURN
      END
```

```
      SUBROUTINE THERMK(P,XN,AFT,XM,RU,CP,CKMIX)
      DIMENSION PHI(2,2),CK(2),XMU(2),XM(2),XN(2),X(2),CP(2),
     .SIGMA(2),EPK(2),ZZ(2),XX(2),EPKT(2)
      COMMON/DDDX/EPKD,SIGMAD
      COMMON/DDX/OMEGAD
      DATA EPK(1)/79./,SIGMA(1)/3.711/,EPK(2)/144./,SIGMA(2)/3.796/
      ZZ(1)=22000.
      ZZ(2)=22000.
      EPKT(1)=AFT/EPK(1)
      EPKT(2)=AFT/EPK(2)
      EPKD=SQRT(EPK(1)*EPK(2))
      SIGMAD=(SIGMA(1)+SIGMA(2))/2.
      DO 1 I=1,2
      XX(I)=EPKT(I)-4.4
      IF(XX(I)) 2,2,3
    3 OMEGA=.813-.004*EPKT(I)+1.325*EXP(-SQRT(EPKT(I)))
      GO TO 4
    2 OMEGA=.8567+.08654*EPKT(I)-.014957*EPKT(I)**2+2.1916/EXP
     .(1.2*EPKT(I))
    4 CONTINUE
      XMU(I)=2.669E-5*SQRT(XM(I)*AFT)/SIGMA(I)**2/OMEGA
      R=RU/XM(I)
      CKMON=15.*R*XMU(I)/4.
      CV=CP(I)-R
      XINT=1.-EXP(-2./3.*CV/R/ZZ(I))
      CALL COEFFD(AFT,XM(1),XM(2),P,CKDA,EPKT(I),SIGMA(I))
      XXX=1.201*OMEGA/OMEGAD
      CK(I)=CKMON+(XXX-3.*R/2./CV*(5./2.-XXX)*XINT)*(CP(I)-5./2.*R
     .)*XMU(I)
      X(I)=XN(I)/(XN(1)+XN(2))
    1 CONTINUE
      C  CALCULATION OF CKMIX
      CKMIX=0.0
      DO 5 I=1,2
      DENOM=0.0
      DO 6 J=1,2
      PHI(I,J)=(1.+(XMU(I)/XMU(J))**.5*(XM(J)/XM(I))**.25)**
     .2/SQRT(8.*(1.+XM(I)/XM(J)))
      DENOM=DENOM+X(J)*PHI(I,J)
    6 CONTINUE
      CKMIX=CKMIX+X(I)*CK(I)/DENOM
    5 CONTINUE
      RETURN
      END
```

```
      SUBROUTINE LEWISNO(AFT,P,XM,RU,CKDA,LE,XN,CP)
      COMMON/RR/XX,CKMIX,CPMIX,YO,HC,E,RHOO,TROOM
      DIMENSION XM(2),XN(2),CP(2),X(2)
      REAL LE
      X(1)=XN(1)/(XN(1)+XN(2))
      X(2)=XN(2)/(XN(1)+XN(2))
      XMMIX=XM(1)*X(1)+XM(2)*X(2)
      RHO=101.325*XMMIX/8314.3/AFT
      RHOO=101.325*XMMIX/8314.3/TROOM
      CPMIX=(X(1)*XM(1)*CP(1)+X(2)*XM(2)*CP(2))/XMMIX
      LE=CKDA*RHO*CPMIX/CKMIX
      RETURN
      END



      SUBROUTINE IGNTEM(T,E,N,TROOM,LE,TIGN)
      REAL N,LE
      R=1.98588
      N=1.
      CON=R*T**2/E
      DT=T-TROOM
      TT=(LE-1.0)/CON*DT-N*LE
      TD=N*LE/DT*CON+1.0
      TIGN=T+CON*TT/TD
      RETURN
      END
```

```
      SUBROUTINE SPECIES(XMUS)
      COMMON/DDD/RR(1380),CPX,HCX
      COMMON B(1380),XLE(1380),T(1380),NX,NELEM,G
      COMMON/RR/XRR,A(1380),ESR,TIGN
      DO 1 I=2,NX
      IF (T(I).LT.TIGN)XL=0.
      AAA=1./(1.+.175E10*1.3E-3*300./T(I)*XLE(I-1)/G*XL/EXP(ESR
     ./T(I)))*A(I-1)
      A(I)=A(I)+(AAA-A(I))*XMUS
      XL=1.
    1 CONTINUE
      RETURN
      END
```

```
      SUBROUTINE TRIDIAG(N)
      DIMENSION BETA(1380),GAMA(1380)
      COMMON/TRI/D(1380),A(1380),B(1380),C(1380)
     C--------
     C    PROGRAM TO SOLVE A TRIDIAGONAL SYSTEM BY ELIMINATION
     C
     C                    L E G E N D
     C
     C    N     = NUMBER OF UNKNOWNS
     C    D     = DIAGONAL ELEMENTS OF MATRIX
     C    C     = RIGHT HAND SIDE, USED TO STORE THE UNKNOWNS
     C    B     = BELOW DIAGONAL ELEMENTS OF MATRIX
     C    A     = ABOVE DIAGONAL ELEMENTS OF MATRIX
     C                  -----------
     C    F O R W A R D   S U B S T I T U T I O N
     C
      BETA(1)=D(1)
      GAMA(1)=C(1)/BETA(1)
      DO 10 I=2,N
      BETA(I)=D(I)-B(I)*A(I-1)/BETA(I-1)
      GAMA(I)=(C(I)-B(I)*GAMA(I-1))/BETA(I)
   10 CONTINUE
     C------
     C    B A C K    S U B S T I T U T I O N
     C
      C(N)=GAMA(N)
      DO 29 I=2,N
      J=N-I+1
      C(J)=GAMA(J)-A(J)*C(J+1)/BETA(J)
   29 CONTINUE
      RETURN
      END
```

```
      SUBROUTINE PRINT(CK)
      COMMON/RAR/TFLAME.
      COMMON/NC/N1,N2,N3,N4,N5,N6
      COMMON/PRRR/F(1380)
      COMMON X(1380),XLE(1380),TEMP(1380),NX,NELEM,G
      COMMON/DDD/RR(1380),CPX,HCX
      COMMON/PR/XLEWIS,XLAMBDA,CP,YO,HC,E,RHOO,TROOM
      COMMON/RR/XRR,ALPHA(1380),ESR,TIGN
      DIMENSION RRR(1380)
      VEL=G/RHOO
      PRINT 90
   90 FORMAT(//T10,*THE FOLLOWING NUMBERS SHOULD MATCH FOR A GOOD
     .SOLUTION TO BE FOUND...*,/T10*THE FIRST NO IS THE THEORETICAL
     .  FLAME TEMPERATURE AND THE SECOND IS THE FINAL PROFILE TEMP*,//)
      PRINT*,TFLAME
      PRINT*,TEMP(NELEM)
      NNN=NX-N6+2
      DO 53 J=1,NELEM
      JJ=J+1
      RRR(J)=RR(J)*(ALPHA(JJ)+ALPHA(J))/2.
      IF(RRR(J).GT.RMAX)RMAX=RRR(J)
      IF(TEMP(J).GT.TMAX)TMAX=TEMP(J)
      IF(RRR(J).EQ.RMAX)TRMAX=(TEMP(J)+TEMP(J+1))/2.
      IF(RRR(J).EQ.RMAX)IRMAX=J
      IF(TEMP(J).EQ.TMAX)ITMAX=J
   53 CONTINUE
      RMIN=RMAX*.0004
      NNN=0.
      DO 544 J=1,NX
      IF(RRR(J).GT.RMIN)NNN=1
      IF(RRR(J).LT.RMIN.AND.NNN.EQ.1)GO TO 545
      IF(RRR(J).LT.RMIN)NBEGIN=J
  544 CONTINUE
  545 NEND=J
      X(NBEGIN)=0.
      DO 45 I=NBEGIN,NELEM
      II=I+1
      X(II)=X(I)+XLE(I)
   45 CONTINUE
      XRMAX=X(IRMAX)
      XTMAX=X(ITMAX)
      DO 236 L=1,NBEGIN
      IF(TEMP(L).LT.301.)NPREHOT=L
  236 CONTINUE
      DO 132 I=2,NBEGIN
      J=NBEGIN-I+1
      JJ=J+1
      X(J)=X(JJ)-XLE(J)
  132 CONTINUE
      NNNN=NEND+100
      NXPRE=(NBEGIN-NPREHOT+2)/3
      NXXPRE=NXPRE+NPREHOT
  560 FORMAT(1H1,10X,*THE FOLLOWING TABLE SHOWS TEMPERATURE IN THE
     .PREHEAT ZONE OF THE FLAME*,///)
```

```
      XFLAME=X(NEND)
      PRINT 1,XLEWIS,XLAMBDA,CP,YO,G,VEL,XFLAME,TIGN,HC
    1 FORMAT(10X,*LEWIS NUMBER                          = *,F12.5
     ./      10X,*THERMAL CONDUCTIVITY(CAL/CM-S-K)= *,F12.5,
     ./      10X,*SPECIFIC HEAT(CAL/GM-K)          = *,F12.5,
     ./      10X,*FUEL FRACTION(INITIAL)           = *,F12.5,
     ./      10X,*VOLUME FLOW RATE(GM/S/CM**2)     = *,F12.5,
     ./      10X,*FLAME VELOCITY(CM/SEC)           = *,F12.5,
     ./       10X,*FLAME WIDTH (CENTIMETERS)         = *,F12.5,
     ./       10X,*CUTOFF TEMPERATURE               = *,F12.5,
     ./       10X,*ENTHALPY OF REACT OF FUEL(CAL/G)= *,F12.2,///)
      PRINT 560
      PRINT 541
    541 FORMAT(12X,* NO  ! DISTANCE   !  TEMPERATURE   ! NO  ! *
     ,,* DISTANCE  !  TEMPERATURE   !  NO   !  DISTANCE  ! TEMPERATURE *
     .,///)
      DO 326 I=NPREHOT,NXPRE
      II=I+NXPRE
      III=II+NXPRE
      PRINT 237 ,I,X(I),TEMP(I),II,X(II),TEMP(II),III,X(III),TEMP(III)
    237 FORMAT(10X,*! *,I3,* ! *,F10.7,* ! *,F14.7,* ! *,I3,* ! *,
     ,F10.7,* ! *,F14.7,* ! *,I3,* ! *,F10.7,* ! *,F14.7,
     ,* !*)
    326 CONTINUE
      PRINT 901
    901 FORMAT(//10X,*THE FOLLOWING TABLE GIVES PARAMETERS IN THE FLAME
     .ZONE*,//)
      PRINT 4
    4 FORMAT(1X,*NO*,T7,*DISTANCE*,T17,*TEMP*,T31,*FUEL*,T40,
     ,*R.RATE*,T50,*UPWIND*,T63,*NO*
     .,T69,*DISTANCE*,T79,*TEMP*,T92,*FUEL*,T100,*RRATE*,T112,
     ,*UPWIND*,///)
      NXXXX=(NEND-NBEGIN+1)/2
      NXXX=NXXXX+NBEGIN
      DO 2 I=NBEGIN,NXXX
      II=I+NXXXX
      PRINT 3,I,X(I),TEMP(I),ALPHA(I),RRR(I),F(I),II,
     ,X(II),TEMP(II),ALPHA(II),RRR(II),F(II)
    3 FORMAT(1X,I3,T5,5(F9.4,2X),T62,I4,T66,5(F9.4,2X))
    2 CONTINUE
      RETURN
      END
```